THE EFFECT OF RESIN TYPE AND GLASS CONTENT ON THE FIRE ENGINEERING PROPERTIES OF TYPICAL FRP COMPOSITES

by

Melissa Barter Avila

A Thesis

Submitted to the Faculty

of the

WORCESTER POLYTECHNIC INSTITUTE

in partial fulfillment of the requirements for the

Degree of Master of Science

in

Fire Protection Engineering

May 2007

APPROVED:

_____

Professor Nicholas A. Dembsey, Major Advisor

_____

Dr. Patricia A. Beaulieu, Co-Advisor, FM Global

_____

Mr. Chris Lautenberger, Reader, University of California, Berkeley

_____

Professor Ali S. Rangwala, Reader

_____

Professor Kathy A. Notarianni, Head of Department

Abstract

This study is designed to provide the composites industry as well as the fire engineering industry baseline data for pyrolysis modelling of common fiber reinforced polymer (FRP) systems. Four resin systems and three glass contents will be considered. This matrix of FRP systems has been carefully fabricated and documented so as to provide "transparency" as to the system compositions. An important and interesting aspect of these FRP systems is that all the resins used are listed by the manufacturers as Class 1 or Class A per ASTM E 84. The FRP systems are being evaluated in bench scale modern fire test apparatuses (FPA, ASTM E 2058, and Cone, ASTM E 1354); detailed information on the FPA is provided. These apparatuses provide a range of measurements such as heat release rate that can be used to calculate engineering "properties" of these FRP systems. The "properties", such as minimum heat flux for proper ignition (found to range from 20 to over 100 kW/m^2) and the b flame spread parameter, can then be used to compare the fire performance (flashover potential) of these FRP systems according to resin type and glass content. Additional instrumentation has also been added to the specimens to allow surface and in-depth temperatures to be measured. The additional measurements are used to complete a set of data for pyrolysis modelling and for calculating thermal properties of the composites. The effect of environmental oxygen concentration and flaming and non-flaming decomposition are investigated in terms of fundamental pyrolysis behavior of the FRP systems. A general conclusion is that the phenolic composite has better fire engineering "properties" than the polyester composite but the glass is the controlling component of the composite with regards to temperature profile and resulting thermal properties.

Acknowledgements

I would like to thank my advisor, Professor Nicholas Dembsey, for his patient support and thoughtful discussions all the way to the end of this project. I gained much valuable experience and a wealth of knowledge from him over the years. I would also like to thank the WPI FPE department for their continued support throughout the project, especially Linda Malone.

This project would not have been possible without the donation of the FPA and additional financial support from FM Global (FM Global Fellow Avila and FM Global Scholar Dembsey). Dr. Patricia Beaulieu at FM Global was always available to have a technical discussion or lend a hand, especially issues relating to setting up experimentation and instrumentation. Many thanks also to Mr. Stephen Ogden, Mr. Dana Capron and Mr. Lawney Crudup at FM Global for their technical support as I was setting up the FPA at WPI. Discussions with Mr. Chris Lautenberger at the University of California, Berkeley regarding data useful for pyrolysis modelling was instrumental in creating the testing matrix. Many thanks also to Professor Ali Rangwala for providing insightful comments on this paper.

I would like to thank Mr. Charlie Dore, from Cinnabar FL and Abate Fire Technologies, from whom I learned a great deal about composites and their manufacture. Many thanks for the materials donated by: Mr. Trevor Humphries of VectorPly, Phoenix City, AL (glass); and Mr. Chad Fester of Airtech International Inc. of Huntington Beach, CA (vacuum bagging and peal ply) as well as Cinnabar, FL (lamination of the FRP composite panels). Information regarding the heat of combustion and other properties of the composites used in this study by Mr. Mike Stevens from Ashland was very useful.

Many thanks also to Mr. Randall Harris, Ms. Mihyun (Esther) Kim and Ms. Jacqueline Shea at WPI for performing the Cone tests. Also, a special thank you goes to Esther Kim for her undying support as my project was winding down by preparing and burning the last round of FPA tests. Thanks also to my husband, Marc Avila, and my family in Kentucky for their continued support and patience throughout this project. Another special thank you goes to Marc and our two dogs for the many hours hanging out with me on the couch with the laptop as I finished this piece of work.

Table of Contents

List of Figures

List of Tables

Chapter 1: Introduction

Traditionally, the manufacture of composites is largely a guess and check operation with regards to fire characteristics. The original design composite is tested via standard fire tests but the composite would need to be re-tested if the resin type or glass content was changed, possibly without knowing if the change will positively affect the test results. The testing cycle can be time consuming and expensive. However, if the manufacturer had an idea of how changing the resin type or glass content would affect the results, this would provide a guideline to ease the time and financial commitment of manufacturing fire-safe composites. The current work aims to provide a beginning to systematic research into how changing the resin type and glass content affects the fire characteristics of typical fiber reinforced polymer composites.

The standard fire test that would typically be used for composites is the UL Steiner Tunnel Test, ASTM E84.[1] The sample in the Tunnel Test is placed horizontally on a ceiling of a tunnel-like test apparatus. Although it has been used for over 50 years, the Tunnel Test has a number of important shortcomings. First, the results of the test only provide a classification scheme for ranking materials; the results do not include useful engineering data. Second, some materials do not behave in the Tunnel Test as they would in a real fire scenario. Since the sample in the Tunnel Test is a horizontal sample, upward flame propagation is not modelled.[2,3] A more appropriate test would be one in which both concurrent and opposed flow flame spread were possible, such as in the room/corner test (ISO 9705[4], NFPA 265[5] and NFPA 286[6]). In this test method, a large ($4m^2$) sample is placed on the walls as well as the ceiling of a corner in a standard test room. The corner is then exposed to an incident heat flux from a large flame. This more closely represents a realistic fire scenario but has the disadvantages of being expensive and time-consuming. Therefore, many different researchers have worked toward developing a model to use bench-scale data (such as the Fire Propagation Apparatus (FPA), ASTM E 2058[7], or the Cone Calorimeter, ASTM E 1354[8]) to predict room/corner test results.[2, 3]

In this study, properties such as the heat release rate, minimum heat flux for proper ignition and the Quintiere[9] flame spread parameter, b, will be used to differentiate the composite systems based on resin type and glass content. The b parameter will also be used to estimate whether flashover might occur in the room/corner test from bench-scale experiments done in the FPA and the Cone Calorimeter.

These bench-scale apparatuses also provide useful data needed by a fire model in order to simulate burning. In the fire community, using data similar to that which will be developed in this study as parameters in a fire model in order to simulate the end use of the material is the long-term goal.[10] Significant steps were taken toward this goal with the development of the Fire Dynamics Simulator (FDS) developed at the National Institute for Standards and Technology[11] and other computational fluid dynamics (CFD) based fire models.[12,13] A subset of these more comprehensive models is the pyrolysis model, which describes the heating and decomposition of the material. A good review of pyrolysis models is available in the literature.[14] From the composites literature,[15,16,17,18] there is a significant amount of work studying the temperature profile with regards to thermo-mechanical stability of composites. These studies incorporate a comprehensive pyrolysis model but focus more on temperatures at depth instead of temperatures at or close to the surface, which are more important for reaction to fire characteristics.

The current work aims to obtain data from bench-scale test apparatuses that can be used to both differentiate the composites according to resin type and glass content as well as provide a good data set for calibration of pyrolysis models such as that being developed at the University of California, Berkeley.[19] While traditional bench-scale measurements such as heat release rate and mass loss rate will be used, measuring surface and in-depth temperatures as well as changing the environment to which the sample is exposed give additional insight into the behavior of the composites and provide the beginning of a data set useful for modelling purposes. A simple parameter estimation to determine the thermal diffusivity, thermal conductivity and specific heat was completed in an attempt to further differentiate the composites.

Organization

This thesis has a main body, which consists of a paper that will be submitted to a journal for publishing, as well as appendices. The appendices detail all of the work that was completed that did not fit within the realm of the paper. The information in each of the appendices is detailed below.

Appendix A discusses the operator independent ignition method and evaluates the use of the Savitzky-Golay and Fast Fourier transform methods of smoothing data.

Appendix B details the calibration of the FPA at WPI, including finding the calibration equations and sensitivity of the instruments as well as learning general information about the instruments that make up the FPA. The appendix also details uncertainties of other measurements discussed in this thesis.

Appendix C explains, in detail, the data reduction macro in Excel that was created for the FPA.

Appendix D details secondary checks that were performed on the WPI FPA, since it was a new apparatus at WPI at the beginning of this study. The appendix discusses measurement of the air flow in the air chamber, mapping of the heat flux for a horizontal sample, attempts to reduce the noise in the load cell and relative humidity measurements of the gas analyzer samples.

Appendix E is an explanation of modifications that were made to the WPI FPA.

Appendix F details instrumentation that was installed for this project including the infrared thermometer, thermocouples and heat flux gage.

Appendix G regards different material properties that were determined for the composite materials including heat of combustion, ash percent for the resin systems, elemental analysis, time to ignition using a variety of methods and the b flame spread parameter. This appendix also gives more detailed information on the makeup of the composites.

Appendix H is a copy of a paper written and presented by the author and two co-authors for the Composites 2006 conference in St. Louis, MO.

Appendix I is a copy of a paper written by the author and two co-authors that was presented at the Fire and Materials 2007 conference in San Francisco, CA by Nicholas Dembsey.

References

[1] Standard Test Method for Surface Burning Characteristics of Building Materials, ASTM E 84-05, ASTM, 100 Barr Harbor Drive, West Conshohocken, PA, U.S.

[2] Dembsey, N.A., J.J. Alston and S.D. Ayers, "Using Cone Calorimeter Data and Half-Scale Corner Test Data to Assess the Fire Performance of Composite Materials," submitted to Cinnabar-Florida, Orlando, FL, USA as part of the project *Phenolics vs. Other Thermosets for Theme Parks* (2001).

[3] Williamson, R.B. and F.W. Mowrer, "The Role of Interior Finish in Fire Development," *Fire Protection Engineering*, 2004, No. 24, pp. 26-40.

[4] Fire Tests – Full-Scale Room Test for Surface Products, ISO 9705, International Standards Organization, Geneva, Switzerland, 1993.

[5] Standard Methods of Fire Tests for Evaluating Room Fire Growth Contribution on Textile Coverings of Full Height Panels and Walls, NFPA 265, National Fire Protection Association, Quincy, MA.

[6] Standard Methods of Fire Tests for Evaluating Contribution of Wall and Ceiling Interior Finish to Room Fire Growth, NFPA 286, National Fire Protection Association, Quincy, MA.

[7] Standard Methods of Test for Measurement of Synthetic Polymer Material Flammability Using a Fire Propagation Apparatus (FPA), ASTM E 2058-03, ASTM, 100 Barr Harbor Drive, West Conshohocken, PA, U.S.

[8] Standard Test Method for Heat and Visible Smoke Release Rates for Materials and Products Using an Oxygen Consumption Calorimeter, ASTM E 1354-02, ASTM, 100 Barr Harbor Drive, West Conshohocken, PA, U.S.

[9] Cleary, T. and J. Quintiere, "A Framework for Utilizing Fire Property Tests," *Fire Safety Science, Proceedings of the Third International Symposium,* International Association of Fire Safety Science (IAFSS), Scotland, U.K., Cox and Langford Editors, Elsevier Applied Science London and New York, July 8-12 (1991) 647-656.

[10] Bill, R.G. and Croce, P.A., "The International FORUM of Fire Research Directors: A position paper on small-scale measurements for next generation standards," *Fire Safety Journal*, 2006; 41: 536-538.

[11] McGrattan, K.B. and Forney, G.P. "Fire Dynamics Simulator (Version 4), User's Guide," NIST Special Publication 1019, National Institute of Standards and Technology, Gaithersburg, Maryland, July 2004.

[12] Olenick, S.M. and Carpenter, D.J., "An updated international survey of computer models for fire and smoke." Journal of Fire Protection Engineering 2003; 13:87-110.

[13] Cox, G. and Kumar, S., "Chapter 3-8: Modeling Enclosure Fires Using CFD." The SFPE Handbook of Fire Protection Engineering. Ed. Philip J. DiNenno. National Fire Protection Association, Quincy, MA, 2000.

[14] Lautenberger, C. and Fernandez-Pello, C., "Pyrolysis modeling, thermal decomposition, and transport processes in combustible solids," Transport Phenomena in Fires. Ed. M. Faghri and B. Sunder, WIT Press, 2007.

[15] Ramroth, W.T., Krysl, P., Asaro, R.J. "Sensitivity and uncertainty analyses for FE thermal model of FRP panel exposed to fire." Composites A 2006; 37:1082-1091.

[16] Davies, J.M., Wang, Y.C., Wong, P.M.H. "Polymer Composites in Fire." Composites A 2006; 37:1131-1141.

[17] Lattimer, B.Y., Ouellette, J. "Properties of composite materials for thermal analysis involving fires." Composites A 2006; 37:1068-1081.

[18] Ramroth, W.T., Asaro, R.J. and Krysl, P., "Finite element modeling of fire degraded FRP composite panels using a rate dependent constitutive model," Composites A 2006; 37:1015-1023.

[19] Lautenberger, C and Fernandez-Pello, C., "A Generalized Pyrolysis Model for Simulating Charring, Intumescent, Smoldering, and Noncharring Gasification," 2006, University of California eScholarship Repository, <http://repositories.cdlib.org/cpl/fs/LautenbergerGenPyro>.

Chapter 2: Effect of Resin Type and Glass Content on the Reaction to Fire Characteristics of Typical FRP Composites

Abstract

This study is designed to provide the composites industry as well as the fire engineering industry baseline data for pyrolysis modelling of common fiber reinforced polymer (FRP) systems. Four resin systems and three glass contents will be considered. This matrix of FRP systems has been carefully fabricated and documented so as to provide "transparency" as to the system compositions. An important and interesting aspect of these FRP systems is that all the resins used are listed by the manufacturers as Class 1 or Class A per ASTM E 84. The FRP systems are being evaluated in bench scale modern fire test apparatuses (FPA, ASTM E 2058, and Cone, ASTM E 1354). These apparatuses provide a range of measurements that can be used to characterize these FRP systems. The engineering "property" minimum heat flux for proper ignition (found to range from 20 to over 100 kW/m^2) has been used to compare these FRP systems according to resin type and glass content. Additional instrumentation has also been added to the specimens to allow surface and in-depth temperatures to be measured. The additional measurements are used to complete a set of data for pyrolysis modelling and for calculating thermal properties of the composites. The effect of environmental oxygen concentration and flaming and non-flaming decomposition are investigated in terms of fundamental pyrolysis behavior of the FRP systems.

Introduction

Traditionally, the manufacture of composites is largely a guess and check operation with regards to fire characteristics. The original design composite is tested via standard fire tests but the composite would need to be re-tested if the resin type or glass content was changed, possibly without knowing if the change will positively affect the test results. The testing cycle can be time consuming and expensive. However, if the manufacturer had an idea of how changing the resin type or glass content would affect the results, this would provide a guideline to ease the time and financial commitment of manufacturing fire-safe

composites. The current work aims to provide a beginning to systematic research into how changing the resin type and glass content affects the fire characteristics of typical fiber reinforced polymer composites.

Bench-scale apparatuses such as the Fire Propagation Apparatus (FPA, ASTM E 2058[1]) and the Cone Calorimeter (ASTM E 1354[2]) are used in this study to provide useful data which can be used in a fire model to simulate burning. In the fire community, using data similar to that which will be developed in this study as parameters in a fire model in order to simulate the end use of the material is the long-term goal.[3] Significant steps were taken toward this goal with the development of the Fire Dynamics Simulator (FDS) developed at the National Institute for Standards and Technology[4] and other computational fluid dynamics (CFD) based fire models.[5,6] A subset of these more comprehensive models is the pyrolysis model, which describes the heating and decomposition of the material. A good review of pyrolysis models is available in the literature.[7] From the composites literature,[8,9,10,11] there is a significant amount of work on the temperature profile of composites with regards to thermo-mechanical stability. These studies incorporate a comprehensive pyrolysis model but focus more on temperatures at depth instead of temperatures at or close to the surface, which are more important for reaction to fire characteristics.

The current work aims to obtain data from bench-scale test apparatuses that can be used to both differentiate the composites according to resin type and glass content as well as provide a good data set for calibration of pyrolysis models such as that being developed at the University of California, Berkeley.[12] While traditional bench-scale measurements such as heat release rate and mass loss rate will be used, measuring surface and in-depth temperatures as well as changing the environment to which the sample is exposed give additional insight into the behavior of the composites and provide the beginning of a data set useful for modelling purposes. The minimum heat flux for proper ignition, a common fire engineering "property," was determined for all of the composites by varying the applied heat flux to the material. A simple parameter estimation to determine the thermal diffusivity, thermal conductivity and specific heat was completed in an attempt to further differentiate the composites.

Testing Equipment and Materials

Composite Systems

In the following discussion, the term "system" will be used to differentiate between resin types (e.g. System 1 is a polyester). The term "sample" will be used to differentiate between glass contents (e.g. sample 1A has a lower glass content than sample 1B). Lastly, the term "specimen" will be used to represent one individual composite from the sample that will be tested.

Eleven different fiber reinforced polymer (FRP) samples are being tested for the current work. There is a total of four different resin systems, each with three different glass contents (except for System 3, which has only two glass contents). Table 1 shows the base resin and the glass content for all of the FRP composites that were tested in the current study. From the table, it can be seen that there was a variability of 6-10.5mm in thickness over all of the composite systems used. Antimony trioxide was added to the polyester (System 1) as a smoke inhibitor. The neat resole phenolic (System 3) is comprised of formaldehyde and phenol and was modified with the addition of a char forming, fire retardant plasticizer that lowers the viscosity of the resin and further enhances its physical and resistance properties. An inorganic fire retardant for System 4 is used to create a high charring effect while an organic fire retardant for System 5 creates an intumescent effect. All of the composites used in this study are geometrically stable during burning; the intumescent phenolic has a very thin intumescent layer that does not visibly expand during testing. All of the resins used in this study are listed as Class 1 or A with regards to ASTM E 84.[13]

There are three different types of fiberglass used in each of the composites: Owens Corning chopped strand mat (67.8g/m^2), Fiber Glass Industries (FGI) 2-end satin roving (882g/m^2) and St. Gobain plain cloth (332g/m^2). The pattern of fiberglass, which has properties similar to E-glass, repeats 3, 4 and 5 times to create the lowest, medium and highest glass contents. The layers of glass, which are a special tight weave, are fully wetted with the resin and held together with a very thin 15 mil phenolic binder veil by Schmelzer, Inc.. The ability of the individual layers of glass to fully wet with the resin is unknown and the glass/resin ratio will be assumed to be constant throughout the cross section of the composite. A prominent glass layer which is thought to be the FGI 2-end satin roving layer can be seen from the cross section of the composite

and thus allows for a measurement of the distance between repeats of the fiberglass pattern. The FGI fiberglass has a 5 by 7mm weave and a 5-7mm stitch can be seen on the cross section of the composites so the assumption of the prominent glass layer is thought to be valid. From the measurements, the fiberglass pattern repeats every 1-2mm.

The FPA and the Cone Calorimeter

The FPA[1] is a bench-scale fire test apparatus in which the sample is heated by four radiant lamps. Each IR lamp consists of 6 bulbs with a tungsten wire in argon gas, which provides a uniform heat flux (to within 5kW/m^2, determined from testing) over the specimen surface of up to 60kW/m^2. The lamps emit with spectral energy peaks of 1.15 and 0.89 microns.[14] A long quartz tube can be used to create an atmosphere for the test that is different than the ambient (i.e. from pure nitrogen to 40% enhanced oxygen). A flow rate of air at 200lpm is run through the bottom of the air chamber so that the sample is in a flow field during the test. The ignition source is a 10mm long blue pilot flame located 10mm above the center of the sample. The FPA can be used to calculate useful engineering data such as heat release rate, mass loss rate, smoke yield and smoke extinction coefficient. The standard specifies a carbon dioxide generation based heat release rate, which will be used for the FPA in this study.[1]

The Cone Calorimeter[2] is similar to the FPA but it also has some important differences. The heater in the Cone is an electrically heated rod in the shape of a cone, instead of the IR lamps in the FPA. The sample in the Cone is exposed to the ambient environment and is not in a flow field so the apparatus can only perform tests under ambient conditions. The ignition source is an intermittent sparker instead of the pilot flame used by the FPA. The Cone standard specifies an oxygen consumption based heat release rate, which will be used for the Cone in this study.[2]

The difference in the radiant source between the Cone and the FPA is noteworthy because the FPA radiation apparently tends to absorb at depth into the composites evaluated in this study while the Cone does not. This difference causes a discrepancy in the time to ignition between results obtained from the Cone and the FPA. Testing performed with thermocouples to demonstrate differences between FPA and Cone test results were inconclusive. The temperature begins to rise a bit slower in the Cone; after the

initial period however, the thermocouple traces for identical tests performed on the two apparatuses match each other fairly well. An attempt was also made to resolve the absorption issue by applying carbon black powder to the surface of the specimen in the FPA to prevent in-depth absorption. The carbon black decreased the time to ignition in the FPA to match that of the Cone, indicating that the FPA does experience some in-depth absorption.

Sample Holder

Instead of the non-insulated aluminium dish that is specified in ASTM E 2058,[1] an insulated sample dish described by de Ris and Khan[15] is used. The sample is surrounded by Cotronics® paper insulation on the back and sides, as shown in Figure 1, to provide a barrier to heat loss. The assumptions that can be made based on the presence of the insulation (e.g. no heat loss from the back face or sides of the sample) are very useful in modelling the sample's reaction to the applied heat flux. The sample holder is also beneficial for installing embedded and back face thermocouples as well as embedding a heat flux gage to lie flush with the sample surface.

Instrumentation Installation

In order to install the thermocouples at depth, 1.25mm diameter holes were drilled at appropriate depths from the surface. The holes were drilled 38-50mm (1.5-2 inches) into the edge of the sample. From testing with both thermocouples at different radii as well as with the heat flux gage, it was found that there is a zone of uniformity with regards to temperature and heat flux within a 32mm (1.25inch) radius from the center of the specimen. Since the specimens have a diameter of approximately 102mm (4 inches) diameter, the thermocouple bead was located within this zone of uniformity. In order to eliminate air gaps in the holes drilled for the thermocouples, excess thermal grease (OmegaTherm Thermally Conductive Silicone Paste, Model OT-201 from Omega Engineering) was inserted along with the thermocouples (Omega Precision Fine Wire Thermocouples, Model 5TC-GG-K-30-36 from Omega Engineering). The back face thermocouple was affixed to the middle of the back surface with Krazy glue, which is inexpensive, dries very fast and has proven to be consistent and repeatable for back face temperature measurements. The

surface thermocouple was attached with a thin layer of high temperature adhesive (Resbond 907 Industrial Strength Fireproof Adhesive from Cotronics Corp.). The surface thermocouple was located one inch from the edge of the sample so that the bead was in the zone of uniformity but not affected by the pilot flame (the ignition source used in the FPA).

Originally, an infrared thermometer was used to measure sample surface temperature. In the FPA, the IR thermometer is mounted on a bracket and has a spot size that is 2.3cm (0.9inch) in diameter whose center is located approximately one inch from the edge of the sample to avoid the pilot flame. In the Cone, the infrared thermometer is closer to the sample surface, resulting in a spot size of 1.3cm (0.5inch) and is situated to view the center of the sample. Unfortunately, the infrared thermometer did not provide repeatable results for the polyester composites and did not provide results consistent with the surface thermocouple for any of the composites. The reason for this is not known but there are a number of theories in the literature including absorption of the emitted radiation by gases coming from the sample such as CO, CO_2 and H_2O[16,17] or the transmissive properties of the resin material.[18] Due to issues with results from the infrared thermometer, the surface thermocouple will be used for surface temperature measurements and the IR thermometer will not be further discussed.

A heat flux gage was also embedded in the sample to lie flush with the surface. The dual heat flux gage (MedTherm model number 32-15TKS-15R(S)-21846) that was used was able to partition the heat flux into both convective and radiative fractions. However, a resin condensate layer formed on the gage just before ignition or after a prolonged period of non-flaming decomposition. The formation of this layer caused the radiometer to read essentially zero heat flux and caused a change in the reading of the total heat flux gage. Even though the reading from the total heat flux gage after the condensate formation is still being interpreted, the information obtained before this time from both the total and radiative heat flux gage can be used to partition the heat flux from the FPA and Cone into its radiative and convective portions.

Uncertainties

The uncertainty for the different variables was determined via statistical analysis performed on data from tests with identical conditions. All uncertainties listed in this study are full scale (as opposed to ± half

scale). The uncertainty in the heat release rate (45kW/m^2) was determined from calibration tests done with PMMA, acetone, methane and propylene in the FPA; it is an average value. The analysis for the uncertainty in the time to ignition, burn duration and mass loss rate for the FPA is based on three PMMA tests performed at 50kW/m^2. A sample set of three is believed to be sufficient in this case because the FPA standard calls for three identical tests to be performed to correctly determine other properties.[1] From these tests, the maximum uncertainty in the time to ignition and the burn duration were found to be 9s and 101s, respectively. The uncertainty in the mass loss rate was found to be 17mg/s (2.4g/sm^2). The uncertainty in the critical mass flux at proper ignition was found to have a maximum uncertainty of 6.5g/sm^2 from population statistics on PMMA and composite samples.

The uncertainty in the thermocouple measurements was determined from comparing the traces from identical tests, including PMMA and composite testing. Population statistics were calculated based on this comparison for a number of tests and the average, across all tests, of the maximum deviation between two traces was found. The thermocouple measurements have, on average, a maximum deviation of 27°C with a standard deviation of 18°C; the maximum deviation will be used to evaluate significant differences in the thermocouple traces.

The uncertainties calculated above for the FPA will also be used for evaluating significant differences in Cone tests. The heat release rate uncertainty in the Cone is governed by the C factor, which is determined by calculating the heat release rate of a methane fire at different mass flow rate steps and inserting the subsequent values into an equation for the C factor that is provided in ASTM E 1354.[2] The required uncertainty from the standard is 5% and it is known that the Cone meets this requirement. Therefore, no additional calibration testing was required on the Cone for the purposes of this study.

Proper Ignition Concept and Testing Matrix

Proper and Improper Ignition

The concept of proper ignition that was used in this study is an extension of the concept of "sustained flaming" that was developed in ASTM E 2058.[1] The standard defines sustained flaming as the "existence of flame on or over most of the specimen surface for at least a 4s duration".[1] Since one of the goals of this

study is to produce useful data for the development of pyrolysis models, a fully developed flame cone is necessary to make the simplifying assumption of one-dimensional burning. Another benefit to this definition is that it does not count edge burning as significant burning because the end use of this product (i.e. a wall, ceiling, floor) would usually be so large that edge effects would be very minor. A flame is considered to be effectively one-dimensional if it is even over the entire sample surface and is unified into a single flame cone (not necessarily axisymmetric). A distinction was made between cellular burning (flamelets over most or all of the surface) and edge burning. If a sample started to burn with cellular flaming and then progressed into a flame cone, it was still called proper ignition for the purposes of this study. Visual observations were made as to the time of the beginning and end of the flame cone so that data could be properly truncated for modelling purposes.

The concept of a critical mass flux is used by modellers as an ignition criterion and sometimes as an extinction criterion. When the mass flux reaches a critical value, the sample is assumed to have ignited and when it decreases past this value near the end of the test, the flame is assumed to have gone out.[19] The critical mass flux at proper ignition was determined for the samples studied and the results are displayed in Table 2. As can be seen from the table, there is a high degree of uncertainty in the critical mass flux. The critical mass flux is based on the time to ignition (uncertainty of 9s) and on the mass loss rate (uncertainty of 17mg/s or 2.4g/sm^2) and therefore has a high degree of variability (6g/sm^2). Also, all tests that experienced proper ignition, including FPA and Cone tests at a variety of heat fluxes, were included to obtain the statistics displayed in the table. Despite the high degree of uncertainty, it is interesting to note that there is a significant downward trend in the critical mass flux at proper ignition with increasing glass content for the system 1 composites (polyester). The PMMA is included as a reference from the literature to ensure consistency. PMMA has a critical mass flux at ignition of 4-5g/sm^2,[19] which matches with the value obtained with the FPA (within the uncertainty). Another interesting note with regards to the table is that the critical mass flux at proper ignition is approximately 10g/sm^2 for all of the materials studied, including the PMMA and all of the composite systems.

Testing Matrix

Tests were performed on the composite systems to determine the minimum heat flux for proper ignition. The minimum heat flux for proper ignition represents the condition under which the material will experience ignition but not necessarily fire spread and will help to rank the materials according to resin type and glass content. If the value of the minimum heat flux is low, the resin is less stable and the probability that it will experience fire spread are increased over those materials that have a higher minimum heat flux. With regards to fire modeling, the idea of minimum heat flux for proper ignition as defined in this study is important since it represents the heat flux at which the concept of one-dimensional burning is applicable. Systems 3, 4 and 5 (the phenolic samples) did not properly ignite at 50kW/m^2 so some tests were also performed at 60kW/m^2. None of the System 3, 4 and 5 composites would properly ignite in the FPA at 60kW/m^2, which is the highest heat flux that the FPA can achieve. Therefore, the minimum heat flux for proper ignition for these systems had to be determined in the Cone,[2] which can achieve up to 100kW/m^2. The minimum heat flux for proper ignition for the System 1 (polyester) composites was determined with the FPA.

A testing matrix was created in an effort to compile a good set of data for modeling purposes. The matrix consisted of tests to fully develop potential differences with glass content and resin type for certain composites, perform non-flaming tests, study environmental effects and compare results between the Cone and the FPA. The difference between results from the Cone and the FPA is discussed above. All tests had instrumentation including embedded and back face thermocouples; some later tests also had a surface thermocouple to measure sample surface temperature. Separate tests were performed with an embedded heat flux gage. The added instrumentation provides good data for both boundary conditions (surface temperature and surface heat flux up to the development of condensate on the gage) and parameter estimation (temperature profile in the specimen). Non-flaming tests are important because the decomposition kinetics of the sample can be tested without the added complexity of the flame. Tests were performed under different environments (with no pilot flame in order to lengthen the non-flaming condition) to determine if the decomposition kinetics would significantly change.

In order to better determine differences with glass content and resin type, tests were done with the polyester composites at all three glass contents in the FPA at 50kW/m^2 and with the neat phenolic with the

highest glass content at 70kW/m^2 in the Cone; all of these tests experienced proper ignition. Tests were also done with the 1A and 3C samples at 50kW/m^2 in the FPA under nitrogen, air and 40% oxygen enhanced air atmospheres as well as with 1A samples at 50kW/m^2 in the FPA and the Cone. A heat flux of 50kW/m^2 was chosen as a representative heat flux for the tests because it is a common heat flux in the literature and it represents a mid-range value for the two testing apparatuses used in this study. If the sample did not properly ignite at 50kW/m^2 and proper ignition was necessary for the test, a heat flux of 70kW/m^2 was used.

Results

Many aspects of the composites were studied through the use of an extensive testing matrix geared toward calibration of a pyrolysis model and comparing glass content and resin type of the different composites. As discussed in the previous section, tests were also done with 1A and 3C in the FPA at 50kW/m^2 under air, nitrogen and 40% oxygen enhanced air. Since no difference in the temperature profile was determined and this is not the main focus of the current study, these results will not be further discussed below.

Minimum Heat Flux for Proper Ignition

The only composite system that properly ignited in the FPA[1] was System 1 so the rest of the samples had to be tested in the Cone[2] at higher heat fluxes. The last column in Table 1 gives the minimum heat flux for proper ignition as a range. A change in the minimum heat flux for proper ignition range is considered to be significant if it is greater than or equal to the step that is being taken (i.e. 5kW/m^2 or 10kW/m^2).

There is a significant change in the minimum heat flux for proper ignition over all of the systems with resin type. The polyester resin (System 1) has a lower minimum heat flux for proper ignition range than any of the phenolic resins. Among the phenolics, the neat phenolic (System 3) has the lowest minimum heat flux for proper ignition, which shows that the additives (Systems 4 and 5) have a significant effect on the fire performance. The intumescent additive, System 5, tends to have a significantly higher minimum heat flux for proper ignition than the charring additive, System 4.

There also appeared to be a trend for most of the systems with changing glass content, except for System 1. The data in Table 1 indicate that the minimum heat flux for proper ignition increases as the glass content increases. That is, as the glass content of the sample increased, more energy was needed to overcome the blocking effect of the glass and release enough vapors at the sample surface to create a steady flame cone over the entire surface.

System 1 seems to have an effect that is unexpected; the lowest glass content has the lowest minimum heat flux for proper ignition. However, more tests should be done to fully confirm this effect. Only one test was done with each sample at each heat flux.

System 3 appears to show a significant change with glass content. It should be noted that 3A was tested in the FPA at 50kW/m^2 and did not properly ignite due to significant delamination and violent popping early in the test. This is due to the release of chemically bonded water in the phenolic composite.[9] In the Cone, the 3A sample properly ignited before severe popping and delamination occurred. The difference in reaction of the 3A sample between the two different apparatuses is thought to be due to some in-depth absorption of the FPA lamp's wavelength into the specimen, as discussed before. Therefore, the 3A sample was tested in the Cone even though the minimum heat flux for proper ignition range would indicate that it could be successfully tested in the FPA.

System 4 showed an increase in minimum heat flux for proper ignition at each change in glass content (i.e. 4A, 4B and 4C all have different minimum heat flux for proper ignition ranges) while System 5 only demonstrated a change for the highest glass content. Sample 5C has a minimum heat flux for proper ignition that is higher than the maximum applied heat flux that the Cone can achieve.

Effect of Glass Content

Polyester

Figure 2 is a graph of the heat release rate traces from FPA tests done at 50kW/m^2 for the System 1 composites. The end of the trace is truncated based on visual observations of the loss of the fully developed flame cone although data was collected throughout the entire test. Recalling that the heat release

rate uncertainty for the FPA is 45kW/m^2, it can be seen that the top layer has a significantly higher heat release rate than the rest of the layers for 1A and 1B but 1C does not have a significant initial peak. Considering the difference in the initial peak with changing glass content, it can be seen that the magnitude of the initial peak is significantly different between 1A and 1B as well as between 1A and 1C but there is not a significant difference between the initial peaks of 1B and 1C. However, the graph shows a trend that as the glass content is increased, the magnitude of the initial peak decreases. These differences are believed to be related to the surface texture. The surface texture of 1A and 1B is smooth and 1A is highly glossy, which seems to indicate that there is a resin film on the surface. However, 1C has a very bumpy surface due to the weave from the glass layers, which may indicate that there is much less resin near the surface than for 1A or 1B and thus a less significant initial peak in the heat release rate trace.

Given the accuracy with which the heat release rate can be determined in the FPA, the difference in the plateau region of the curve is insignificant (see Figure 2) across all of the System 1 samples. Once the top layer of resin is burnt off, the glass layers block the heat transfer into and the mass transfer out of the specimen, slowing the decomposition of the resin. This effect appears to be present irregardless of the glass content for the range of glass contents studied.

From the test data, the time to ignition for samples 1A, 1B and 1C are 124s, 145s and 159s, respectively. Given that the uncertainty in the time to ignition is 9s, there is a significant increase in the time to ignition with glass content for all of the polyester composites. In Figure 2, the test is truncated at the loss of flame cone, which is approximately the same for all three glass contents if the time axis is normalized with the thickness of the specimen, as it appears in the graph. This result apparently indicates that the three different glass contents reach the same sort of condition at the loss of the flame cone but more work is needed to understand the results.

A comparison of surface and in-depth temperatures for the specimen can further demonstrate differences with glass content for the polyester composites, as shown in Figure 3 and Figure 4. Since the samples are different thicknesses, the time axis is normalized by the thickness of the sample. The normalization uses a nondimensional Fourier number, assuming that all of the samples have the same thermal diffusivity. The temperature axis is a temperature rise to eliminate any differences in initial temperature between the thermocouples. The temperatures at a depth of one-third from the surface as well

as the back face were also recorded but are not shown in the graph to reduce clutter; they follow a similar trend. From Figure 3, it can be seen that there is not a significant difference in the in-depth temperature with glass content for the polyester composites. Referring to Figure 4 for the surface temperatures, there is a significant difference with glass content for all of the polyester composites before ignition but all of the traces plateau within the uncertainty shortly after ignition. From the composites literature,[20] the thermal conductivity of the E-glass is an order of magnitude higher than that of the composite. The materials being studied are layered composites so if there is more glass closer to the surface, there will be a higher local thermal conductivity at the surface. The local thermal conductivity at the surface is thought to be higher for the higher glass content due to the surface texture (as discussed above), resulting in a lower surface temperature. As the test progresses and the resin is consumed, the temperatures for all of the different glass contents plateau to a similar surface temperature. In Figure 4, one of the 1A samples is with a pilot flame and the other is not. However, the test with no pilot flame autoignites and exhibits the same surface temperature behavior as the test with the pilot flame.

Phenolic

Figure 5 is a graph of the heat release rate traces from Cone tests done at 70kW/m^2 for the System 3 (neat phenolic) composites. The end of the trace is truncated based on visual observations of the loss of the fully developed flame cone. Recalling that the heat release rate uncertainty for the FPA is 45kW/m^2, it can be seen that there is no significant difference with glass content for the neat phenolic composites. One of the 3A tests, the neat phenolic with the low glass content, ignited and then went out before the sparker was removed. The sparker was left in and the sample reignited into a fully developed flame cone. Considering that the time to ignition for samples 3A and 3C are 50, 57 and 47, 43s, respectively, there is not a significant difference in time to ignition for the neat phenolic composites.

In-depth and back face temperatures for the phenolic composites are shown in Figure 6. There does not appear to be any significant difference with glass content for the phenolic composites. Surface temperature was recorded for the high glass content but not the low glass content and thus cannot be compared; see Figure 13 for typical traces for 3C.

Effect of Resin Type

The polyester and the neat phenolic with the highest glass contents were compared to one another in order to determine any differences with resin type. From Figure 7, it can be seen that there is not a significant difference in the value of the peak heat release rate between the two composites but there is a large difference in burn duration. Recalling that the data in the graph is truncated at loss of flame cone, it can be seen that the polyester composite exhibits significant burning for a much longer period than the phenolic composite. Both composites ignite around 30s but the polyester composite sustains a flame cone on the sample surface for 190s versus only 55s for the phenolic. By comparing the in-depth temperature histories of the two different resins, see Figure 8, it can be seen that the phenolic (3C) has a steeper linear trend than the average polyester (1C), which decreases with time. The difference in the trends is potentially related to the thermal stability of the resins: the polyester is less stable than the phenolic as shown in Figure 7.

Analysis

Parameter Estimation

The thermal diffusivity, thermal conductivity and specific heat can be estimated using an inert homogenous solid solution for the temperature profile with no absorption at depth. The assumption of no absorption at depth was investigated with PMMA in the FPA by comparing actual temperature profiles to the analytical solution for absorption at depth into an inert homogeneous solid, as solved for in the literature,[12] up to half the time to ignition. This cutoff point was used since the equation assumes that the material is inert. It was found from the analysis that 33% of the incident heat flux is absorbed 0.75mm into the sample while the remainder is absorbed at the surface. Since the uncertainty in the location measurements for the thermocouples is on the order of 1mm, it is assumed that this absorption depth is negligible since it is within the location uncertainty of the instrument being used to determine the temperature profile.

The absorption at depth for the composites could not be determined the same way as PMMA since there are too many unknown parameters in the equation (i.e. absorption coefficient and thermal properties). As discussed in previous sections, it is known from experimentation that the ignition time is slightly longer in the FPA than it is in the Cone for the same material and that applying carbon black to the sample surface in the FPA lowers the ignition time to that of the Cone. This indicates that there is some absorption at depth in the FPA but not in the Cone, since it matches the ignition time for the test with the carbon black. However, the temperature profiles observed in the same sample tested in the Cone and the FPA are the same, within the uncertainty, indicating that the absorption at depth in the FPA is insignificant.

Therefore, the thermal properties can be estimated using an inert homogenous solid solution for the temperature profile with no absorption at depth. The equation is available in the literature[21] and is repeated below.

$$T = T_0 + \frac{\dot{q}''_{absorbed}}{H}[erfc(\frac{x}{2\sqrt{\delta t}}) - \exp(\frac{Hx}{k} + \frac{\delta H^2 t}{k^2})erfc(\frac{x}{2\sqrt{\delta t}} + \sqrt{\frac{\delta H^2 t}{k^2}})]$$

In the equation, T is the temperature (K), T_0 is the initial temperature (K), $\dot{q}''_{aborbed}$ is the absorbed heat flux (W/m^2), H is the linearized heat transfer coefficient (W/m^2K), x is the depth from the surface (m), δ is the thermal diffusivity (m^2/s), t is time (s) and k is the thermal conductivity (W/mK). The absorbed heat flux is assumed to be equal to the applied heat flux.

The heat transfer coefficient is an important parameter in the equation but it is inherently difficult to calculate. From tests performed with the embedded heat flux gage, it was found that convection does not play a significant role in heating or cooling of the embedded gage in the period before formation of the condensate layer (i.e. before the radiometer reads a value of zero). It is interesting to note that there appeared to be convective heating in the FPA (possibly due to the forced air flow causing a stagnant area above the sample surface) and convective cooling in the Cone (which is natural convection). However, the difference was a maximum of $6kW/m^2$, which is the uncertainty of the heat flux gage.

Beaulieu[22] determined an average heat transfer coefficient, H, of $30W/m^2K$ considering a temperature range of 20-350°C in an apparatus similar to the FPA. The same temperature range is found for the tests performed in this study, up to the cutoff point of half the time to ignition. Since the convective portion of the heat flux is insignificant, it is assumed that the radiation emitted from the surface dominates

the heat loss. Therefore, it is assumed that the heat transfer coefficient from Beaulieu can be used to analyze both Cone and FPA test results. Beaulieu found that the deviation between the actual and predicted temperature profiles was 20°C using this value of H.

In order to estimate thermal properties, the actual temperature data was compared to the theoretical temperature derived from the analytical solution given above up to half the time to ignition. At half the time to ignition, there is no significant visual decomposition and the temperature rise at the back face is no more than 100°C (as measured by a back face thermocouple) for all of the composites considered in the parameter estimation exercise. Since the thermal diffusivity is the controlling parameter in the equation, it was changed until the global residual between the actual and the analytical temperature profiles was at a minimum. The thermal conductivity was then changed until the same condition was achieved and the values were reported. The residual was defined as the sum of the difference between the actual and predicted values at each time step for each of the temperature measurements; all of these sums were then summed to obtain an overall global residual. The value of the specific heat (c) is directly related to the thermal diffusivity (δ), thermal conductivity (k) and density (ρ) by $\delta=k/\rho c$. The value of the density was measured prior to the test while the thermal conductivity and thermal diffusivity were found from the procedure above, so the specific heat of the material was also found indirectly and is reported in the results. For the tests performed without the surface thermocouple, the surface temperature is not included in the optimization procedure. After the addition of the surface thermocouple late in the testing regime (see discussion in Instrumentation section above), additional tests were performed using the same method including the surface temperature measurement.

The initial values that were used for the PMMA and the composites were taken from the literature over the temperature range 300-475K. This temperature range was used since PMMA begins to decompose at 475K.[22] The literature values for PMMA[23] in the temperature range considered are shown in Table 3; they do not change significantly over the given temperature range. Since only the thermal conductivity, specific heat and density were given in the literature,[23] the diffusivity was found by the equation used above to determine specific heat from the optimized thermal parameters (i.e. $\delta=k/\rho c$).

The initial values for the composites were taken from an average of the values reported in the literature for the thermal conductivity and specific heat of similar virgin composites,[8-10] assuming that a

vinylester resin is essentially equivalent to a polyester resin. The initial values used for the polyester and the phenolic composites are listed in Table 4. From the literature, the thermal conductivity does not change more than 0.02W/mK in the temperature range 300-475K and the specific heat in this temperature range was 1081-1098J/kgK[20] and 1221-1361J/kgK.[9] The thermal conductivity of E-glass, which is similar to the glass used in the current study, alone was found to have a much higher value than the composite and was equal to 1.09W/mK.[20] The value of the global residual was mapped versus the thermal diffusivity and then the thermal conductivity by a range of plus and minus one order of magnitude, which covers a wide range of materials,[24] in order to ensure that the residual was a global minimum.

Figure 9 shows a comparison of the temperature profiles for the 1C composite at applied heat fluxes of 50kW/m^2 and 70kW/m^2. The temperature axis is nondimensionalized using the analytical solution detailed above so that the effect of heat flux on the temperature profile is removed. The graph shows that there is not a significant difference in the heating rate of the composite with applied heat flux, which indicates that the assumption of constant properties is valid under the given conditions.

The method was attempted first on the PMMA tests to determine how well the parameters could be estimated using the method described above; the results are shown in Table 3. Although the method is a bit crude, the results are decent when compared to the published literature values for PMMA.

Since the method was determined to produce proper values for PMMA, it was then used on the composite materials to estimate the thermal properties to further determine differences with glass content and resin type. The results are shown in Table 4. The results in the table are average optimal thermal parameters from multiple tests and the surface temperature is not included. A typical graph of the actual temperature curves versus the average predicted temperature profile with optimized values of thermal diffusivity and thermal conductivity is shown in Figure 10 for the polyester composite. From the graph, it can be seen that the model uncertainty is larger than the 20°C found from Beaulieu[22] which is to be expected since the uncertainty of the thermocouples alone is 27°C. Figure 11 shows the predicted temperatures from average optimized properties for the neat phenolic with the high glass content (3C). From the figures, it can be seen that the average values provide a good representation of the temperatures from the two different tests even though the uncertainty is higher than that reported by Beaulieu.[22] From Table 4, it can be seen that there is no significant difference with resin type or glass content with regards to

the estimated thermal properties. Since the temperature profile in the composites was found to be similar with resin type and glass content (see Figure 3, Figure 6 and Figure 8), the similarity in the estimated thermal properties is expected.

Tests were performed with surface thermocouples and the surface temperature was then included in the optimization procedure; the results are shown in Table 5. From the table, there is not a significant difference in the effective thermal properties with glass content. However, there may be a significant difference (evaluated using the standard deviation from Table 4) with resin type. This result is consistent with the findings of a difference in surface temperature with resin type (compare Figure 12 and Figure 13) and only a slight difference with glass content (see Figure 4); more testing is needed with the surface thermocouple to verify these results. Graphs of actual versus average predicted values for the polyester and phenolic composites are shown in Figure 12 and Figure 13, respectively. From the graphs, it can be seen that the theory matches the surface temperature and the 1/3 depth thermocouple to within the uncertainty from Beaulieu,[22] indicating that the surface thermocouple is providing reasonable and consistent results. The 2/3 depth thermocouple is under-predicted for the polyester composite, which may be due to the temperature at the back face (less than 100°C as discussed above) and the resultant thermal wave affecting the results for the deeper thermocouple.

Conclusions and Future Work

The results of this study are important to the composites industry because it is the beginning of systematic research into how the resin type and the glass content affect the overall fire performance of composites. The resin type was found to affect the resultant fire performance, however the effect of glass content is a little more subtle. For example, there is a difference in the peak heat release rate (see Figure 2) with glass content for the System 1 composites but there is no significant difference in the average heat release rate in the plateau region of the trace. There is an increase in the time to ignition and a decrease in the burning time with glass content for the System 1 composites (see Figure 2). The minimum heat flux for proper ignition greatly changed with resin type with the polyester resin (System 1) having a significantly lower minimum heat flux for proper ignition range than the phenolic resins and the phenolics with additives

(Systems 4 and 5) improving over the performance of the neat phenolic (System 3). Except for System 1, the minimum heat flux for proper ignition increased with glass content (see Table 1).

The in-depth temperatures were slightly steeper for the phenolic resin than the polyester resin but were only slightly outside of the uncertainty. The surface temperature significantly decreased with glass content for the polyester composites. Therefore, there is only a slight change with resin type and glass content for the thermal profile. Since the temperature profile and the plateau region of the heat release rate trace were not affected by the glass content, it is thought that the glass is controlling the thermal properties of the composite. The glass has a much higher thermal conductivity than the composite, which could cause it to become the dominant component in the material. Also, it can be seen from Figure 9 that the heating rate is constant with applied heat flux. Since the properties of the glass are constant with temperature,[23] the figure provides additional support to the argument that the glass is the controlling component in the composites. From the parameter estimation exercise, it was found that the thermal properties may change significantly with resin type but are invariant with regards to glass content; further testing with the surface thermocouple is needed to verify this result. These results seem to indicate that the resin type should be chosen carefully when manufacturing fire safe composites but a wide range of glass contents is suitable.

This work is also very important to the fire industry because it provides data specifically useful for calibration of fire models, including surface temperature, in-depth temperatures and radiative and convective portions of the heat flux prior to ignition. Tests were also completed with extended periods of a non-flaming condition, which is useful for pyrolysis models because there is no added complexity due to the flame. Currently, the heat flux data is only applicable up to the formation of the resin condensate on the gage face (i.e. when the radiometer reads zero) even though the gage is left in the sample and provides a reading for the entire test. It would be beneficial to determine if the reading from the total heat flux gage could be used after the formation of this condensate. More tests with the surface thermocouple would also be very beneficial.

Acknowledgements

The continued significant support for this project from FM Global Research (FM Global Fellow Avila and FM Global Scholar Dembsey) is greatly appreciated. The technical support of Patricia Beaulieu, Steve Ogden, Dana Capron and Lawney Crudup at FM Global throughout this project was very helpful. Discussions with Chris Lautenberger at the University of California, Berkeley regarding data useful for pyrolysis modelling was instrumental in creating the testing matrix. The authors greatly appreciate the materials donated by: Trevor Humphries of VectorPly, Phoenix City, AL (glass); and Chad Fester of Airtech International Inc. of Huntington Beach, CA (vacuum bagging and peal ply) as well as Cinnabar, FL (lamination of the FRP composite panels). Information regarding the heat of combustion and other properties of the composites used in this study by Mike Stevens from Ashland was very useful. Many thanks also to Randall Harris, Mihyun (Esther) Kim and Jacqueline Shea at WPI for performing the Cone tests and to Esther Kim for performing the last round of FPA tests.

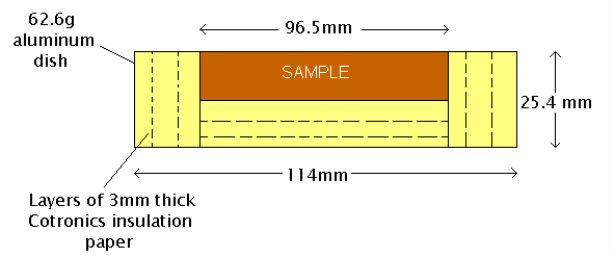

Figure 1: Insulated Sample Holder Designed by de Ris and Khan[15]

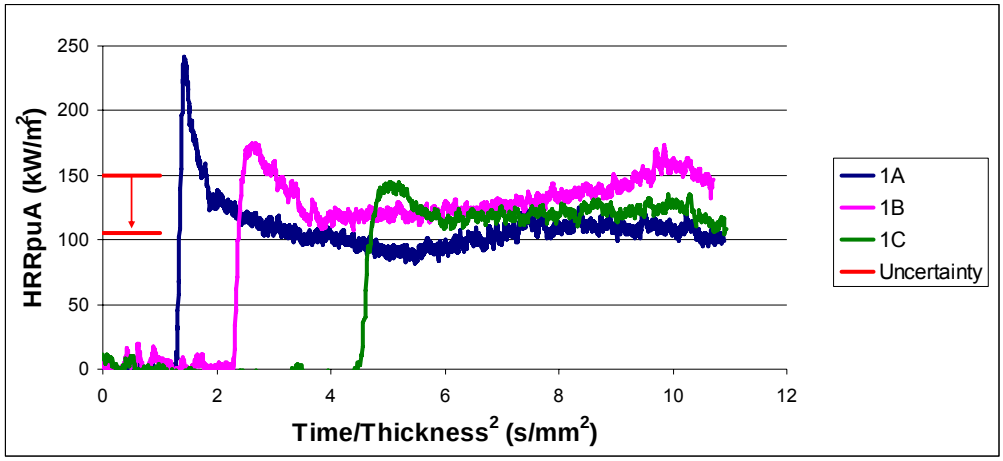

Figure 2: Comparison of the Generic CO_2 Based Heat Release Rate per Unit Area (HRRpuA) for System 1 (Polyester) Composites at Three Different Glass Contents. All tests were performed in the FPA[1] at an applied heat flux of 50kW/m^2, truncated at loss of flame cone. Time zero is start of exposure. The thicknesses of the samples are (in mm): 1A 10, 1B 8 and 1C 6.

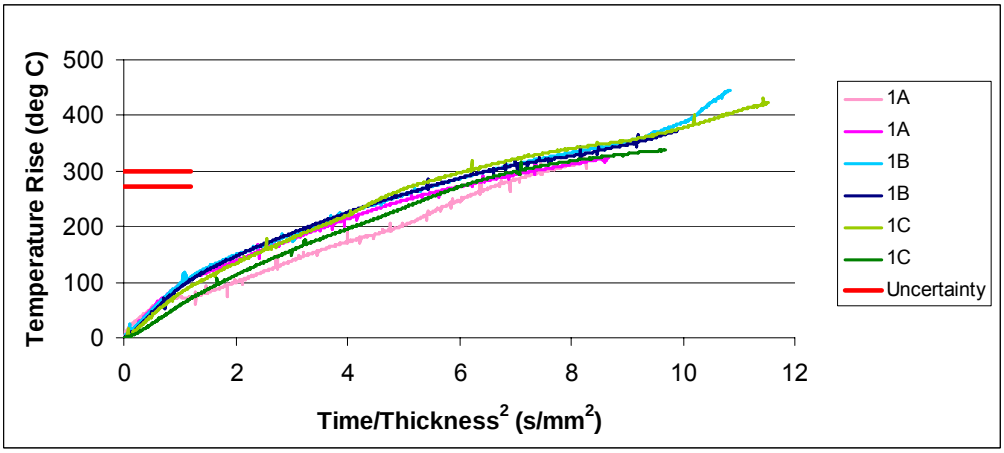

Figure 3: Comparison of 2/3 In-Depth Temperatures for the System 1 (Polyester) Composites at Three Different Glass Contents. All tests were performed in the FPA[1] at an applied heat flux of 50kW/m^2, truncated at loss of flame cone. Time zero is start of exposure. The thicknesses of the samples are (in mm): 1A 10, 1B 8 and 1C 6.

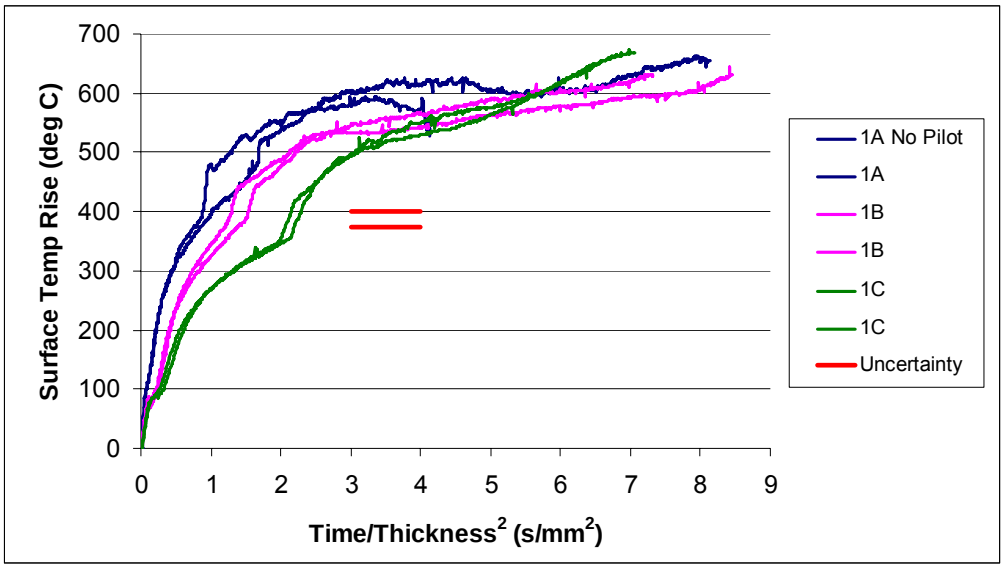

Figure 4: Comparison of Surface Temperatures for the System 1 (Polyester) Composites at Three Different Glass Contents. All tests were performed in the FPA[1] at an applied heat flux of 50kW/m^2, truncated at loss of flame cone. Time zero is start of exposure. The thicknesses of the samples are (in mm): 1A 10, 1B 8 and 1C 6. Ignition occurs when there is a discontinuous jump in the surface temperature.

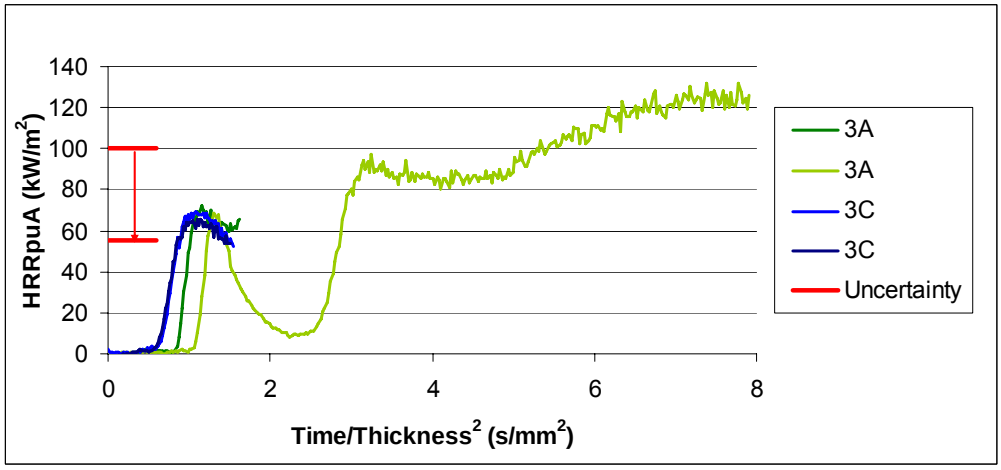

Figure 5: Comparison of the Generic O_2 Based Heat Release Rate per Unit Area (HRRpuA) for System 3 (Neat Phenolic) Composites at Two Different Glass Contents. All tests were performed in the Cone[2] at an applied heat flux of 70kW/m^2, truncated at loss of flame cone. Time zero is start of exposure. The thicknesses of the samples are (in mm): 3A 6.5 and 3C 7.5.

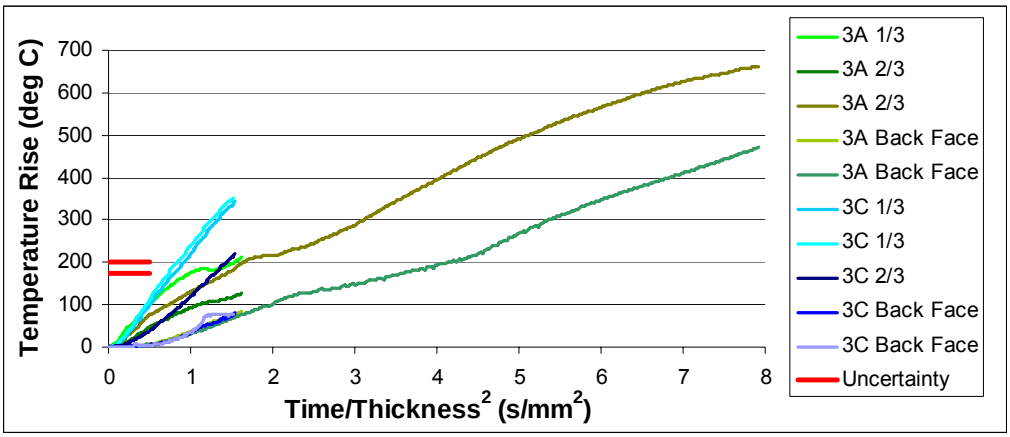

Figure 6: Comparison of In-Depth Temperatures for the System 3 (Neat Phenolic) Composites at Two Different Glass Contents. All tests were performed in the Cone^2 at an applied heat flux of 70kW/m^2, truncated at loss of flame cone. Time zero is start of exposure. The thicknesses of the samples are (in mm): 3A 6.5 and 3C 7.5. The 1/3 thermocouple for 3A may provide erroneous data after significant popping began at a normalized time of 0.92s/mm^2.

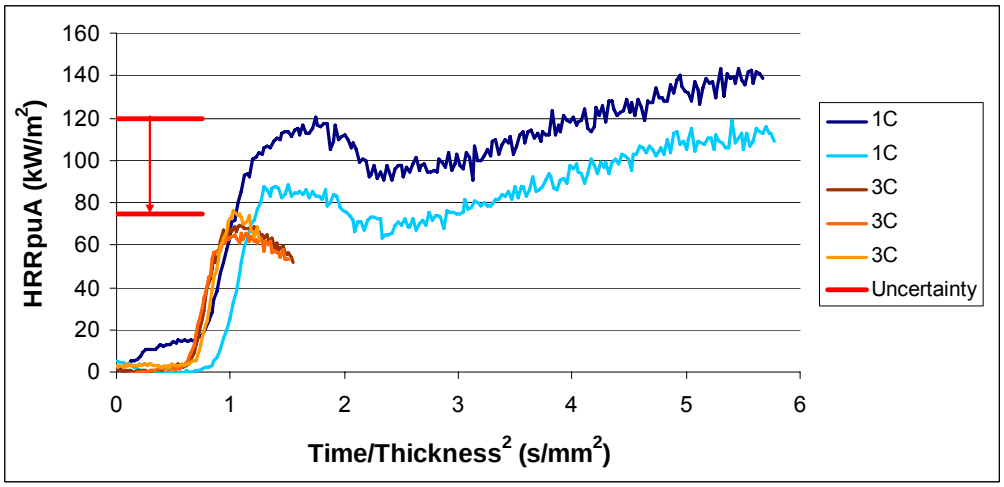

Figure 7: Comparison of the Generic O_2 Based Heat Release Rate per Unit Area (HRRpuA) for 1C and 3C Composites. All tests were performed in the Cone^2 at an applied heat flux of 70kW/m^2, truncated at loss of flame cone. Time zero is start of exposure. The thicknesses of the samples are (in mm): 1C 6.2 and 3C 7.5.

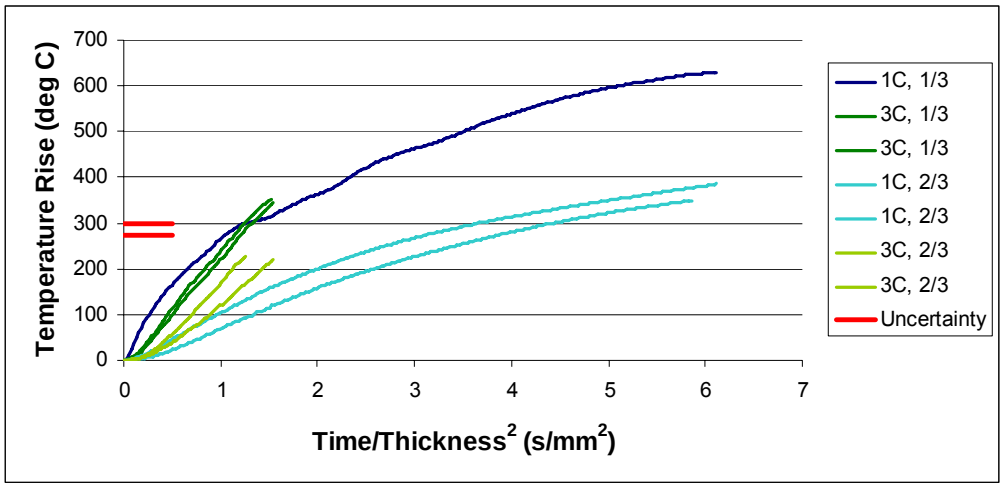

Figure 8: Comparison of In-Depth Temperatures for 1C and 3C Composites. All tests were performed in the Cone^2 at an Applied Heat Flux of 70kW/m^2, truncated at loss of flame cone. Time zero is start of exposure. The thicknesses of the samples are (in mm): 1C 6.2 and 3C 7.5.

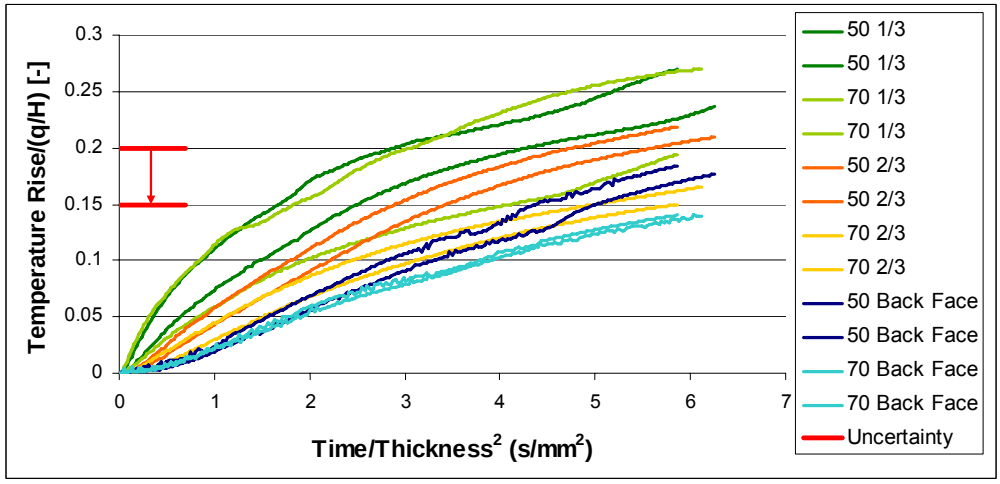

Figure 9: Comparison of Temperature Profiles for 1C at 50kW/m^2 and 70kW/m^2 in the Cone. The temperature axis is non-dimensionalized and the time axis is normalized.

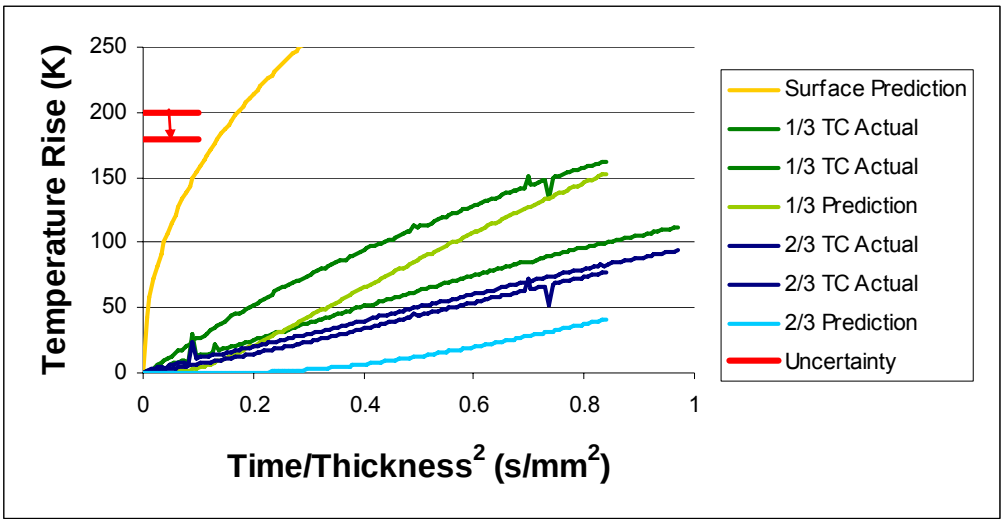

Figure 10: Comparison of Actual and Predicted Temperatures Using Average Estimated Values for 1B (Polyester). The tests were performed in the FPA[1] at an applied heat flux of 50kW/m^2, truncated at half the time to visual ignition. The 20°C uncertainty is from Beaulieu.[22]

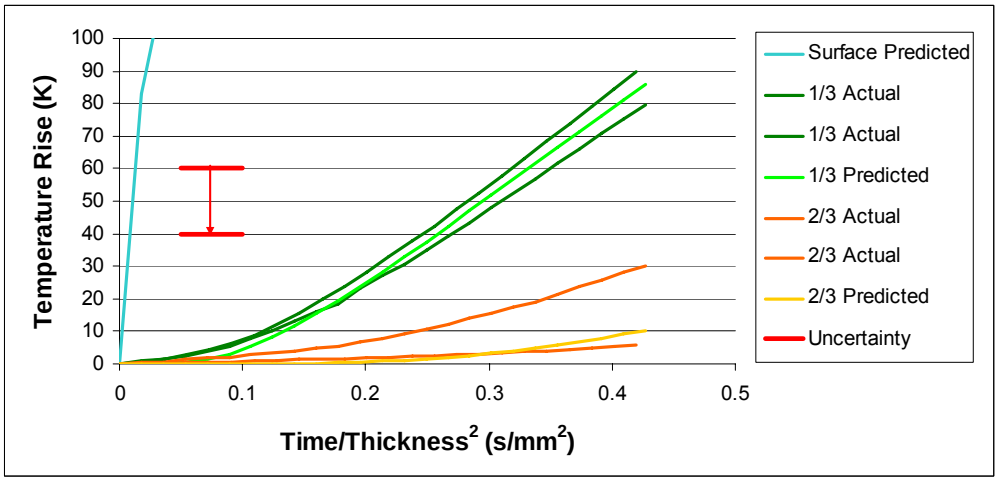

Figure 11: Comparison of Actual and Predicted Temperatures Using Average Estimated Values for 3C (Neat Phenolic). The test was performed in the Cone[2] at an applied heat flux of 70kW/m^2, truncated at half the time to visual ignition. The 20°C uncertainty is from Beaulieu.[22]

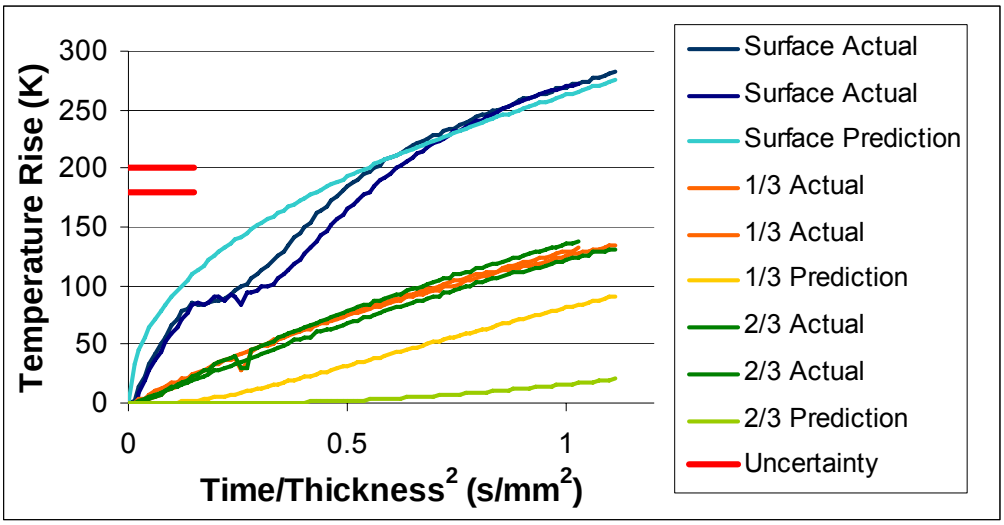

Figure 12: Comparison of Actual and Predicted Temperatures Using Average Estimated Values for 1C (Polyester), including surface thermocouple data. The tests were performed in the FPA[1] at an applied heat flux of 50kW/m^2, truncated at half the time to visual ignition. The 20K uncertainty is from Beaulieu.[22]

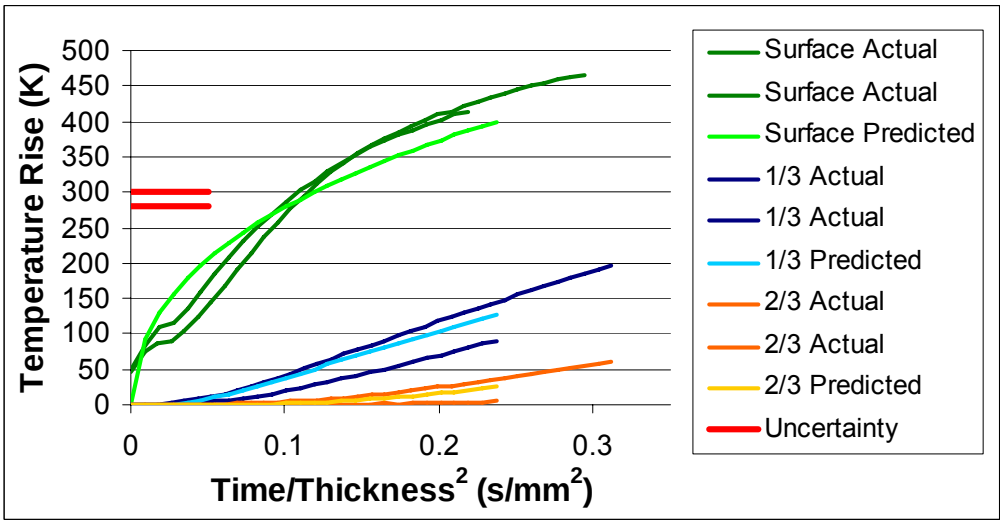

Figure 13: Comparison of Actual and Predicted Temperatures Using Average Estimated Values for 3C (Phenolic), including surface thermocouple data. The tests were performed in the Cone[2] at an applied heat flux of 70kW/m^2, truncated at half the time to visual ignition. The 20°C uncertainty is from Beaulieu.[22]

Table 1: Description of the FRP Composites and the Minimum Heat Flux for Proper Ignition Range for each Composite System. The Sample Thickness and the Minimum Heat Flux for Proper Ignition (determined in the FPA[1] for System 1 and in the Cone[2] for all others) are listed as ranges. %RFG =%Refined Glass Content.

FRP Sample	Resin System	Glass (%RFG)	Thickness (mm)	Min HF (kW/m^2)
1A	Brominated Polyester	33	8.5-10	25-30
1B	Brominated Polyester	46.5	8.0-9.0	20-25
1C	Brominated Polyester	73.3	6	20-25
3A	Neat Resole Phenolic	38	6-9.5	40-50
3C	Neat Resole Phenolic	79.1	7-8	60-65
4A	Resole Phenolic w/ Charring Additive	30	7-8	50-60
4B	Resole Phenolic w/ Charring Additive	38	7.5-8	70-80
4C	Resole Phenolic w/ Charring Additive	48	8.5-10.5	90-100
5A	Resole Phenolic w/ Intumescent Additive	30	6	90-100
5B	Resole Phenolic w/ Intumescent Additive	45	8-9	90-100
5C	Resole Phenolic w/ Intumescent Additive	59	8-9	>100

Table 2: Table of Critical Mass Flux at Proper Ignition. 5A and 5B are based on only one test.

Sample	Average (g/sm^2)	Standard Deviation (g/sm^2)
PMMA	9	6.5
1A	13	2.9
1B	10	4.1
1C	8	1.5
3A	8	2.6
3C	7	5.3
4A	11	4.5
4C	10	5.2
5A	7	NA
5B	5	NA

Table 3: Parameter Estimation Values for PMMA, not including surface temperature data. The actual literature values are shown in the last row.[23]

Heat Flux (kW/m^2)	Diffusivity (m^2/s)	Conductivity (W/mK)	Specific Heat (J/kgK)
15	1.7E-07	0.24	1300
15	1.3E-07	0.22	1600
28	2.5E-07	0.22	840
60	1.4E-07	0.22	1500
Average	1.7E-07	0.23	1300
Standard Deviation	5.1E-08	0.01	350
Difference From Actual	6.2E-08	0.00	440
Literature Values	1.1E-07	0.22	1700

Table 4: Parameter Estimation Values for the Composite Materials, not including surface temperature data. The values shown are average values from multiple tests. The literature values are shown in the last two rows.[8-10] k=thermal conductivity, c=specific heat and δ=thermal diffusivity.

Sample	δ Avg (m^2/s)	δ Std Dev (m^2/s)	k Avg (W/mK)	k Std Dev (W/mK)	c Avg (J/kgK)	c Std Dev (J/kgK)
1A	1.8E-07	7.0E-08	0.33	0.01	1400	440
1B	1.4E-07	4.2E-08	0.35	0.01	1600	550
1C	1.4E-07	1.0E-08	0.34	0.02	1400	34
3A	2.1E-07	7.0E-08	0.30	0.01	970	320
3C	9.1E-08	1.7E-08	0.28	0.00	2300	400
Lit. Polyester	1.8E-07	NA	0.32	No Uncertainty Given	1155	No Uncertainty Given
Lit. Phenolic	1.5E-07	NA	0.28	No Uncertainty Given	1334	No Uncertainty Given

Table 5: Parameter Estimation Values for the Composite Materials, including the surface thermocouple data. k=thermal conductivity, c=specific heat and δ=thermal diffusivity.

Sample	δ (m^2/s)	k (W/mK)	c (J/kgK)	ρ (kg/m^3)
1A	1.0E-07	0.32	1900	1600
1B	6.1E-08	0.33	3500	1600
1B	5.4E-08	0.32	3800	1600
1C	7.5E-08	0.32	2300	1900
1C	7.6E-08	0.33	2300	1900
3C	3.0E-07	0.23	550	1400
3C	4.4E-07	0.27	450	1400

References

[1] Standard Methods of Test for Measurement of Synthetic Polymer Material Flammability Using a Fire Propagation Apparatus (FPA), ASTM E 2058-03, ASTM, 100 Barr Harbor Drive, West Conshohocken, PA, U.S.

[2] Standard Test Method for Heat and Visible Smoke Release Rates for Materials and Products Using an Oxygen Consumption Calorimeter, ASTM E 1354-02, ASTM, 100 Barr Harbor Drive, West Conshohocken, PA, U.S.

[3] Bill, R.G. and Croce, P.A., "The International FORUM of Fire Research Directors: A position paper on small-scale measurements for next generation standards," *Fire Safety Journal*, 2006; 41: 536-538.

[4] McGrattan, K.B. and Forney, G.P. "Fire Dynamics Simulator (Version 4), User's Guide," NIST Special Publication 1019, National Institute of Standards and Technology, Gaithersburg, Maryland, July 2004.

[5] Olenick, S.M. and Carpenter, D.J., "An updated international survey of computer models for fire and smoke." Journal of Fire Protection Engineering 2003; 13:87-110.

[6] Cox, G. and Kumar, S., "Chapter 3-8: Modeling Enclosure Fires Using CFD." The SFPE Handbook of Fire Protection Engineering. Ed. Philip J. DiNenno. National Fire Protection Association, Quincy, MA, 2000.

[7] Lautenberger, C. and Fernandez-Pello, C., "Pyrolysis modeling, thermal decomposition, and transport processes in combustible solids," Transport Phenomena in Fires. Ed. M. Faghri and B. Sunder, WIT Press, 2007.

[8] Ramroth, W.T., Krysl, P., Asaro, R.J. "Sensitivity and uncertainty analyses for FE thermal model of FRP panel exposed to fire." Composites A 2006; 37:1082-1091.

[9] Davies, J.M., Wang, Y.C., Wong, P.M.H. "Polymer Composites in Fire." Composites A 2006; 37:1131-1141.

[10] Lattimer, B.Y., Oullette, J. "Properties of composite materials for thermal analysis involving fires." Composites A 2006; 37:1068-1081.

[11] Ramroth, W.T., Asaro, R.J. and Krysl, P., "Finite element modeling of fire degraded FRP composite panels using a rate dependent constitutive model," Composites A 2006; 37:1015-1023.

[12] Lautenberger, C and Fernandez-Pello, C., "A Generalized Pyrolysis Model for Simulating Charring, Intumescent, Smoldering, and Noncharring Gasification," 2006, University of California eScholarship Repository, <http://repositories.cdlib.org/cpl/fs/LautenbergerGenPyro>.

[13] Standard Test Method for Surface Burning Characteristics of Building Materials, ASTM E 84-05, ASTM, 100 Barr Harbor Drive, West Conshohocken, PA, U.S.

[14] User's Guide for the Fire Propagation Apparatus (FPA) ASTM E-2058, Fire Testing Technology Limited, PO Box 116, East Grinstead, West Sussex, England.

[15] de Ris, J.L. and Khan, M.M., "A sample holder for determining material properties," *Fire and Materials*, 24, 219-226 (2000).

[16] Omega, Inc. "IR Thermometers and Pyrometers" 02 February 2007 <http://www.omega.com/literature/transactions/volume1/thermometers1.html>.

[17] Blair, B. "Atmospheric Transmission." John Hopkins University, Department of Physics and Astronomy. 02 February 2007 <http://fuse.pha.jhu.edu/~wpb/spectroscopy/atm_trans.html>.

[18] Clausing, L.T. "What you really need to know to begin using infrared cameras." The American Society for NonDestructive Testing, May 2006. 02 February 2007 <http://www.asnt.org/publications/materialseval/solution/may06solution/may06sol.htm>.

[19] Nelson, M., "Combustion of Polymers: The critical mass flux concept", 2004, University of Wollongong, Australia <http://www.uow.edu.au/~mnelson/review.dir/cmf.html>.

[20] Lua, J., O'Brien, J., Key, C.T., Wu, Y., Lattimer, B.Y. "A temperature and mass dependenent thermal model for fire response prediction of marine composites." Composites A 2006; 37:1024-1039.

[21] Carslaw, H.S. and Jaeger, J.C. "Chapter 2-8 Semi-Infinite Solid." Conduction in Solids 2nd Edition. Oxford University Press, Oxford, 1959.

[22] Beaulieu, P.A. "Flammability Characteristics at Heat Flux Levels Up to 200kW/m^2 and The Effect of Oxygen on Flame Heat Flux" PhD Dissertation, Worcester Polytechnic Institute, 2005.

[23] Polymers: A Property Database (Online CD), CRC Press, 2000.

[24] "Appendix B: Thermophysical Property Data." The SFPE Handbook of Fire Protection Engineering. Ed. Philip J. DiNenno. National Fire Protection Association, Quincy, MA, 2000.

Chapter 3: Conclusions and Future Work

The work being done in this study is important to the composites industry because it is a beginning of systematic research into how the resin type and the glass content affect the overall fire performance of the composites. The resin type was found to affect the resultant fire performance, however the effect of glass content is a little more subtle. For example, there is a difference in the peak heat release rate (see Figure 2) with glass content for the System 1 composites but there is no significant difference in the average heat release rate in the plateau region of the trace. There is an increase in the time to ignition and a decrease in the burning time with glass content for the System 1 composites (see Figure 2). The minimum heat flux for proper ignition greatly changed with resin type with the polyester resin (System 1) having a significantly lower minimum heat flux for proper ignition range than the phenolic resins and the phenolics with additives (Systems 4 and 5) improving over the performance of the neat phenolic (System 3). Except for System 1, the minimum heat flux for proper ignition range increased with glass content (see Table 2).

The in-depth temperatures were slightly steeper for the phenolic resin than the polyester resin but were only slightly outside of the uncertainty. The surface temperature significantly decreased with glass content for the polyester composites. Therefore, there is only a slight change with resin type and glass content for the thermal profile. Since the temperature profile and the plateau region of the heat release rate trace were not affected by the glass content, it is thought that the glass is controlling the thermal properties of the composite. The glass has a much higher thermal conductivity than the composite, which could cause it to become the dominant component in the material. Also, it can be seen from Figure 9 that the heating rate is constant. Since the properties of the glass are constant with temperature,[23] the figure provides additional support to the argument that the glass is the controlling component in the composites. From the parameter estimation exercise, it was found that the thermal properties may change significantly with resin type but are invariant with regards to glass content; further testing with the surface thermocouple is needed to verify this result. These results seem to indicate that the resin type should be chosen carefully when manufacturing fire safe composites but a wide range of glass contents is suitable.

This work is also very important to the fire industry because it provides data specifically useful for calibration of fire models, including surface temperature, in-depth temperatures and radiative and

convective portions of the heat flux prior to ignition. Tests were also completed with extended periods of a non-flaming condition, which is useful for pyrolysis models because there is no added complexity due to the flame. Another aspect of the work that is very important to the fire industry are the results from the b parameter as well as comparisons between the Cone and the FPA. The industry is learning toward performance based design in modern building codes, which requires determining whether a room will flashover or not. From the results of the b parameter, it is expected that the FRPs with the polyester resin (System 1) would flashover in a room/corner test while the phenolics (Systems 3, 4 and 5) are not expected to flashover based on tests done at 50kW/m^2. Based on the large uncertainty in the b parameter and to verify the results of this study, it would be very interesting to perform large scale room/corner tests with the specimens. The comparison between the FPA and the Cone is significant since the FPA is a relatively new apparatus and much work has already been completed on the Cone Calorimeter.

Future work to be done includes additional work with the embedded heat flux gage and the surface thermocouple. Currently, the heat flux data is only applicable up to the formation of the resin condensate on the gage face (i.e. when the radiometer reads zero) even though the gage is left in the sample and provides a reading for the entire test. It would be beneficial to determine if the reading from the total heat flux gage could be used after the formation of this condensate. The surface thermocouple has been found to provide excellent results and should be used for all future tests to provide additional insight for modelling purposes.

Appendix A: Operator Independent Ignition

Introduction

The 1st and 2nd derivatives of the mass history from the WPI FPA need to be used to obtain useful data such as mass loss rate[1] and the operator independent ignition time.[2] However, the mass loss data from the Fire Propagation Apparatus (FPA, ASTM E 2058[3]) has a fair amount of white noise; this noise is further amplified when the 1st and 2nd derivative of the data are found. In order to determine meaningful data from the mass history and its derivatives, the data must be smoothed to reduce the amount of noise in the signal. A number of different smoothing techniques are compared, including Savitzky-Golay (the smoothing technique used in the operator independent ignition paper[2]), Fast Fourier Transform and a simple 10 point smooth. The Fast Fourier Transform was found to provide the best smoothing for the FPA mass loss rate.

Savitzky-Golay (SG)

The general premise of the SG method of smoothing data is to fit a polynomial of a certain degree and of a certain number of points to the original data; it is essentially a sophisticated moving average filter. A table of coefficients for each combination of degree and number of points is available[4] while corrections were made to the tables at later dates.[5,6] These coefficients are then applied to the following equation[7]:

$$x_{i,new} = \sum_{j=-p}^{p} c_j x_{i+j}$$

Different coefficients are also available for the 1st and 2nd derivatives of the data. These can be applied directly to the data using the equation above instead of using an independent method of obtaining the derivative (e.g. the ASTM E 1354 equation for mass loss rate).

There is a tradeoff between the elimination of noise and the flattening of the signal itself when determining the number of points that should be used for a specific scenario. In the literature, there is some discrepancy regarding the degree of the polynomial and the number of points that are best suited to the case of a mass history. De Ris and Khan[2] suggest that a 25 point, 4th degree SG smoothing should be used for the 2nd derivative and that 19 points of the same degree should be used for the 1st derivative. Staggs[8] determined that a SG smooth with 11 points and a degree of 2 worked the best for smoothing the mass history from the cone calorimeter. A number of different combinations will be considered for this study to determine the one best suited for use in smoothing the FPA mass history and its derivatives.

Fast Fourier Transform (FFT)

The FFT is a general name for a class of efficient algorithms to compute the discrete Fourier transform (DFT). The DFT is defined as[9]:

$$H_n = \sum_{k=0}^{N-1} W^{nk} h_k$$

where W is defined as $W = e^{\frac{2\pi \cdot i}{N}}$. For large data sets, like those that are going to be encountered in the use of the FPA, the DFT is extremely inefficient because it requires N^2 operations.

A number of FFT algorithms have been developed over the years to reduce the computation time to the order of $N\log_2 N$ operations. The most widely used FFT is the Danielson-Lanczos Lemma. The idea behind this FFT algorithm is to split the original DFT into even and odd parts[9]:

$$F_k = \sum_{j=0}^{N-1} e^{\frac{2\pi \cdot i \cdot j \cdot k}{N}} f_j$$

$$F_k = \sum_{j=0}^{\frac{N}{2}-1} e^{\frac{2\pi \cdot i \cdot k \cdot (2j)}{N}} f_{2j} + \sum_{j=0}^{\frac{N}{2}-1} e^{\frac{2\pi \cdot i \cdot k \cdot (2j+1)}{N}} f_{2j+1}$$

This division can be performed until F_k is simply the addition of N one point DFTs. A single point DFT is an identity operation that copies the information in the input array element to the appropriate output array element. In order to obtain the one point DFTs, the original input array must be an integer power of two. If it is not a power of two, data should be deleted or zeros should be added at the end of the data set to make the number of data points an even power of two. In the end, each one point transform will have come through a series of even and odd arrays[9]:

$$F_k^{eoeeoeo\ldots oee} = f_n$$

In order to build up the one point DFTs into 2 point DFTs to 4 point DFTs, etc, up to the N point DFT, the correct placement of the one point DFT result in the output array is essential. In fact, the binary of the correct output element is the bit reverse number of the order of the e's and o's in the statement above where o=1 and e=0.

The algorithm that was used is specifically outlined for MS Excel.[10] It follows the Danielson-Lanczos Lemma and is ready to be inserted into Visual Basic and applied directly as a macro in Excel. The macros, one for the forward transform (ForwardFT) and the inverse transform (InverseFT), are shown after the text in this appendix, along with their submacros. ForwardFT and InverseFT are driver macros that simply set a variable to 1 or -1, depending on which one is called and then passes this value to the Fourier macro. The Fourier macro simply does some checks (e.g. makes sure the data is an integer power of two, makes sure there are 3 columns in the input array, etc.) and then calls the macro FT. FT is the macro which actually calculates the Fourier transform. It first rearranges the data into bit reversed order and then it calculates the successive groups of transforms (e.g. groups of 2 point DFTs, then 4 point DFTs and so on)

until it reaches the N point DFT. This result is then rearranged into the correct format by the Fourier macro and output into Excel.[10]

The macro itself does not smooth; the forward and inverse macros are inverse operations. The forward transform is performed on the data to obtain the real and imaginary parts of the transform versus frequency. The magnitude of the signal and noise combination at each frequency can be found by taking the square root of the sum of the squares of the real and imaginary parts of the transform. The magnitude is plotted versus frequency and the plot is examined; the frequency at which the magnitude drastically changes is assumed to be when the noise takes over the signal. The real and imaginary parts of the frequencies above the selected frequency are zeroed and the inverse transform is performed on the partially zeroed data. This then produces a graph in which the frequencies which have been assumed to be predominantly noise have been eliminated, resulting in a much smoother signal.[10,11,12]

1st Derivative of Mass History

The first derivative is always reviewed after a fire test because it represents the rate at which mass is lost. Therefore, it is important that it be smooth enough so that useful conclusions may be derived from the graph. Besides the actual mass loss rate, another feature of the first derivative curve is the frequency at which the sample "puffs". This is represented by periodic peaks and valleys in the steady state portion of the MLR curve. This will be different than the puffing frequency of the fire because the MLR will be representing the reaction of the sample to the puffing frequency of the fire, which will be damped. Beaulieu[13] found that the frequency is approximately 0.03-0.05Hz.

The puffing frequency (flame flicker) will be calculated for reference purposes from an equation in the literature.[14] Note that this equation is for a natural fire, while the fire in the FPA is not:

$$f = (0.5 \pm 0.04)(g / D)^{\frac{1}{2}} Hz$$

$$f = (0.5 \pm 0.04)(\frac{9.81 m/s^2}{0.0958 m})^{\frac{1}{2}} Hz$$

$$f = 4.6 Hz -> 5.5 Hz$$

This is much higher than the frequencies observed in the MLR from the FPA.

A black PMMA sample which was 3.77" in diameter and 0.63" thick and weighing 135.1g was placed in an insulated sample holder that was explained by De Ris and Khan.[2] The sample was tested in the FPA and the mass history, among other channels, was recorded. In order to make all of the results comparable, the original mass history was taken and the MLR equation from ASTM E 1354[1] was used to calculate the derivatives, unless otherwise noted. No smoothing was performed before the calculation of the derivatives. The smoothing in the load cell controller was turned off.

The original 1st derivative with no smoothing or averaging is shown in Figure 14.

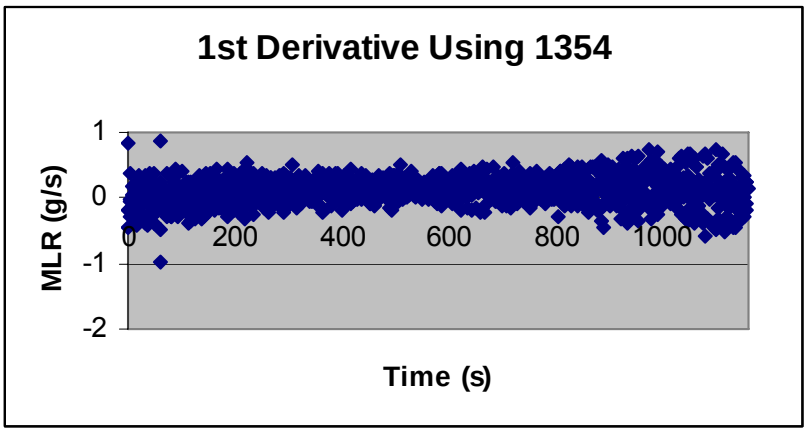

Figure 14: The 1st Derivative Curve (Mass Loss Rate) from a Test done in the FPA with a PMMA sample. No smoothing or averaging on the data.

As can be seen, the graph is much too noisy to determine a trend. The various smoothing techniques that were explored are discussed in the sections below. The beginning and end of the test are fairly noisy due to the shutter down noise. In all cases, the last minute was removed from the data and, in the case of the 2nd derivative, the first and last minute was taken off of the data to get rid of the shutter down noise; most of the data removed was baseline data.

Savitzky-Golay

After the first derivative was taken using the MLR equation in ASTM E 1354, the data was smoothed using SG. The suggestion given for the first derivative by de Ris and Khan was to use a 19 point 4th order SG smooth.[2] The result is shown in Figure 15.

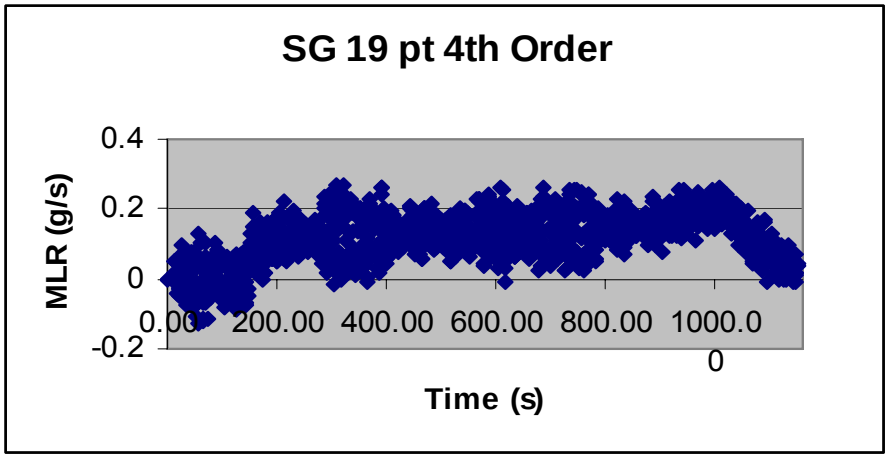

Figure 15: The 1st Derivative Curve (Mass Loss Rate) from a Test done in the FPA with a PMMA sample. The data was smoothed with a SG 19 point 4th Order Smoothing Algorithm.

Although the periodic frequency during steady state is difficult to discern due to data scatter, the peaks and valleys appear to have a period of 12s (0.0833Hz). However, the data is still very noisy.

The other suggestion for the first derivative, made by Staggs,[8] was to use an 11 point 2nd order SG smooth. The result is shown in Figure 16.

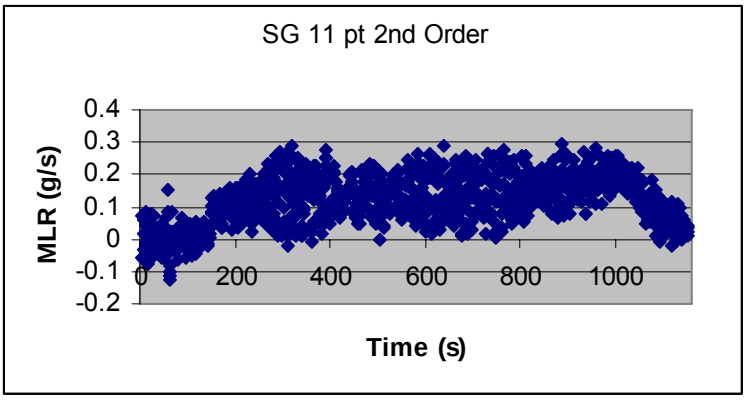

Figure 16: The 1st Derivative Curve (Mass Loss Rate) from a Test done in the FPA with a PMMA sample. The data was smoothed with a SG 11 point 2nd Order Smoothing Algorithm.

Again, the periodic frequency is very difficult to discern and the graph is too noisy to provide useful data. The periodic frequency is estimated to be 10-20s (0.05-0.1Hz).

From the data, it is determined that the current setup of the load cell in the FPA does not have a resolution good enough to use the SG method alone. It has worked for others[2,8] when dealing with the mass history because their resolution is much better than the level being achieved in the WPI FPA. De Ris and Khan have an effective resolution of approximately 10mg while Staggs used the data from the WPI cone calorimeter, which has an effective resolution of approximately 13mg. The effective resolution on the WPI FPA is 120mg.

Fast Fourier Transform

The first step in the smoothing of the MLR using FFT is to perform the forward transform and then create the power spectrum (i.e. magnitude versus frequency plot). The power spectrum was created, see Figure 17, and the cutoff frequency was estimated to be 0.03-0.04Hz. The cutoff frequency is the frequency at which there is an abrupt change in the trend of the power spectrum. In Figure 17, the curve starts out high at a frequency of 0 and then ramps down to when it suddenly flattens out around 0.03-0.04Hz. When the power spectrum is flat, there is no periodicity in that region and it is said to represent white noise (i.e. noise that is independent of frequency).[10]

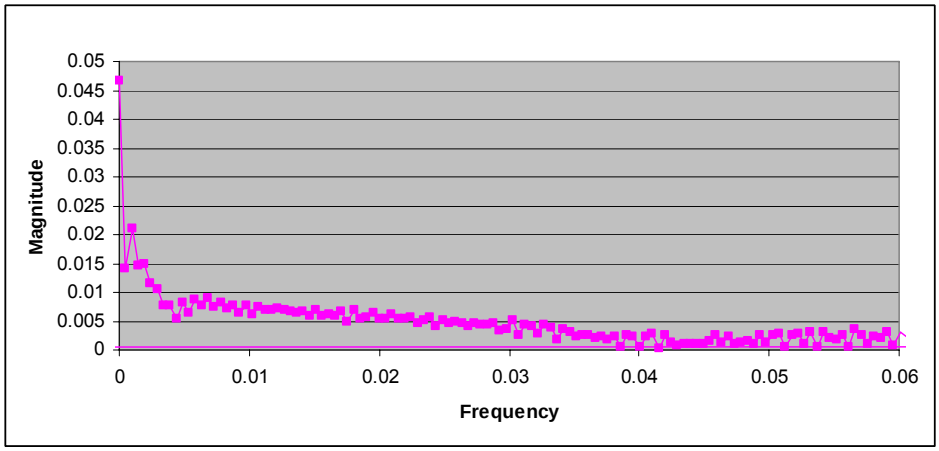

Figure 17: The Power Spectrum for the 1st Derivative Curve (Mass Loss Rate) from a Test done in the FPA with a PMMA sample.

Since the cutoff frequency was determined to be 0.03-0.04Hz from the power spectrum, that's where the frequency was zeroed. The inverse transform was then performed on the partially zeroed data and a smooth mass loss rate was created, as shown in Figure 18 and Figure 19 below.

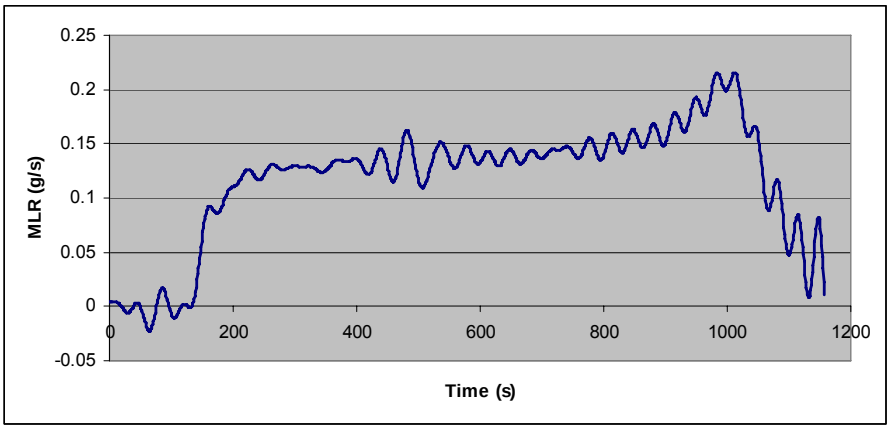

Figure 18: The 1st Derivative Curve (Mass Loss Rate) from a Test done in the FPA with a PMMA sample. The data was smoothed using FFT with a cutoff frequency of 0.03Hz.

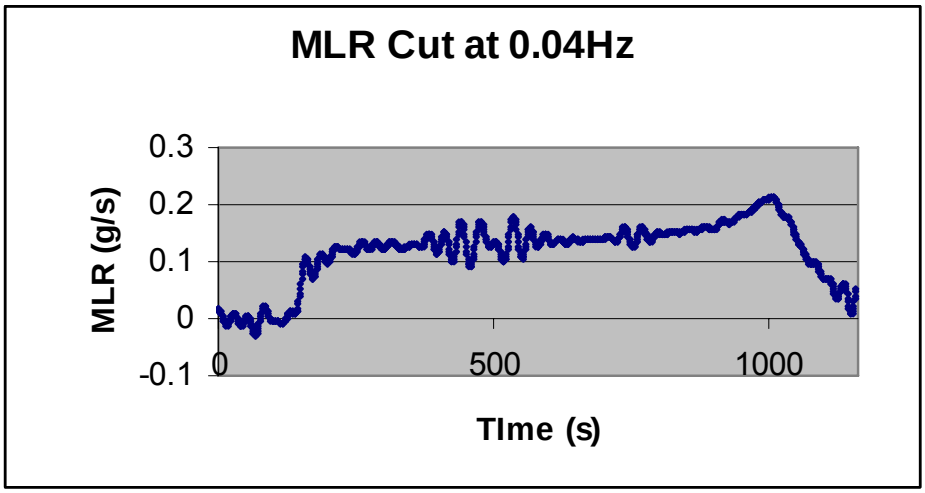

Figure 19: The 1st Derivative Curve (Mass Loss Rate) from a Test done in the FPA with a PMMA sample. The data was smoothed using FFT with a cutoff frequency of 0.04Hz.

The period of the peaks and valleys in the steady state portion of the graph is 34-39s (0.026-0.029Hz) when the cutoff point is 0.03Hz and 25-35s (0.029-0.04Hz) when the cutoff point is 0.04Hz. As can be seen from the graphs, the mass loss rate has been smoothed and represents a typical mass loss rate curve for PMMA.

In order to determine an upper and lower bound for the cutoff point, additional cutoff points were explored. When the frequency cutoff was changed to 0.02Hz, Figure 20 was obtained.

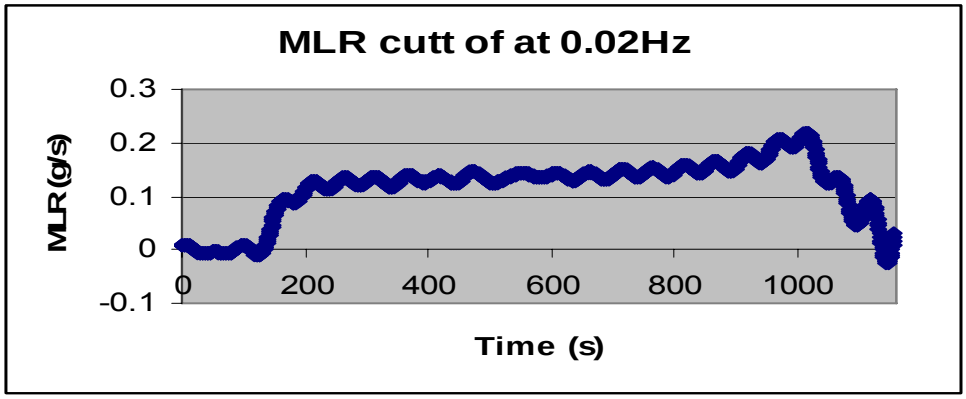

Figure 20: 1st Derivative Curve (Mass Loss Rate) from a Test done in the FPA with a PMMA sample. The data was smoothed using FFT with a cutoff frequency of 0.02Hz.

The period is 45-55s (0.018-0.022Hz). By looking at the curve, it appears as though certain features have been taken out by cutting the data at such a low frequency. Since this cutoff point removes more than just noise, this is not a good choice for a cutoff frequency.

Two cutoff frequencies that were higher than the cutoff frequency observed in the power spectrum were also tried. The 0.06Hz cutoff is shown in Figure 21 and 0.08Hz cutoff is shown in Figure 22.

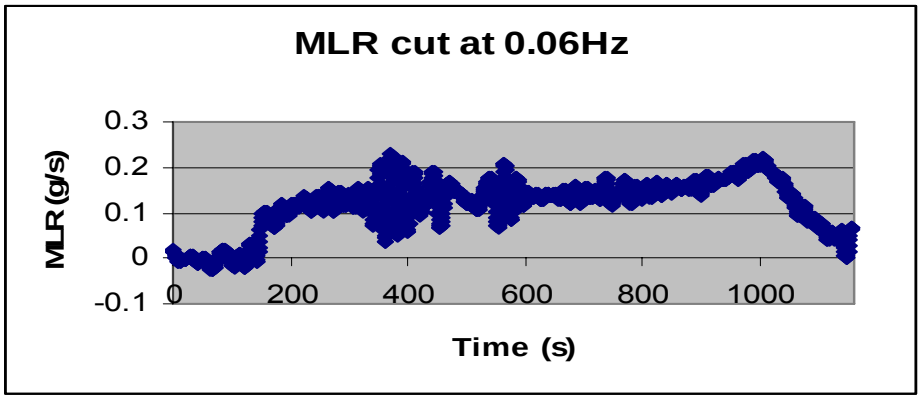

Figure 21: 1st Derivative Curve (Mass Loss Rate) from a Test done in the FPA with a PMMA sample. The data was smoothed using FFT with a cutoff frequency of 0.06Hz.

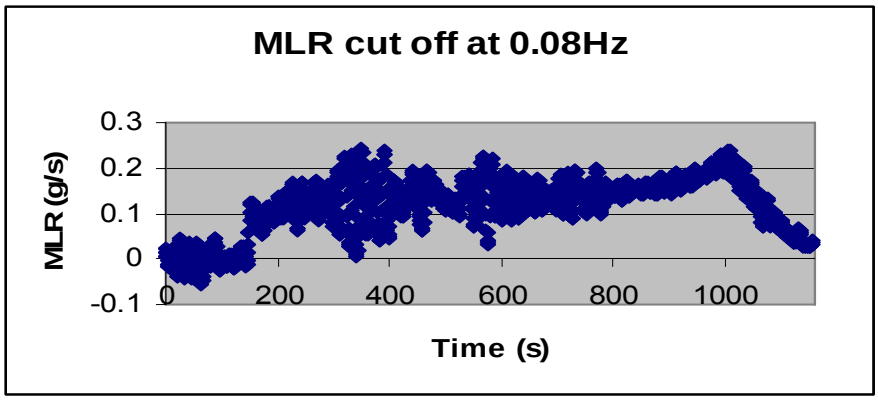

Figure 22: 1st Derivative Curve (Mass Loss Rate) from a Test done in the FPA with a PMMA sample. The data was smoothed using FFT with a cutoff frequency of 0.06Hz.

The period of the 0.06Hz cutoff frequency FFT smooth is 18-22s (0.045-0.056Hz); that of the 0.08Hz cutoff frequency smooth is 12-15s (0.067-0.083Hz). As can be seen, when the frequency is cutoff at 0.08Hz, the data becomes fairly noisy. Therefore, it is seen that the cutoff point of 0.03-0.04Hz based on the first derivative is indeed an optimal cutoff frequency when the quality of the curve is taken into consideration.

10 Point Moving Average

A simple 10 point moving average was applied to the 1st derivative data (i.e. the data that was obtained from the original mass history using the ASTM E 1354 mass loss rate equation). A second pass (a 10 point average of the 10 point average) and a third pass were also done on the data. The first pass is shown in Figure 23; the second pass is shown in Figure 24 and the third pass is shown in Figure 25.

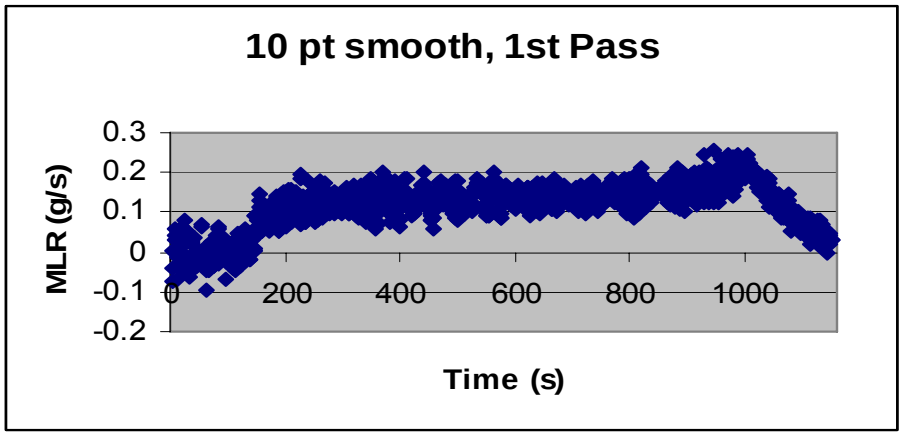

Figure 23: 1st Derivative Curve (Mass Loss Rate) from a Test done in the FPA with a PMMA sample. The data was smoothed using one pass of a 10 point smooth.

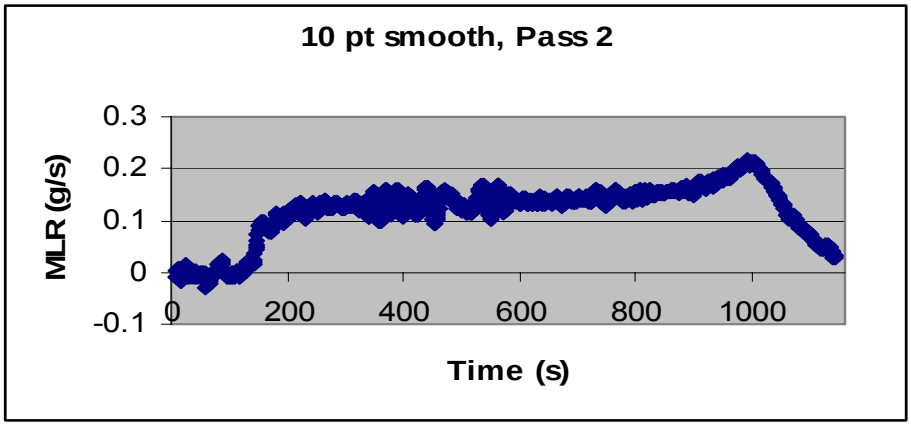

Figure 24: 1st Derivative Curve (Mass Loss Rate) from a Test done in the FPA with a PMMA sample. The data was smoothed using two passes of a 10 point smooth.

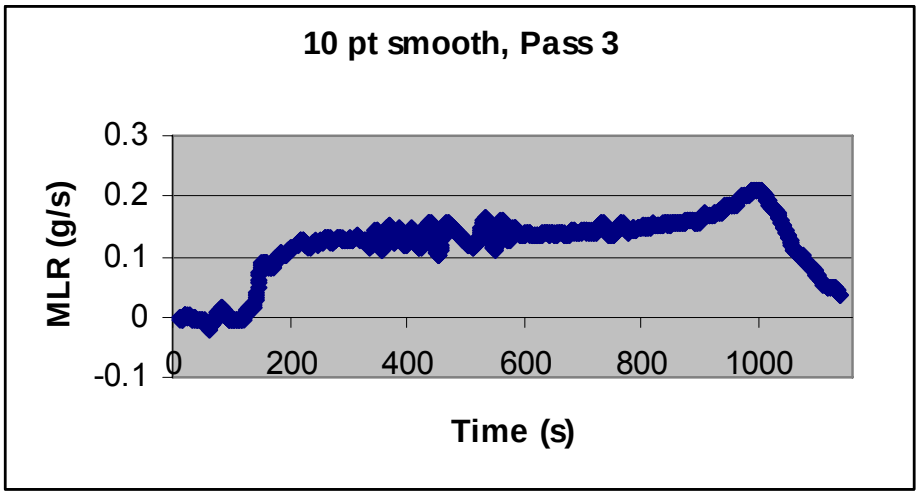

Figure 25: 1st Derivative Curve (Mass Loss Rate) from a Test done in the FPA with a PMMA sample. The data was smoothed using three passes of a 10 point smooth.

The data from the first pass is still very noisy and a lot of the peaks and valleys were not discernible. However, the period did appear to be approximately 15-25s (0.04-0.067Hz). The data from the second pass is much better but it is apparent that the curve could use a more intelligent smoothing technique due to the sharpness of the peaks and valleys. The period had a range of 10-30s (0.033-0.1Hz). It is hypothesized that the range is so wide due to the simple moving average technique used. It appears as though the data from the 3rd pass has been smoothed too much due to the flat parts now showing in the curve. The period in the 3rd pass is 25-35s (0.029-0.04Hz).

Combinations

The different smoothing algorithms were combined in order to determine if any additional insight is achieved.

1st Derivative Using SG and a 10 Point Smooth

Since all of the smoothing techniques have their advantages and disadvantages, it is sometimes useful to use a combination of filters to obtain the desired result.[7] A few different combinations of the SG filter and the 10 point moving average were tried. The combination that produced the best result with the least amount of smoothing was the combination in which the original mass data was smoothed using 1st derivative 19 point 4th order SG convolutes and then that curve, which is now the 1st derivative, was smoothed with one pass of a 10 point moving average. The result is given in Figure 26.

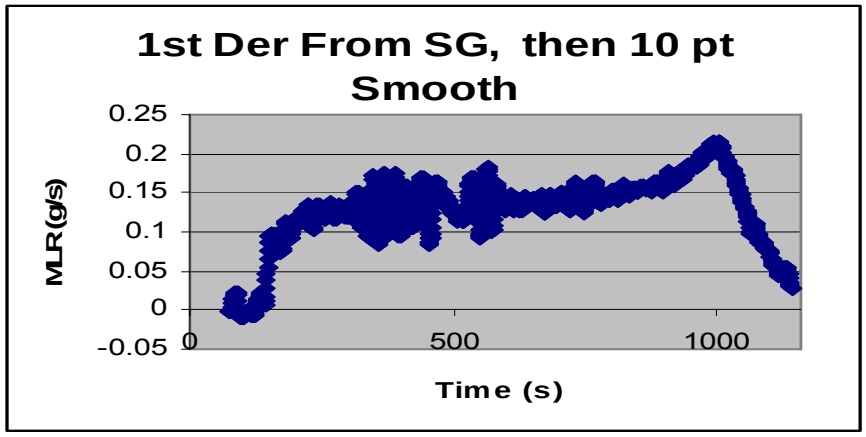

Figure 26: 1st Derivative Curve (Mass Loss Rate) from a Test done in the FPA with a PMMA sample. The data was smoothed using 19 point 4th Order SG 1st Derivative convolutes and then one pass of a 10 point moving average.

The period, which was very steady and easily identifiable in most cases, was 15-20s (0.05-0.067Hz).

It is also interesting to note that there is a fairly significant difference between the derivative that was calculated using ASTM E 1354 and then smoothed using SG versus the derivative that was calculated directly from SG convolutes. The two graphs are shown below in Figure 27.

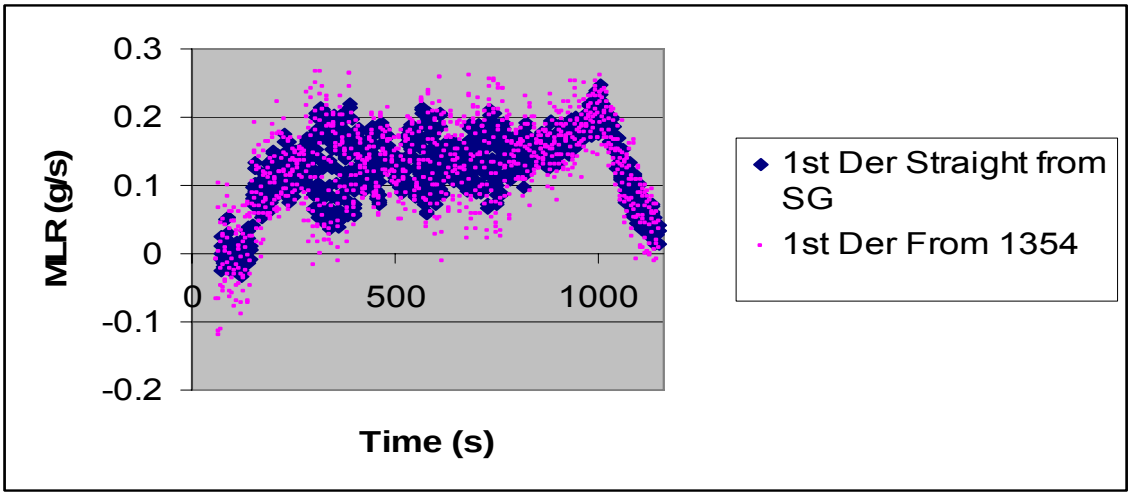

Figure 27: Comparing the 1st Derivative Calculated Directly from SG and the other Just Smoothed from SG

As can be seen, the 1st derivative calculated using ASTM E 1354 is noisier than that obtained straight from SG even though the derivative from ASTM E 1354 was smoothed using SG.

1st Derivative Using SG and a FFT Smooth

It appears as though obtaining the derivative directly from SG produces slightly better results than if the ASTM E 1354 equation is used. It also appears, from Figure 18 of this document, that the FFT power spectrum method produces the cleanest graph. However, the FFT graph could be better and it is hypothesized that a combination of both SG, to obtain the derivative, and FFT, to complete the smoothing of the curve, could be beneficial. The derivative was obtained using 1st derivative 19 point 4th order SG convolutes and the power spectrum for the data was created, as before; it is shown in Figure 28.

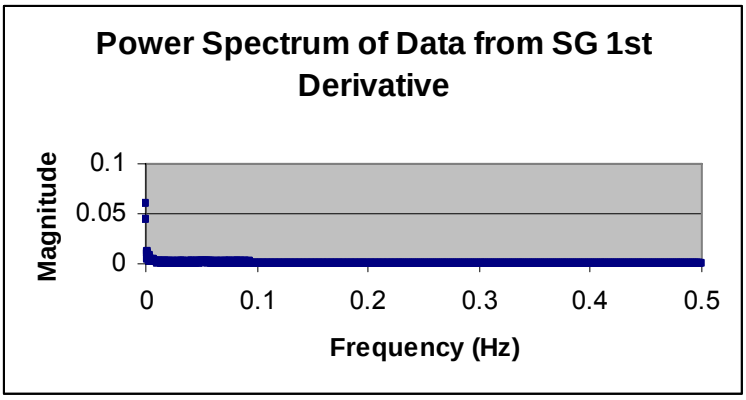

Figure 28: Power Spectrum for the 1st Derivative Curve (Mass Loss Rate) from a Test done in the FPA with a PMMA sample. The data was smoothed using a 19 point 4th order SG 1st derivative convolutes and then the power spectrum was determined.

The cutoff frequency was determined to be 0.1Hz from the power spectrum of the data. Therefore, the frequency was cut off at 0.1Hz and the period of the peaks and valleys was 12-33s (0.0303-0.0833Hz). The graph is shown below in Figure 29.

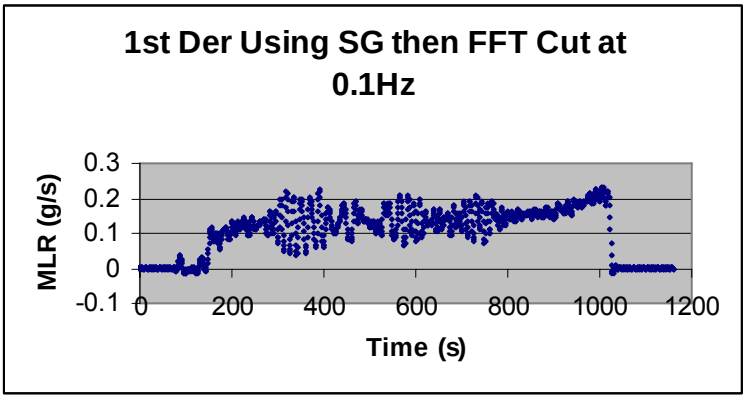

Figure 29: 1st Derivative Curve (Mass Loss Rate) from a Test done in the FPA with a PMMA sample. The data was smoothed using a 19 point 4th order SG 1st derivative convolutes and then a FFT smooth with a cutoff point of 0.1Hz was applied.

This graph is still fairly noisy so a cutoff frequency of 0.04Hz was used because this was the cutoff frequency when the MLR equation from ASTM E 1354 was used to obtain the first derivative. The graph is shown in Figure 30.

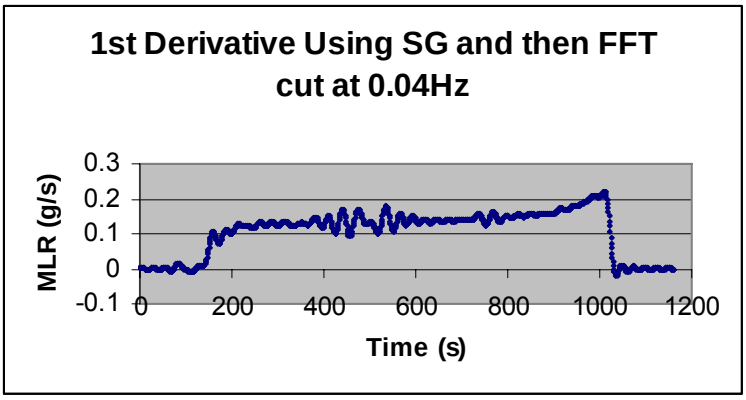

Figure 30: 1st Derivative Curve (Mass Loss Rate) from a Test done in the FPA with a PMMA sample. The data was smoothed using a 19 point 4th order SG 1st derivative convolutes and then a FFT smooth with a cutoff point of 0.04Hz was applied.

The period between the peaks and valleys is 29-35s (0.0286-0.0345Hz). The graph is much less noisy because more of the frequencies have been removed.

As a method of comparison, Figure 30 and Figure 19 were plotted on the same graph. The graph is shown in Figure 31 below.

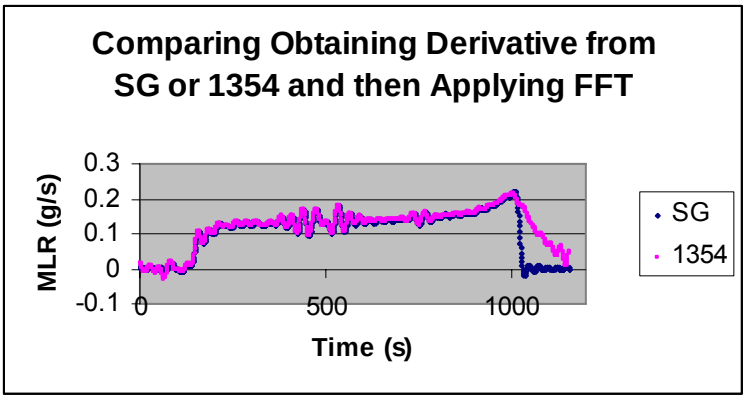

Figure 31: 1st Derivative Curve (Mass Loss Rate) Comparison from a Test done in the FPA with a PMMA sample. Both curves were smoothed with FFT and a cutoff point of 0.04Hz. The first derivative was calculated using SG convolutes on one curve and ASTM E 1354 for the other.

They basically follow the same path until the very end. At the end, the derivative obtained using SG drops off sharply while the ASTM E 1354 derivative ramps down. It seems as though the SG method is cutting off some important phenomenon at the end. Therefore, it is concluded that the method of using ASTM E 1354 to calculate the derivative and then applying FFT is the best method for reducing the noise but preserving the phenomenon in the first derivative.

FFT on Mass History then Derivatives

Perhaps if the original mass history were smoothed to a suitable effective resolution, the derivates could be taken from the mass history without any additional smoothing. The mass history is a fairly nice curve; the trend can be seen very clearly and the white noise is not very prominent. The resolution on the original mass history data for this particular test was ±60mg. The graph is shown in Figure 32 below.

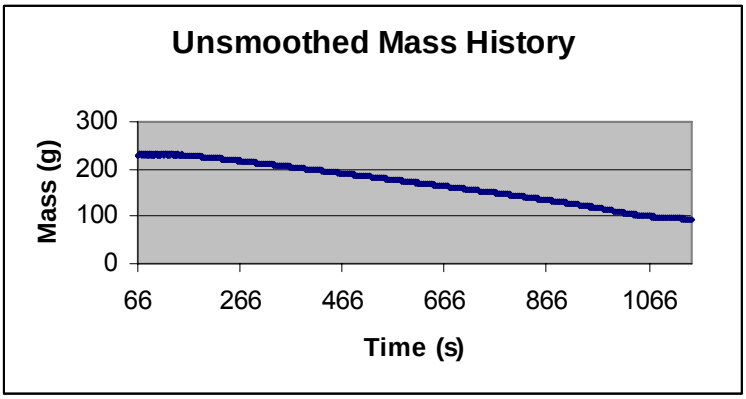

Figure 32: Original Mass History from a Test done in the FPA with a PMMA sample. The data is not smoothed.

Note that the first and last minute were cut off to eliminate the shutter down noise at the beginning and end of the test.

The same FFT procedure as was used on the 1st derivative (explained above) was used on the original unsmoothed mass history. The power spectrum that was obtained is shown in Figure 33 below.

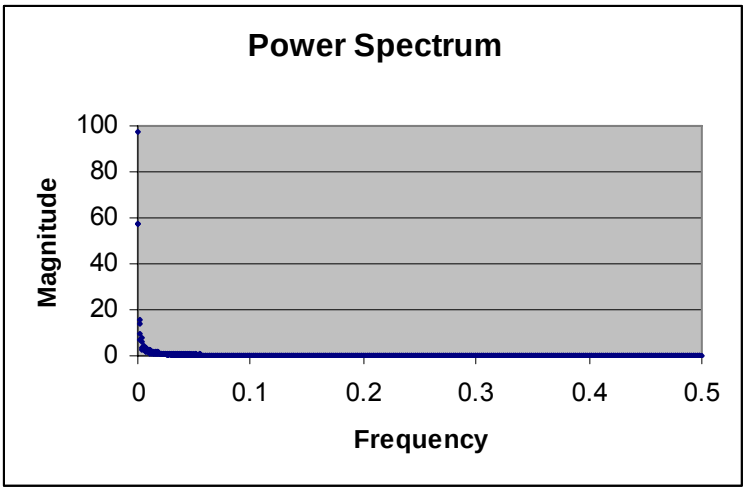

Figure 33: Power Spectrum for the Original Mass History from a Test done in the FPA with a PMMA sample.

As can be seen from the power spectrum, the magnitude of the frequency goes to zero at 0.06Hz. Therefore, all frequencies above 0.06Hz were cut off and the following "mass history" was obtained.

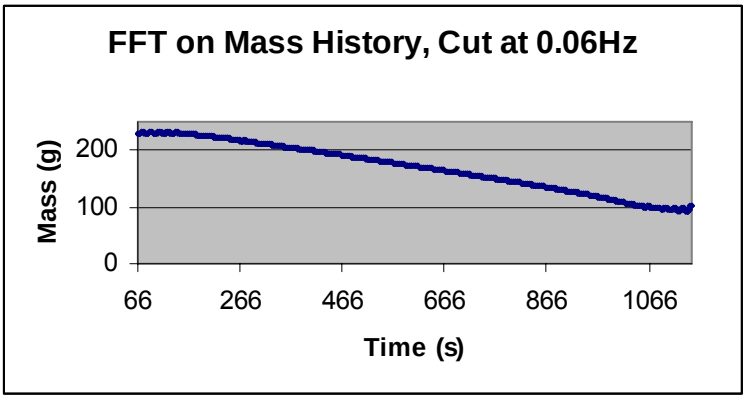

Figure 34: Original Mass History from a Test done in the FPA with a PMMA sample. The data is smoothed using FFT with a cutoff point of 0.06Hz.

As can be seen from comparing Figure 32 and Figure 34, using the FFT power spectrum method on the original unsmoothed mass history introduces a distinct periodicity in the graph which was not there before. This can be seen even more prominently when the graph is blown up and it is shown that the effective resolution of the mass history in Figure 34 is ±250mg. When the derivatives are taken on this data, the results will be even worse than if the derivatives were calculated from the original mass history due to this periodicity.

It is unclear why the data gets less smooth when the FFT is applied to the original data. A number of different cutoff frequencies were used (0.025Hz, 0.045Hz, 0.1Hz, 0.12Hz and 0.14Hz) and they all produced results that were worse than the original unsmoothed mass history. There is a phenomenon known as Gibb's Phenomenon in which ripples are introduced into the data when the frequencies are abruptly cut off, as they are in this case. The way to fix the ripples is to slowly decline from one to zero when cutting off the frequencies in which noise dominates.[15] However, a smooth decline from one to zero was tried using a linear 10 point decline and there was no improvement in the mass history. Therefore, it is hypothesized that the rippling effect is coming from another phenomenon.

2nd Derivative of Mass History

The second derivative is interesting as well because the largest negative peak of the 2nd derivative represents the operator independent ignition time of the sample. It is sometimes difficult, especially with materials such as composites, to visually determine the time to ignition. This operator independent way of determining the time to ignition could help to alleviate this problem.[2]

The 2nd derivative was obtained from applying the mass loss rate equation from ASTM E 1354 to the 1st derivative data, unless otherwise noted. The noise in the data is amplified by the derivatives so the 2nd derivative is even noisier than the first if no smoothing is done. The original 2nd derivative obtained from ASTM E 1354 with no smoothing is shown in Figure 35.

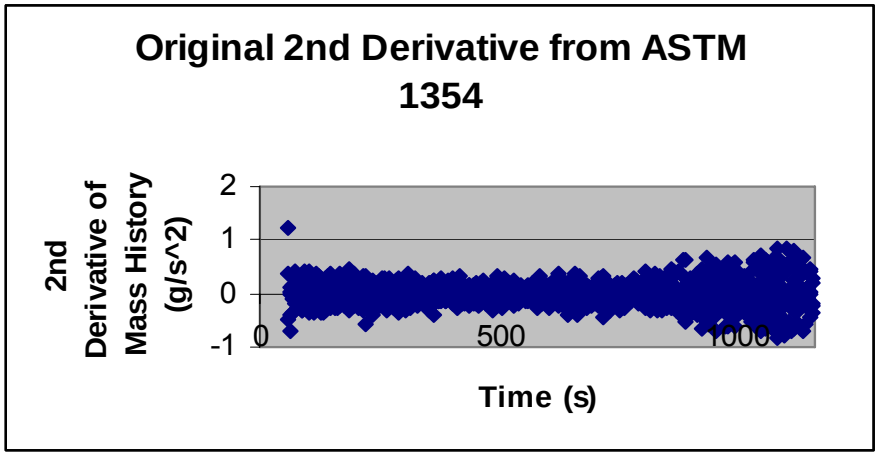

Figure 35: Original 2nd Derivative of the Mass History from a Test done in the FPA with a PMMA sample. The data is not smoothed.

The first and last minute of the test were cut off to eliminate shutter down noise; the noise from the shutter was amplified significantly by the 2nd derivative. As can be seen, the 2nd derivative is so noisy that nothing can be concluded from it. Therefore, it needs to be smoothed. The same methods as for the first derivative will be used so they will not be fully explained again. The only difference is that the first minute is also cut off in the 2nd derivative. Also, now the operator independent ignition (OII) time is looked for in the graph and the periodic frequency is of no relevance. The visual ignition time for the test was 146s.

Savitzky-Golay

The suggestion given for the second derivative by de Ris and Khan was to use a 19 point 4th order SG smooth. The result is shown in Figure 36.

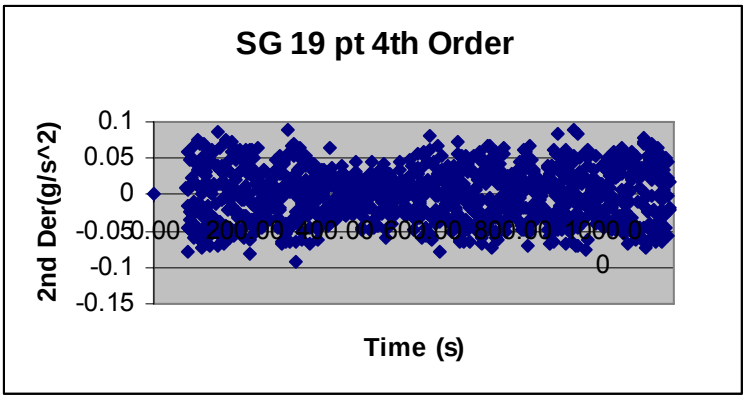

Figure 36: Original 2nd Derivative of the Mass History from a Test done in the FPA with a PMMA sample. The data is smoothed using a 19pt 4th Order SG Algorithm.

The data is extremely noisy and the OII time is impossible to discern.

The other suggestion for the derivative, made by Staggs, was to use an 11 point 2nd order SG smooth. The result is shown in Figure 37 below.

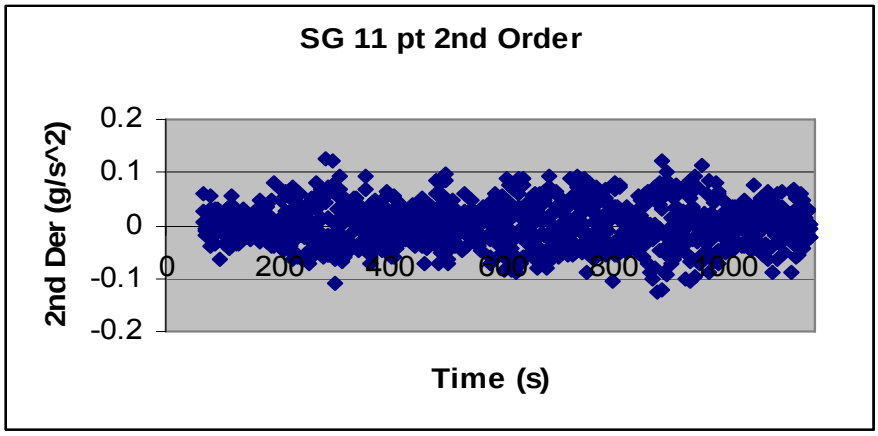

Figure 37: Original 2nd Derivative of the Mass History from a Test done in the FPA with a PMMA sample. The data is smoothed using an 11pt 2nd Order SG Algorithm.

The OII time cannot be determined.

Fast Fourier Transform

The power spectrum was determined in the same fashion as before for the 1st derivative data. It is shown in Figure 38.

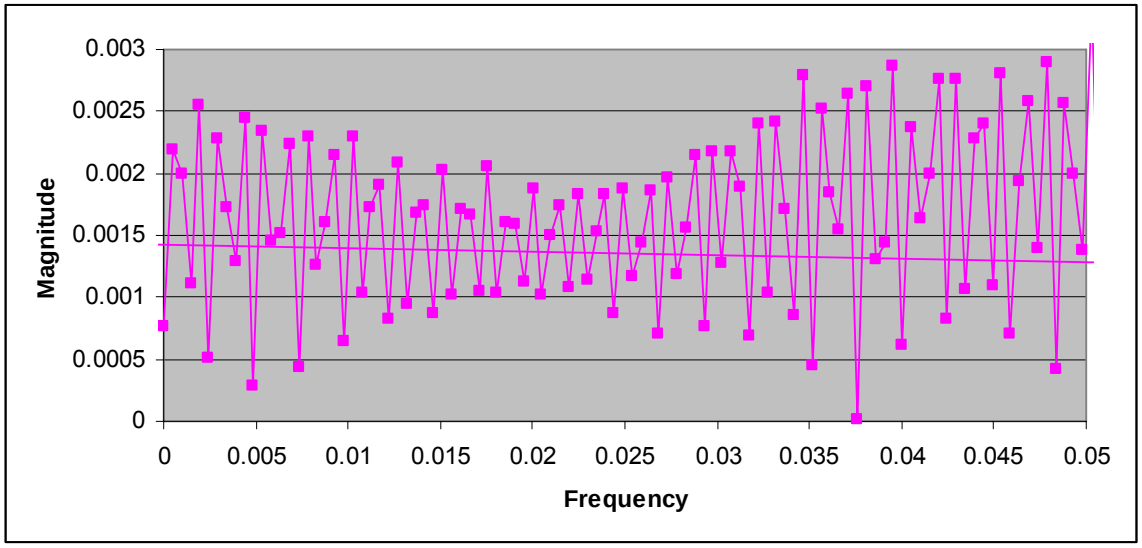

Figure 38: Power Spectrum for the Original 2nd Derivative of the Mass History from a Test done in the FPA with a PMMA sample.

The frequency cutoff was determined to be approximately 0.02-0.25Hz. The same frequency cutoffs as for the first derivative were used, except for 0.03Hz. They are shown in Figures 26-29 below.

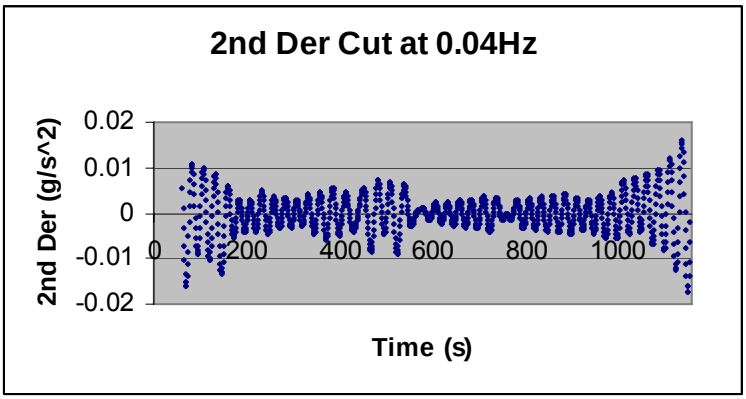

Figure 39: The 2nd Derivative of the Mass History from a Test done in the FPA with a PMMA sample. The derivative is smoothed with FFT using a cutoff frequency of 0.04Hz.

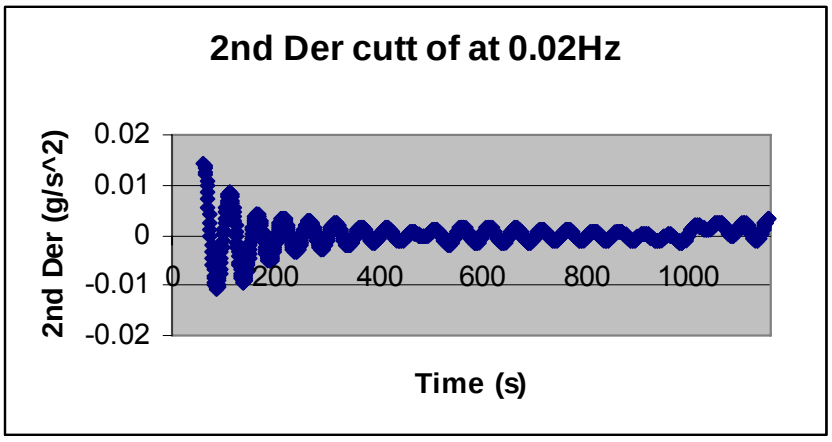

Figure 40: The 2nd Derivative of the Mass History from a Test done in the FPA with a PMMA sample. The derivative is smoothed with FFT using a cutoff frequency of 0.02Hz.

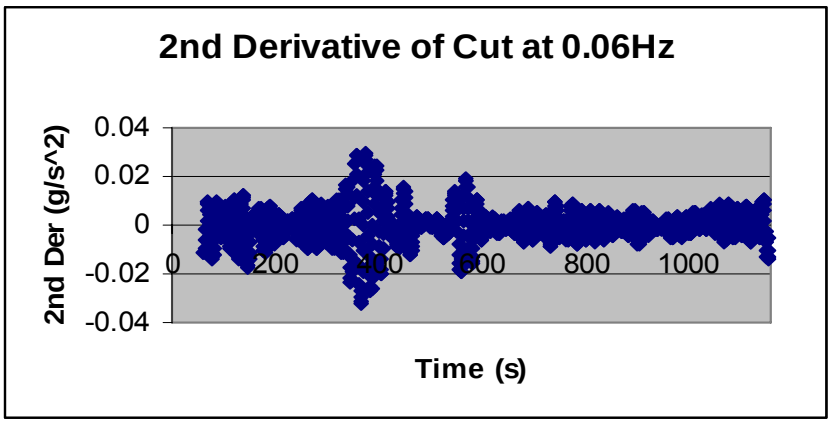

Figure 41: The 2nd Derivative of the Mass History from a Test done in the FPA with a PMMA sample. The derivative is smoothed with FFT using a cutoff frequency of 0.06Hz.

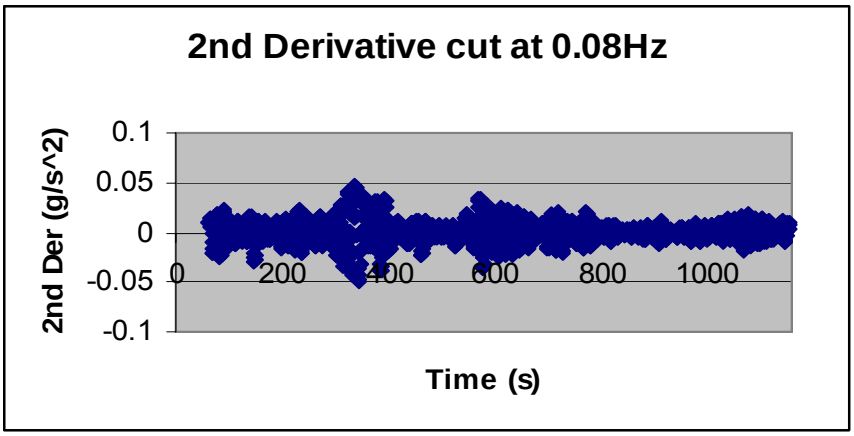

Figure 42: The 2nd Derivative of the Mass History from a Test done in the FPA with a PMMA sample. The derivative is smoothed with FFT using a cutoff frequency of 0.08Hz.

The 2nd derivative cut off at 0.04Hz correctly determines the time to ignition of 146s. Unfortunately, it is not a global peak due to the shutter down noise. However, the shutter will be padded and the noise from it will not be as amplified in the future, if at all. If the 2nd derivative is cut off at 0.02Hz, the OII time is 141s. Cut off at 0.06Hz, the OII time is 147s; at 0.08Hz, it is 148s. As can be seen, the cutoff frequency does not have a huge effect on the OII time, especially considering the uncertainty in the visual ignition is 9s.

10 Point Moving Average

In the first pass, the data is much too scattered to determine the OII time. However, in the 2nd pass, the data is still scattered but the point at 149s is the lowest point on the graph (i.e. the global negative peak). The graph is shown in Figure 43.

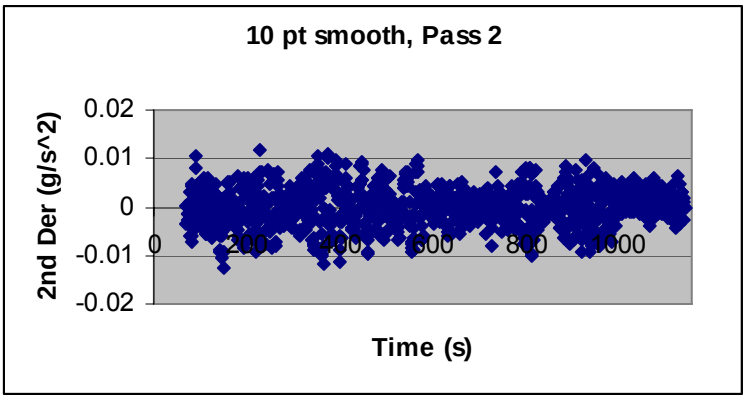

Figure 43: The 2nd Derivative of the Mass History from a Test done in the FPA with a PMMA sample. The derivative is smoothed using two passes of a 10 point moving average.

It is beneficial if the peak is a global peak because then the whole method can be completely automatic. The third pass makes the peak even more pronounced and it is very obvious that the maximum negative peak is located at 145s. The graph is shown in Figure 44.

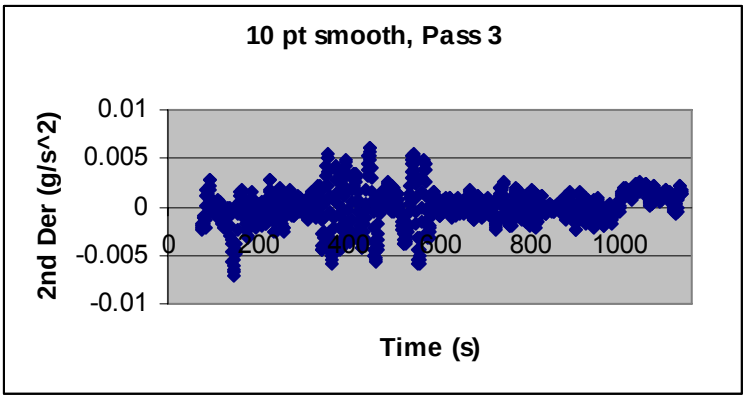

Figure 44: The 2nd Derivative of the Mass History from a Test done in the FPA with a PMMA sample. The derivative is smoothed using three passes of a 10 point moving average.

Therefore, a simple moving average, applied multiple times, is able to make the maximum negative peak clearly visible using data produced by the WPI FPA.

Combinations

The different smoothing algorithms were combined in order to determine if any additional insight is achieved.

2nd Derivative Using SG and a 10 Point Smooth

The same combination that was used for the first derivative will be used here except that a 25 point 4th order 2nd derivative SG smooth will be used. The OII time was difficult to tell from the 1st and 2nd pass with the 10 point smooth. However, on the third pass, it became a global negative peak right at 146s. The graph is shown in Figure 45.

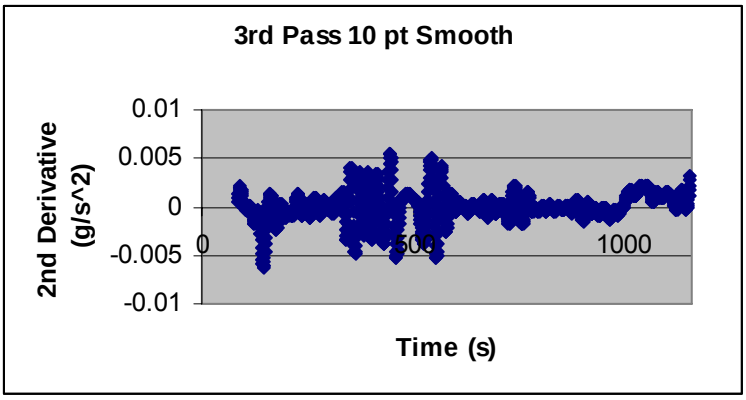

Figure 45: 2nd Derivative of the Mass History from a Test done in the FPA with a PMMA sample. The data was smoothed using a 25 point 4th order SG 2nd derivative convolutes and then three passes of a 10 point moving average smooth were applied.

The problem with this method is the large number of steps involved in the process.

2nd Derivative Using SG and a FFT Smooth

The derivative was obtained using 2nd derivative 25 point 4th order SG convolutes and then the FFT was used to smooth the curve. The power spectrum from the data is shown in Figure 46 below.

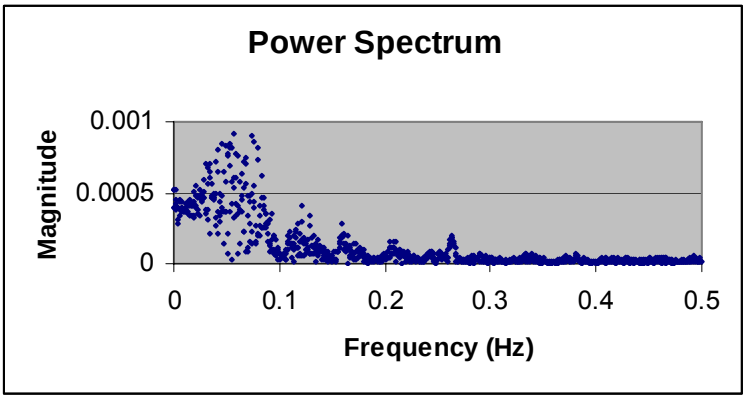

Figure 46: Power Spectrum for the 2nd Derivative of the Mass History from a Test done in the FPA with a PMMA sample. The 2nd derivative was found using a 25 point 4th order SG 2nd derivative convolutes.

The cutoff frequency appears to be 0.28Hz. This was the cutoff frequency that was tried first. The result is shown in Figure 47 below.

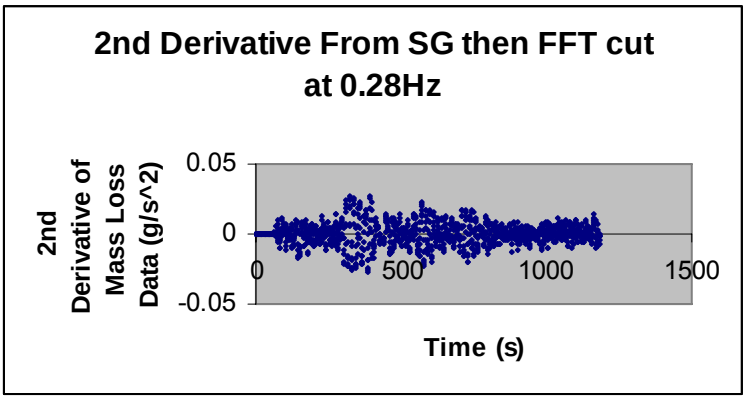

Figure 47: Power Spectrum for the 2nd Derivative of the Mass History from a Test done in the FPA with a PMMA sample. The 2nd derivative was found using a 25 point 4th order SG 2nd derivative convolutes and then the data was smoothed using FTT with a 0.28Hz cutoff frequency.

As can be seen, the data is very noisy and, although there is a small peak at 146s, the OII time is not clearly discernible. It is hypothesized that the cutoff frequency is so much higher when the derivative is obtained using SG because it smoothes the periodicity in the data, which the FFT power spectrum method depends upon to determine the difference between the actual signal (i.e. periodical) and the noise (assumed to be white noise).

For completeness, the frequency was also cut off at 0.04Hz. The result is shown in Figure 48.

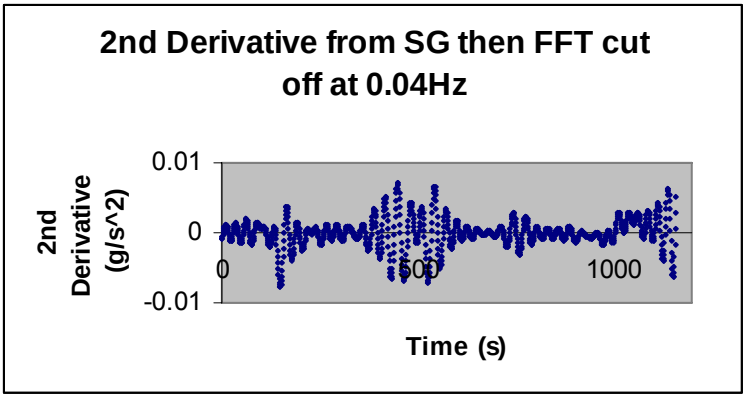

Figure 48: Power Spectrum for the 2nd Derivative of the Mass History from a Test done in the FPA with a PMMA sample. The 2nd derivative was found using a 25 point 4th order SG 2nd derivative convolutes and then the data was smoothed using FTT with a 0.04Hz cutoff frequency.

There is a global negative peak around the time to ignition. However, it is at 150s while the visual ignition time was 146s. Again, it is hypothesized that the dampening of the periodicity by the SG method is disrupting the FFT smoothing; it is better to obtain the derivative from ASTM E 1354 than apply SG.

Conclusions

It is found that the best way to obtain the relevant information from the first and second derivatives of the mass history from the WPI FPA is to take the derivatives using the MLR equation from ASTM E 1354 and then apply the FFT power spectrum method. This method uses the best combination of the least number of steps in the process, the reduction of noise, preservation of phenomenon and accuracy compared to visual ignition time. This document was simply an example of the different types of smoothing that are available. As the first tests in the FPA were smoothed, it was determined that the power spectrum from the 2^{nd} derivative gave more repeatable cutoff frequencies than that from the first derivative. Therefore, the cutoff point determined from the 2^{nd} derivative power spectrum should be used for both the first and second derivatives of the mass history. It was found that, for all samples, the cutoff frequency is between 0.02 and 0.03Hz. It was shown in Figure 38 above that there was a change in the trend of the PMMA sample around 0.02-0.025Hz in the 2^{nd} derivative power spectrum. In order to make the process fully objective for consistency purposes, a magnitude within this frequency range has to be used as the cutoff. From performing multiple tests on many different samples (e.g. PMMA and composite materials), it was found that a suitable cutoff magnitude within the range 0.02-0.03Hz was 0.00025 or, if this magnitude was not achieved during the given range, the highest magnitude in that range. The method described here has displayed results consistent from test to test including mass loss rate, time to visual ignition and heat release rate (when the mass loss rate is used to determine a heat release rate). It also produces data that match those produced by others.[13] The FFT power spectrum method may be able to be fully automated in Excel; this is a recommendation for future work. However, in order to do this, a spring would be needed to soften the shutter down noise so that the operator independent time to ignition would be a global negative peak instead of a local negative peak.

Files for Reference

The data that is displayed in this appendix is available in files: Support Data for FFT VS SG doc mass history.xls; Support Data for FFT VS SG doc 1st Der.xls; Support Data for FFT VS SG doc 2nd Der.xls and Support Data for FFT vs SG doc.xls.

The Macros[10]

```
Sub ForwardFT()
'
' ForwardFT Macro
' This is from the book "advanced excel for scientific data analysis" by robert de levie
'

'
    Dim iSign As Integer
    iSign = 1
    Call Fourier(iSign)
    End Sub


Sub Fourier(iSign)
'
' Fourier Macro
' This is called by ForwardFT to do the Fourier analysis.  This algorithm is from Robert de Levie's book "Advanced Excel for Scientific Data Analysis"
'

'
    ' Check the array length n, which must be a power of 2,
' and be at least 2

Dim cn As Integer, cnMax As Integer, jSign As Integer
Dim n As Integer, NN As Integer
Dim rn As Integer, rnMax As Integer
Dim Length As Single
Dim Check1 As Double, Check2 As Double
Dim Denom As Double, Interval As Double, z As Double
Dim DataArray As Variant, outputArray As Variant
Dim myRange As Range
```

```
Dim Ans, hAnswer

Begin:
n = 0
rnMax = Selection.Rows.Count
Length = CSng(rnMax)
cnMax = Selection.Columns.Count

' If area was not highlighted

If rnMax = 1 And cnMax = 1 Then
  hAnswer = MsgBox("You forgot to highlight" _
    & Chr(13) & "the block of input data." _
    & Chr(13) & "Do you want to do so now?" _
    , vbYesNo, "Fourier transformation")
  If hAnswer = vbNo Then End
  If hAnswer = vbYes Then
    Set myRange = Application.InputBox(Prompt:= _
      "The input data are located in:", Type:=8)
    myRange.Select
  End If
  GoTo Begin
End If

If Length < 2 Then
  MsgBox "There must be at least two rows."
  End
End If
Do While Length > 1
  Length = Length / 2
Loop
If Length <> 1 Then
  MsgBox "The current number of rows is " & rnMax _
    & "which is not an integer power of two."
  End
End If

' Check that there are three input columns

If cnMax <> 3 Then
  MsgBox "There must be three input columns," _
    & Chr(13) & "one for the variable (time, frequen-," _
    & Chr(13) & "cy, etc.), the next two for the real" _
    & Chr(13) & "and imaginary parts of the input data."
  End
End If

' Read the input data

DataArray = Selection.Value

' Check that the first column has its first two elements

Check1 = VarType(DataArray(1, 1))
If Check1 = 0 Then
  MsgBox "Enter the top left value."
```

```
  End
End If
Check2 = VarType(DataArray(2, 1))
If Check2 = 0 Then
  MsgBox "Enter a value in row 2 of the first column."
  End
End If

' Determine what input convention is used:
' jSign = -1 for input data centered around zero,
' jSign = 1 for input data starting at zero

jSign = 0
Interval = (DataArray(2, 1) - DataArray(1, 1)) * rnMax
If DataArray(1, 1) > (-0.5 * Interval / rnMax) And _
  DataArray(1, 1) < (0.5 * Interval / rnMax) Then jSign = 1
If DataArray(1, 1) < (-0.5 * Interval / rnMax) And _
  DataArray(rnMax / 2 + 1, 1) > (-0.5 * Interval / rnMax) _
  And DataArray(rnMax / 2 + 1, 1) < (0.5 * Interval / _
  rnMax) Then jSign = -1
If jSign = 0 Then
  MsgBox "The input format is incorrect." _
    & Chr(13) & "It should either be centered" _
    & Chr(13) & "around zero, or start at zero."
  End
End If

' Read and rearrange the input data

NN = 2 * rnMax
ReDim Term(NN) As Double
If jSign = 1 Then
  For rn = 1 To rnMax
    Term(2 * rn - 1) = DataArray(rn, 2)
    Term(2 * rn) = DataArray(rn, 3)
  Next rn
End If
If jSign = -1 Then
  For rn = 1 To rnMax / 2
    Term(2 * rn - 1) = DataArray(rnMax / 2 + rn, 2)
    Term(2 * rn) = DataArray(rnMax / 2 + rn, 3)
    Term(rnMax + 2 * rn - 1) = DataArray(rn, 2)
    Term(rnMax + 2 * rn) = DataArray(rn, 3)
  Next rn
End If

' Check that the output does not overwrite valuable data

Selection.Offset(0, 3).Select
outputArray = Selection.Value
For rn = 1 To rnMax
  For cn = 1 To cnMax
    z = outputArray(rn, cn)
    If (IsEmpty(z) Or z = 0) Then
      n = n
    Else
```

```
      n = n + 1
    End If
  Next cn
Next rn
If n > 0 Then
  Ans = MsgBox("  There are data in the space where" _
    & Chr(13) & "the output will be written. Proceed " _
    & Chr(13) & "  anyway and overwrite those data?", _
    vbYesNo)
  If Ans = vbNo Then
    Selection.Offset(0, -3).Select
    End
  End If
End If

' Calculate and write the frequency or time scale

If jSign = 1 Then
  For rn = 1 To rnMax / 2
    DataArray(rn, 1) = (rn - 1) / Interval
  Next rn
  For rn = (rnMax / 2 + 1) To rnMax
    If iSign > 0 Then
      DataArray(rn, 1) = (rn - rnMax - 1) / Interval
    Else
      DataArray(rn, 1) = (rn - 1) / Interval
    End If
  Next rn
End If

If jSign = -1 Then
  For rn = 1 To rnMax
    DataArray(rn, 1) = (-(rnMax / 2) + rn - 1) / Interval
  Next rn
End If

' Calculate the Fourier transform

Call FT(Term, NN, iSign)

' Arrange and write the output data

Denom = (rnMax + 1 + iSign * (rnMax - 1)) / 2
If jSign = 1 Then
  For rn = 1 To rnMax
    DataArray(rn, 2) = Term(2 * rn - 1) / Denom
    DataArray(rn, 3) = Term(2 * rn) / Denom
  Next rn
End If
If jSign = -1 Then
  For rn = 1 To rnMax / 2
    DataArray(rn, 2) = Term(rnMax + 2 * rn - 1) / Denom
    DataArray(rn, 3) = Term(rnMax + 2 * rn) / Denom
    DataArray((rnMax / 2) + rn, 2) = _
      Term(2 * rn - 1) / Denom
    DataArray((rnMax / 2) + rn, 3) = Term(2 * rn) / Denom
```

```
  Next rn
End If

Application.ScreenUpdating = False

Selection.Value = DataArray

End Sub
```

Sub FT(Term, NN, iSign)

```
' FT Macro
' This is from de Levie's book and is called by the ForwardFT macro.
'
' The following is the Fourier transform routine FOUR1 from
' J. C. Sprott, "Numerical Recipes: Routines and Examples
' in BASIC", Cambridge University Press, Copyright (C)1991
' by Numerical Recipes Software. Used here by permission.
' Use of this routine other than as an integral part of the
' present book requires an additional license from Numeri-
' cal Recipes Software. Further distribution is prohibited.
' The routine has been modified to yield double-precision
' results, and to conform to the standard mathematical sign
' convention for Fourier transformation.

Dim i As Integer, istep As Integer, j As Integer
Dim m As Integer, mmax As Integer

Dim tr As Double, ti As Double, theta As Double
Dim wtemp As Double, wi As Double, wr As Double
Dim wpi As Double, wpr As Double

j = 1
For i = 1 To NN Step 2
  If j > i Then
    tr = Term(j)
    ti = Term(j + 1)
    Term(j) = Term(i)
    Term(j + 1) = Term(i + 1)
    Term(i) = tr
    Term(i + 1) = ti
  End If
  m = Int(NN / 2)
  While m >= 2 And j > m
    j = j - m
    m = Int(m / 2)
  Wend
  j = j + m
Next i
mmax = 2
While NN > mmax
  istep = 2 * mmax
  theta = 2 * [Pi()] / (-iSign * mmax)
  wpr = -2 * Sin(0.5 * theta) ^ 2
  wpi = Sin(theta)
```

```
  wr = 1
  wi = 0
  For m = 1 To mmax Step 2
    For i = m To NN Step istep
      j = i + mmax
      tr = wr * Term(j) - wi * Term(j + 1)
      ti = wr * Term(j + 1) + wi * Term(j)
      Term(j) = Term(i) - tr
      Term(j + 1) = Term(i + 1) - ti
      Term(i) = Term(i) + tr
      Term(i + 1) = Term(i + 1) + ti
    Next i
    wtemp = wr
    wr = wr * wpr - wi * wpi + wr
    wi = wi * wpr + wtemp * wpi + wi
  Next m
  mmax = istep
Wend

End Sub
```

Sub InverseFT()

```
' InverseFT Macro
' Algorithm to compute the inverse FT transformation from de Levie's Advanced Excel book.
'
Dim iSign As Integer
iSign = -1
Call Fourier(iSign)

End Sub
```

References

[1] Standard Test Method for Heat and Visible Smoke Release Rates for Materials and Products Using an Oxygen Consumption Calorimeter, ASTM E 1354-02, ASTM, 100 Barr Harbor Drive, West Conshohocken, PA, U.S.

[2] M. M. Khan and J. L. de Ris, "Operator Independent Ignition Measurements", *Proceedings Fire and Materials Conference* (2005).

[3] Standard Methods of Test for Measurement of Synthetic Polymer Material Flammability Using a Fire Propagation Apparatus (FPA), ASTM E 2058-03, ASTM, 100 Barr Harbor Drive, West Conshohocken, PA, U.S.

[4] A. Savitzky and M. J. E. Golay, *Anal. Chem.,* **36,** 1627 (1964).

[5] J. Steiner, Y. Termonia and J. Deltour, *Anal. Chem.*, **44**, 1906 (1972).

[6] H. H. Madden, *Anal. Chem.*, **50**, 1383 (1978).

[7] R.G. Brereton "Chemometrics – Data Analysis for the Laboratory and Chemical Plant" John Wiley & Sons, 2003.

[8] J. E. J. Staggs, *Fire Safety Journal*, **40**, 493 (2005).

[9] W. H. Press, W. T. Vetterling, S. A. Teukolsky and B. P. Flannery, "Numerical Recipes in C: The Art of Scientific Computing" Cambridge University Press, 2002.

[10] R. de Levie, "Advanced Excel for Scientific Data Analysis", Oxford University Press, 2004.

[11] M. P Seah, W. A. Dench, B. Gale and T. E. Groves, *J. Phys. E: Sci. Instrum.*, **21**, 351 (1988).

[12] T. O' Haver, "Harmonic Analysis", Dept. of Chemistry and Biochemistry, 2001, The University of Maryland at College Park, 8 September 2005, <http://www.wam.umd.edu/~toh/spectrum/HarmonicAnalysis.html>.

[13] P. A. Beaulieu, "Characterization of Mass Loss Measurement System in AFM," Factory Mutual Research Internal Memo,, 20 August 2001.

[14] D. Drysdale, "An Introduction to Fire Dynamics", John Wiley & Sons, 2003.

[15] E. L. Kosarev and E. Pantos, *J. Phys. E: Sci. Instrum.*, **16**, 537 (1983).

Appendix B: Fire Propagation Apparatus Calibration

Introduction

The first task that was completed on the WPI FPA was to determine the calibration equations for the different instrumentation and to ensure that they were producing reasonable data, since it is a new apparatus at WPI. After the calibration equations were determined, tests were done with well-known materials in an attempt to determine the uncertainty in the time to ignition, burn duration, mass loss rate and heat release rate in the FPA. Tests were performed with PMMA (solid in holder designed by de Ris and Khan[1]), acetone (liquid in uninsulated aluminium dish from ASTM E 2058[2]), methane and propylene (gases coming through the FPA's gas burner); these tests were used to determine the uncertainty in most of the measurements. Identical tests with the composite samples were also used to determine uncertainties in other measurements.

Calibration Equations and Instrument Information

The calibration equations were determined from the instrument manuals or from repeated measurements of the voltage at known conditions. The procedure by which the calibration equation for each of the instruments in the FPA was determined as well as any pertinent information about the instrument is detailed below. The resolution of each of the instruments is listed to provide context for the data truncation that is used in the calculations (see Appendix C: FPA Data Reduction Macro).

Load Cell

The calibration equation for the load cell is specified by the user by way of the load cell controller. The output voltage range of the load cell is 0-10V and the range was set from 0-300g; the calibration equation is then y=30x where y is the mass in grams and x is the voltage output. If needed, this calibration is easily changed using the load cell controller. The resolution of the load cell controller is 100μV.[3] Since there is

no manual for the load cell itself, the uncertainty of the load cell controller was used for truncation of the data. Since the load cell controller needs almost an hour to reach a steady state temperature for accurate readings,[3] it is suggested that the load cell controller be left on at all times. The instrument has two different smoothing algorithms available which are both turned off in the FPA in order to get raw data (in the WPI Cone, the smoothing is turned on). From testing, it was found that the response time of the controller is dramatically increased when the smoothing algorithm is applied. When there is no smoothing in the controller, the response time of the load cell was found to be 500ms from a drop test.

O_2/CO/CO_2 Servomex Analyzer

The output range in the manual for the Servomex gas analyzer is in milliamps instead of volts. There is a resistor on the output of the analyzer in order to supply volts to the data acquisition system. The value of the resistor was determined by running the zero gas through the analyzer and noting the corresponding voltage. The range of the analyzer stated in the manual is 4-20mA while the zero voltage for the oxygen analyzer is 2.25V and for the CO/CO_2 analyzer is 2V. Using the well-known equation V=IR, where V is volts, I is current and R is the resistance, the resistor has a value of 500Ω for the CO/CO_2 analyzer and 562.5Ω for the oxygen analyzers. Using this information, the voltage range of the CO/CO_2 analyzer is 2-10V and for the oxygen analyzers is 2.25-11.25V.

From the manual,[4] the output range of the carbon monoxide analyzer is 0-500ppm, which leads to a calibration equation of y=62.5x-125 where x is in volts and y is in ppm of CO. Following the same path, the output range of the carbon dioxide analyzer is 0-5000ppm, which leads to a calibration equation of y=6250x-1250. The inlet oxygen analyzer has a range of 0-50% oxygen while the combustion oxygen analyzer ranges from 0-25%, which leads to calibration equations of y=(50/9)x-12.5 and y=(25/9)x-6.25, respectively. The manual does not explicitly state the resolution of the instruments so 3 digits after the decimal place will be used in the calculations.

The gas transport time (i.e. the time that it takes the gas to reach the analyzer) and the response time (i.e. the time it takes for the analyzer to record 90% of the actual value after it begins to respond) of the analyzer cells were determined by testing and then were lumped into an overall time delay for the

calculations. The response time was typically a few seconds shorter than the gas transport time. The time was found by using the FPA's gas burner and stepping the mass flow rate of propylene and methane (both were used to produce an average value of the time delay for each analyzer since they produce/consume different levels of the gases for the analyzers) up and down to determine how fast the analyzers registered the change. Three tests were performed and the results were averaged into the following time delays for the Servomex gas analyzer: CO=17s; CO_2=15s; O_2=22s. These time delays are automatically taken into account in the macro (see Appendix C: FPA Data Reduction Macro).

Total Hydrocarbon (THC) Analyzer

The voltage range on the Rosemount THC analyzer is 0-5V. The analyzer has seven different specific ranges for the output of the analyzer. The current range selected (range 5) is a usable range of 0-400ppm and a maximum range of 0-800ppm when the fuel for the analyzer is a mixed fuel as opposed to pure hydrogen (mixed fuel, a hydrogen/nitrogen mix, is used in the WPI FPA). According to the manual, only half of the maximum range should be used.[5] From the information given, the calibration equation for the THC analyzer at this range is y=160x where y is the output in parts per million and x is the output in volts. The reading on the front panel of the analyzer represents the reading in percent of full scale. For example, since the span gas is 101ppm of methane and the full scale range is 0-800ppm, the instrument front panel should read 12.6%.

According to the manual,[5] the precision of the analyzer is ±1% of full scale so the data from the THC analyzer will be rounded to 3 decimal places (one decimal place past the precision of the analyzer). The time lag of the analyzer was found using the same set of tests as for the Servomex gas analyzer; the time delay is 13s. Again, the response time was typically a few seconds shorter than the gas transport time.

Smoke Meter

The smoke meter was assembled by FFT and consists of a Melles-Griot laser and two photodiodes. Since the assembly consists of parts from different manufacturers, there is no manual for the smoke meter itself.

Thus there was no precision or calibration equation given for the smoke meter. The main and compensating photodiode will be rounded to 3 decimal places. As for the calibration equation, four filters were used to ensure that the response of the smoke meter is linear and the calibration equation was determined from the zero and span points. The calibration equation for the main photodiode was determined to be y=0.821x+0.002 where x is the output in volts and y is the fraction of the light from the laser that is reaching the photodiode. This can be used to determine the smoke production rate from the sample, among other calculations.

Unfortunately, the main and compensating photodiode are adjusted using the same potentiometer on the laser and they tend to drift in different directions over time. Therefore, the calibration equation for the compensating photodiode has to be determined daily from the calibration data. The calibration equation for the main photodiode, which is the more important of the two since it represents the actual signal, is kept constant by adjusting the potentiometer.

Mass Flow Meter

The mass flow meter gives a reading of the flow rate of gas going to the FPA's gas burner. Initially, it was determined that the meter was out of calibration since the results obtained from the gas flowrate did not match the heat release rate calculated from the gas analyzers. The heat release rate from the gas flow rate was found using the following conversion.

$$1\,kW \times \frac{1\,kJ}{s \cdot 1\,kW} \times \frac{1\,kg}{50.0\,MJ} \times \frac{1\,MJ}{1{,}000\,kJ} \times \frac{1}{\rho} \times \frac{1{,}000\,L}{1\,m^3} \times \frac{60\,s}{1\,\mathrm{min}} \approx \frac{slpm}{kW}$$

The instrument was recalibrated in-house using a calibrated Teledyne Hastings flowmeter. The meter was calibrated with methane at the normal operating temperature of the FPA and the calibration equation was found to be y=4.717x where y is the flowrate of methane in standard liters per minute (slpm) and x is volts. Correction factors, which can be found in the manual,[6] need to be applied to the calibration equation if another temperature or gas is used. From the manual,[6] the resolution of the mass flow meter is 0.1% of full

scale so the data will be rounded to four decimal places (i.e. one plus the stated resolution of the instrument).

Ambient and Differential Pressure Transducer

The ambient temperature is measured by a Druck sensor and does not need to be calibrated daily. It will be obvious if the sensor malfunctions since it will not read a reasonable ambient pressure. The calibration equation is y=25x+70 where y is the ambient pressure in kPa and x is volts. The equation was determined from the original program that came with the FPA, FPACalc.

The differential pressure transducer does need to be calibrated daily but the calibration includes only a zero point (i.e. no span point) since it is a zero offset device. From information on the instrument, the voltage range is 0.05-10.05V and the range in Pascals is 0-622.7Pa. This information provides a calibration equation of y=622.7(x-0.05) where y is the differential pressure in Pa and x is the voltage.

Lamp Control

The DigiTec display meter for the lamp voltage control is not consistent or repeatable. It is suggested that the heat flux be checked with the calibration heat flux gage at the beginning of each day or whenever the heat flux needs to be adjusted.

Uncertainty

Heat Release Rate

FPA tests were done with methane, propylene and acetone, as well as PMMA, and the heat release rate was calculated using three different methods. The ASTM E 2058[2] and the Beaulieu[7] methods are based on carbon dioxide generation while the Parker[8] method is based on oxygen consumption. All three methods can be formulated as either fuel specific or generic (i.e. published average values). The effective heat of

combustion was found by dividing the cumulative heat release rate by the total mass lost. This effective heat of combustion was compared to the chemical heat of combustion (equal to the published total heat of combustion corrected for the published smoke yield); this method is specified as a heat release rate calibration procedure in ASTM E 2058, using acetone as a model material. The standard states that the effective heat of combustion, calculated using the fuel specific heat release rate equation, must be within ±5% of the published value for acetone.[2] As can be seen from Table 6, the accuracy (defined as the deviation of the average value from all of the tests as compared to the published value; all of the reported uncertainties are full scale as opposed to ± half scale) in the acetone heat of combustion, calculated from the fuel specific equation, was found to be 7.9%. Therefore, the heat release rate for the FPA was found to be calibrated according to ASTM E 2058. Effective heat of combustion accuracies determined using the other methods of calculating heat release rate are also shown in Table 6 to demonstrate that there is not a significant difference between the results from the different methods.

Table 6: Results from FPA[2] Calibration Tests. All of the reported uncertainties are full scale as opposed to ± half scale. EHC=Effective Heat of Combustion; G=Gas; L=Liquid; S=Solid.

EHC--Fuel Specific 2058						
Material	**Phase**	**# Tests**	**Accuracy (%)**	**Precision (%)**	**Avg Deviation (kW)**	**Max Deviation (kW)**
Propylene	G	6	-1.2%	+/-2.5%	0.3	<0.5 *
Methane	G	6	8.6%	+/-1.5%	0.4	<0.5 *
Acetone	L	4	7.9%	+/-5%	0.3	<0.5
PMMA	S	3	-2.9%	+/-2.5%	0.2	<0.5
EHC--Parker						
Material	**Phase**	**# Tests**	**Accuracy (%)**	**Precision (%)**	**Avg Deviation (kW)**	**Max Deviation (kW)**
Propylene	G	6	5.0%	+/-1.5%	0.8	<1*
Methane	G	6	11.0%	+/-2%	0.7	<1 *
Acetone	L	4	9.0%	+/-5%	0.5	<0.5
PMMA	S	3	-1.4%	+/-2%	0.2	<0.5
EHC--Beaulieu						
Material	**Phase**	**# Tests**	**Accuracy (%)**	**Precision (%)**	**Avg Deviation (kW)**	**Max Deviation (kW)**
Propylene	G	6	4.3%	+/-2.5%	0.4	<0.5*
Methane	G	6	14.2%	+/-0.5%	0.6	<1 *
Acetone	L	4	12.2%	+/-5%	0.4	<0.5
PMMA	S	3	3.9%	+/-3%	0.2	<0.5

In Table 6, the number listed as the accuracy in kW is the average or maximum value that the heat release rate trace calculated from the ASTM E 2058,[2] Parker[8] and Beaulieu[7] equations deviates from the reference heat release rate trace (the mass loss rate multiplied by the published chemical heat of combustion). There is an asterisk in the last column for both propylene and methane because both of these gases were coming

from the FPA's gas burner. The mass flow rate of the gas was stepped up and down during the experiment, which increased the heat release rate of the fire. In the case of both propylene and methane, it was found that the absolute difference between the calculated and the reference heat release rate traces got larger as the mass flow rate was increased.

The absolute accuracy in Table 6 is listed in kW even though units of kW/m^2 are generally used. Since the propylene and the methane are in the gaseous state and are coming through the FPA's gas burner, there is no specimen surface to divide by to achieve units of kW/m^2. Since the average specimen surface of the composites is $0.007m^2$, the uncertainty in kW/m^2 is an average of $45kW/m^2$ and a maximum of $70kW/m^2$. These uncertainties are determined by averaging all of the uncertainties in the table, except for the cases in which the maximum deviation was <1 instead of <0.5. These uncertainties are believed to be erroneously high since the gas burner was turned to a high heat release rate during the test, which increased the uncertainty. The average heat release rate uncertainty of $45kW/m^2$ will be used to evaluate differences between the composites in this study.

Time to Ignition, Burn Duration and Mass Loss Rate

The analysis for the uncertainty in the time to ignition, burn duration and mass loss rate for the FPA is based on three PMMA tests. A sample set of three is believed to be sufficient in this case because the FPA standard calls for three identical tests to be performed to correctly determine other properties.[2] Since the uncertainty was based on only three tests, the value represents a maximum uncertainty from the three tests. The burn duration is defined as the time that there is a fully developed flame cone on the sample surface. From these tests, the uncertainty in the time to ignition and the burn duration were found to be 9s and 101s, respectively. The uncertainty in the mass loss rate was found to be 17mg/s. These uncertainties are full scale (as opposed to ± half scale).

The uncertainty in the time to ignition given above is based on visual observations, however the time to ignition can also be determined by operator independent ignition using the 2^{nd} derivative of the mass history (see Appendix A: Operator Independent Ignition) and from the traces from the gas analyzers (O_2, CO, CO_2 and THC). In this study, the main focus was on the visual time to ignition and the operator

independent time to ignition, although the time to ignition for the other methods was tabulated for some tests (see file Comparison of Time to Ignition.xls).

In order to determine the uncertainty of the 2nd derivative time to ignition relative to the visual time to ignition, both composite materials and PMMA were studied, as shown in Table 7.

Table 7: Comparison of Time to Ignition from Visual Observations and 2nd Derivative of Mass History.

Test	Heat Flux (kW/m^2)	tig from 2nd derivative (s)	visual tig (s)	visual - 2nd der tig (s)
1A 20060124	50	121.5	127	5.5
1A 20060314	50	121.5	123.5	2
1B 20060126	50	145.5	150	4.5
1B 20060314	50	137.5	145	7.5
1C 20060126	50	135	138.5	3.5
1C 20060314	50	156.5	158.5	2
PMMA 20051026	50	59	48	-11
PMMA 20051101	50	73	57	-16
PMMA 20051108	50	52	51	-1
1A 20060914 Instrumented	50	118	111.5	-6.5
1A 20061006 Diff Radii	50	130.5	130.5	0
1C 20060914 Instrumented	50	113.5	128.5	15
1C 20061006 Diff Radii	50	156.5	157.5	1
PMMA 20060912 Instrumented	50	37	36	-1
PMMA 20060914 Instrumented	28	97.5	96.5	-1
			Average Difference	0.3

From the table, it can be seen that there is no significant difference, on average, between the visual ignition and the operator independent ignition time from the 2nd derivative.

b Parameter

The b parameter[9] is an important flame spread parameter that can be used to correlate bench-scale tests to room/corner test results,[10] as discussed in Appendix G: Material Properties. The b parameter depends on the heat release rate, time to ignition and burn duration. Given the uncertainties in these parameters, the equation for the propagation of uncertainty[11] was used to determine that the uncertainty in the b parameter is approximately 0.45 full scale (±0.225).

Files for Reference

For additional instrumentation information, including details on how to update the calibration equation for the load cell, see Instrument Info.doc in the FPA Documents folder. For tests from which time delays were derived, see Time Delays folder (includes delays for gas analyzers and load cell).

References

[1] de Ris, J.L. and Khan, M.M., "A sample holder for determining material properties," *Fire and Materials*, 24, 219-226 (2000).

[2] Standard Methods of Test for Measurement of Synthetic Polymer Material Flammability Using a Fire Propagation Apparatus (FPA), ASTM E 2058-03, ASTM, 100 Barr Harbor Drive, West Conshohocken, PA, U.S.

[3] Operator's Manual for INFINITY Strain/DC Current/Voltage Meter, Newport Electronics, Santa Ana, CA, 2002.

[4] Configuration, Operation and Installation Manual for the Servomex Xentra Analyzer, Sugar Land, Texas.

[5] Instruction Manual for the Model 400A Hydrocarbon Analyzer, Rosemount Analytical, Inc., Process Analytic Division, Orrville, OH, 2002.

[6] Instruction Manual for the MKS Type M100B Mass-Flo Controller and M10MB Mass-Flo Meter, MKS, Andover, MA, 1999.

[7] Beaulieu, P.A. and Dembsey, N.A., "Enhanced Equations for Carbon Dioxide and Oxygen Calorimetry," *Proceedings of the 9th International Fire and Materials Conference,* p.49 (2005).

[8] Parker, W.J., "Calculations of the Heat Release Rate by Oxygen Consumption for Various Applications," National Bureau of Standards Report # NBSIR 81-2427 (1982).

[9] Cleary, T. and J. Quintiere, "A Framework for Utilizing Fire Property Tests," *Fire Safety Science, Proceedings of the Third International Symposium,* International Association of Fire Safety Science (IAFSS), Scotland, U.K., Cox and Langford Editors, Elsevier Applied Science London and New York, July 8-12 (1991) 647-656.

[10] Beyler, C., S. Hunt, B. Lattimer, N. Iqbal, C. Lautenberger, N. Dembsey, J. Barnett, M. Janssens, S. Dillon and A. Grenier, "Prediction of ISO 9705 Room/Corner Test Results," US Department of Transportation, Report No. R&DC-215-99, 1999.

[11] Coleman, H. W. and W. G. Steele, Experimentation and Uncertainty Analysis for Engineerings, 2nd Edition, New York: John Wiley & Songs., Inc., 1999.

Appendix C: FPA Data Reduction Macro

Introduction

Originally, the FPA came with a program for data reduction called FPACalc. However, this program did not provide raw volts for further data analysis. Since the Agilent data acquisition system was available in the FPA, the Agilent Benchlink data acquisition program was used to obtain raw volts from the system. However, this system was not entirely suitable for research work since it can only produce data at a rate of one time per second (if all of the necessary channels are included) and it cannot provide instructions to the user as to the operation of the FPA. The industry standard for data acquisition, National Instrument's LabView, was then installed and a virtual instrument, written by WPI Student Todd Hetrick, was created to guide the user through the calibration and test procedures and then to produce raw data.

Since raw data is produced by the data acquisition system, a data reduction macro was created in Microsoft Excel in order to turn the raw volts into useful engineering data. This appendix details how the data reduction macro works as well as how to successfully run the macro.

FPA Data Reduction Workbook

The file FPA Data Reduction.xls contains all of the macros needed to reduce the data as well as instructions on how to run the macro, headers for all of the columns and blank graphs for all of the data. All of the macros can be accessed from this workbook, including the driver macro and all of the submacros. The next section will detail the data reduction macro.

The Data Reduction Macro

The main driver macro is FPADataReduction and starting this macro will automatically run all others, which is its only function; the driver macro consists only of calls to submacros. This design of the main

macro allows for clearer interpretation of the steps to the data reduction and for easier adjustments to the submacros. The subsections below detail the function of each of the submacros; the name of the submacro is the heading of the subsection.

FillInTime

This macro copies the time column from the Test Data worksheet and pastes it into the appropriate worksheets. The purpose of this action is to provide a leftmost column in each worksheet that can be used to automatically fill in the equations to the length of the test.

TruncateData

As discussed in Appendix B: Fire Propagation Apparatus Calibration, all of the data must be rounded to a reasonable number of digits. If the data is not rounded, it will cause additional uncertainty in the calculated data. The truncation is performed on the raw data (i.e. before the calibration equations are applied) using the round() function in Excel.

CalibrationEquations

After the data is truncated, the calibration equations need to be applied to turn the raw volts into meaningful data. The calibration equations that are used for each instrument can be found in Appendix B: Fire Propagation Apparatus Calibration. For the compensating photodiode, the calibration equation is changed daily while all other calibration equations are held constant. Unfortunately, the main and compensating photodiode are adjusted using the same potentiometer on the laser and they tend to drift in different directions over time. The calibration equation for the main photodiode, which is the more important of the two since it represents the actual signal, is kept constant by adjusting the potentiometer.

OxygenConditioning

Since the FPA is not based on oxygen consumption calorimetry, the oxygen analyzer has a higher uncertainty than that used in the Cone Calorimeter. The oxygen analyzer needs to be both drift corrected and smoothed in order to provide a clean data trace for use in the heat release rate equations. A linear drift correction is used based on a 20s average at the beginning and end of the trace. A simple 10 point smoothing algorithm was used to smooth the trace.

Before the drift correction and the smoothing algorithm are applied, a typical curve of the combustion oxygen analyzer (from 1A at 50kW/m^2 in the FPA on 20061201) is shown below.

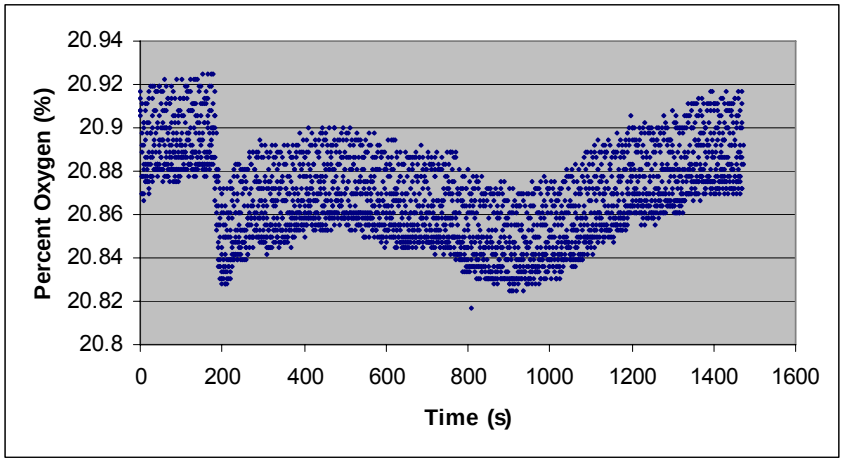

Figure 49: Example of the Combustion Oxygen Analyzer Curve Before the Drift Correction and Smoothing Algorithm is Applied

After the correction and smoothing is applied, the curve is transformed into the following graph.

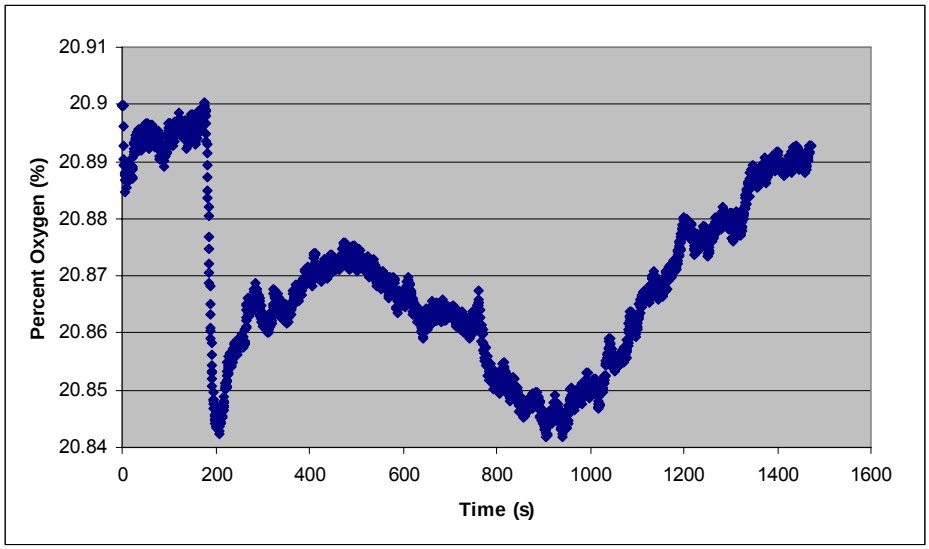

Figure 50: Example of the Combustion Oxygen Analyzer Curve After the Drift Correction and Smoothing Algorithm is Applied

When smoothed traces such as that shown in Figure 50 are used in the oxygen consumption heat release rate equations, the heat release rate will match those determined from the carbon dioxide generation based techniques.

It is unclear at this time why the oxygen analyzer drifts and why it is so noisy. See Appendix D: Secondary FPA Checks for additional discussion on progress with the oxygen analyzer.

AirDensity

First, this macro moves all of the calibrated data columns from the calibrated data worksheet to the calculations worksheet so that they will be easily accessible for the equations. Next, the air density macro calculates the air density from the following equation:

$$\rho = \frac{353 \cdot \frac{P_{atm}}{101}}{T_d} \text{ [kg/m}^3\text{]}$$

Where P_{atm} is the atmospheric pressure (the absolute pressure column) [kPa] and T_d is the gas temperature in the test section duct (the duct temperature column) [K]. The constant 101 is the atmospheric pressure in kPa and 353 is $\rho \cdot T_d$ for air at an atmospheric pressure of 101kPa.[1]

FlowCoefficient

The macro creates the global variable, k, for the flow coefficient in the duct and defines it. The flow coefficient was defined as 0.62 in FPACalc and this is the value that is used in the equations. The pitot tube used is the averaging type.

AverageDPT

The macro creates the global variable, DPT, and defines it as the average of the readings from the differential pressure transducer over the entire test. The trace from the differential pressure transducer is very noisy due to turbulence in the duct and will also cause calculated values that involve the differential pressure transducer to be noisy. Since the average value does not change over the length of the test, it is much easier and more efficient to average the values instead of using a smoothing algorithm.

VolumetricFlow

The volumetric flow rate in the duct, V, is defined as[1]:

$$V = A_d \cdot k \cdot \frac{\sqrt{\frac{2 \cdot \Delta p_m \cdot T_d}{353}}}{\sqrt{\frac{P_{atm}}{101}}} \text{ [m}^3\text{/s]}$$

Where A_d is the area of the duct cross section (where the diameter of the duct is 0.15m from FPACalc) [m^2], k is the flow coefficient defined above [-], $\Delta\rho_m$ is the average reading of the differential pressure

transducer over all scans [Pa], T_d is the duct temperature (as measured by a thermocouple in the duct) [K] and P_{atm} is the atmospheric pressure (as measured by the ambient pressure transducer) [kPa]. The constant 101 is the atmospheric pressure in kPa and 353 is $\rho \cdot T_d$ for air at an atmospheric pressure of 101kPa.

There is a line of code in the macro as follows:

```
If IsEmpty(ActiveCell) Then Exit Sub
   Range(ActiveCell, ActiveCell.Offset(0, -1).End(xlDown).Offset(0, 1)).FillDown
```

This line of code autofills the volumetric flow rate equation to the appropriate length of the test, using the column to its left as a reference. This line of code appears in many of the other macros as well.

MassFlowRate

The macro applies the following equation to calculate the mass flow rate of the gases in the duct[1]:

$$m_d = V \cdot \rho \ \text{[kg/s]}$$

Where V is the volumetric flow rate in the duct [m^3/s] and ρ is the air density [kg/m^3].

SpecificHeat

The macro calculates the specific heat of air in the duct using the following equation[1]:

$$c_p = 1 + 1.34 \times 10^{-4} \cdot T_d - \frac{2590}{T_d^2} \ \text{[kJ/kgK]}$$

Where T_d is the duct temperature (as measured by a thermocouple in the duct) [K].

ConvectiveHRR

The macro calculates the convective heat release rate of the fire using the following equation[1]:

$$Q_c = m_d \cdot c_p \cdot (T_d - T_a) \text{ [kW]}$$

Where m_d is the mass flow rate in the duct as defined above [kg/s], c_p is the specific heat of air in the duct as defined above [kJ/kgK], T_d is the duct temperature (as measured by a thermocouple in the duct) [K] and Ta is the baseline duct temperature (defined as the first 20s of the duct thermocouple trace) [K].

SECwithMandC and SECwithMonly

These macros calculate the smoke extinction coefficient (SEC) using the following equation:[2]

$$D = \frac{\ln(\frac{I_a}{I})}{L} \text{ [1/m]}$$

Where L is the path length of the laser, which is the diameter of the duct (0.15m) in this case. I_a/I can be calculated using both the main (M) and the compensating (C) photodiode (i.e. I_a/I= C/M) or with just the main photodiode (i.e. I_a/I=1/M). The only difference between the macros SECwithMandC and SECwithMonly is that they calculate the expression I_a/I differently.

SFPEfwithMandC and SFPEfwithMonly

The volume fraction of smoke is calculated using the following equation:[3]

$$f_s = \frac{D \cdot \lambda}{\Omega} \text{ [-]}$$

Where D is the smoke extinction coefficient defined above [1/m], λ is the wavelength of the laser [m] and Ω is the coefficient of particulate extinction taken as 7.0 [-] from Tewarson.[3] The wavelength of the laser is 0.6328μm.[4] The only difference between the macros SFPEfwithMandC and SFPEfwithMonly is the value of the smoke extinction coefficient that is used (i.e. whether the compensating photodiode is included in the smoke extinction coefficient or not).

SFPESmokeGenMandC and SFPESmokeGenMonly

The smoke generation rate of smoke is calculated using the following equation:[3]

$$\dot{G}_s'' = \frac{f_s \cdot V \cdot \rho_s}{A} \text{ [g/(m}^2\text{s)]}$$

Where f_s is the volume fraction of smoke as defined above [-], V is the volumetric flow rate in the duct as defined above [m^3/s], ρ_s is the density of smoke given as 1.1E6g/m^3 from Tewarson[3] and A is the total area of the material burning (i.e. the sample surface area) [m^2]. The only difference between the macros SFPESmokeGenMandC and SFPESmokeGenMonly is the value of the volume fraction of smoke that is used (i.e. whether the compensating photodiode is included in the smoke extinction coefficient or not).

MLR

The mass loss rate is derived using the equation in ASTM E 1354:[5]

$$-\left[\frac{dm}{dt}\right]_i = \frac{-m_{i-2} + 8m_{i-1} - 8m_{i+1} + m_{i+2}}{12\Delta t} \text{ for 1<i<n-1 [g/s]}$$

Where m is the value of the mass history at the appropriate relative times [g] and Δt is the time step (typically 0.5s for FPA tests). The mass loss rate derived from this equation is much too noisy to be very useful. Therefore, the mass loss rate curve is smoothed using Fast Fourier Transform in another macro (see Appendix A: Operator Independent Ignition for more information and a description of the macros).

SmokeYields

Two different average smoke yields are calculated using the main and compensating photodiode or the main photodiode only. They are calculated using the same equation, shown below:[3]

$$\gamma_s = \frac{A \cdot \sum_{n=t_0}^{n=t_f} \dot{G}_s''(t_n)\Delta t_n}{M_{loss}} \quad [-]$$

Where A is the total area burning (i.e. the sample surface area) [m^2], $G_s(t_n)$ is the smoke generation rate at the current time [g/m^2s], Δt_n is the time step (typically 0.5s for FPA tests) and M_{loss} is the total mass lost [g]. The constants are named Smoke Yield (M) and Smoke Yield (M&C) in the macro.

VolFractionCOCO2

Since the analyzer reading is in ppm and the equations require a volume fraction of CO and CO_2, this macro simply divides the analyzer readings by 10^6 to get the volume fractions of the gases. Volume fraction is equal to mole fraction for gases.[6]

COandCO2Gen

The generation rates of CO and CO_2 are, respectively:[1]

$$G_{CO} = A_d \cdot K \cdot \sqrt{\frac{P_{atm}}{101}} \cdot \sqrt{2 \cdot \frac{353 \cdot \Delta p_m}{T_d}} \cdot 0.967 \cdot X_{CO} \text{ [kg/s]}$$

$$G_{CO2} = A_d \cdot K \cdot \sqrt{\frac{P_{atm}}{101}} \cdot \sqrt{2 \cdot \frac{353 \cdot \Delta p_m}{T_d}} \cdot 1.519 \cdot X_{CO2} \text{ [kg/s]}$$

Where A_d is the cross sectional area of the test section duct (where the diameter of the duct is 0.15m from FPACalc) [m^2], k is the flow coefficient defined above [-], P_{atm} is the atmospheric pressure (as measured by the ambient pressure transducer) [kPa], $\Delta\rho_m$ is the average reading of the differential pressure transducer over all scans (Pa), X_{CO} is the mole fraction of CO [-] and X_{CO2} is the mole fraction of CO_2 [-]. The constants 0.967 and 1.519 are the ratios of the molecular weight of carbon monoxide (28.01g/mole) and carbon dioxide (44.01g/mole), respectively, to that of air (28.97g/mole).

Generic2058ChemHRR

The macro calculates the heat release rate using the following generic equation from ASTM E 2058:[1]

$$Q_{chem} = \frac{13300 \cdot (G_{CO2} - G^0_{CO2}) + 11100 \cdot (G_{CO} - G^0_{CO})}{A} \text{ [kW/m}^2\text{]}$$

Where A is the total area burning (i.e. the sample surface area) [m^2], G_{CO2} and G_{CO} are the generation rates of carbon dioxide and carbon monoxide, respectively, as defined above and the superscript 0 denotes the baseline generation rates of CO and CO_2 (an average of the first 20 seconds). The numbers 13300 kJ/kg(CO_2) and 11100 kJ/kg(CO) represent the reported average heat of combustion per unit mass carbon monoxide or carbon dioxide for most specimens.

COandCO2Yield

This macro creates and defines constants for the stoichiometric carbon monoxide and carbon dioxide yields. The stoichiometric CO and CO_2 yield are given by COY = 2.33*X_c and CO_2Y = 3.67*X_c where X_c is the mass fraction of carbon in the fuel.[7] See Appendix G: Material Properties for information regarding the mass fraction of carbon in the materials used in this study.

FuelSpecific2058ChemHRR

T he macro calculates the heat release rate using the following fuel specific equation from ASTM E 2058:[1]

$$Q_{chem} = \frac{\frac{\Delta H_T}{k_{CO_2}} \cdot (G_{CO_2} - G_{CO_2}^0) + \frac{\Delta H_T - \Delta H_{CO} \cdot k_{CO}}{k_{CO}} \cdot (G_{CO} - G_{CO}^0)}{A} \quad [\mathrm{kW/m^2}]$$

Where ΔH_T is the net heat of complete combustion of the fuel (determined from testing at Schwarzkopf MicroLabs, see Appendix G: Material Properties for more information) [kJ/kg(fuel)], ΔH_{CO} is the heat of combustion of CO [kJ/kg(CO)],[8] k_{CO} and k_{CO2} are the stoichiometric yield of carbon monoxide and carbon dioxide, respectively, as defined above [-], A is the total area burning (i.e. the sample surface area) [m^2], G_{CO} and G_{CO2} are the generation rates of carbon monoxide and carbon dioxide, respectively, as defined above [kg/s] and the superscript 0 denotes the baseline generation rates of CO and CO_2 (an average of the first 20 seconds).

This equation differs from the generic ASTM E 2058 equation detailed above since the properties of the material being studied are used in the equation (i.e. fuel specific) and not average values from the literature (i.e. generic). Heat release rate is calculated in this way as well as using more advanced equations (see Parker and Beaulieu macros later in this section) in order to determine if they all produced the same results and to better develop an uncertainty in the heat release rate. All of the methods produce the same results, within the uncertainty.

VolFractionO2

This macro calculates the volume fraction of the reading from the oxygen analyzers by multiplying the value by 0.01. The inlet oxygen is defined as an average of the first 20s of the combustion oxygen analyzer baseline. This was done since the two oxygen analyzers do not always start off at the exact same value, which would cause an erroneous heat release rate calculation if the value from the inlet oxygen analyzer were used. As mentioned above, the oxygen analyzers on the FPA are unfortunately not of very good resolution, especially as compared to the oxygen analyzer on the Cone, since the FPA is based on carbon dioxide generation calorimetry instead of oxygen consumption calorimetry.

ParkerO2DepletionFactor

The Parker oxygen depletion factor is needed for the Parker heat release rate equation and is defined as:[9]

$$\phi = \frac{X_{O_2}^0 \cdot (1 - X_{CO_2} - X_{CO}) - X_{O_2} \cdot (1 - X_{CO_2}^0 - X_{CO}^0)}{X_{O_2}^0 \cdot (1 - X_{CO_2} - X_{CO} - X_{O_2})} \quad [-]$$

Where X represents the mole fraction of the gas in the subscript. The superscript 0 represents a baseline value, calculating using the first 20s of the trace. The variables with no superscript represent the exhaust gases (in mole fraction).

VolumetricFlowIntoSystem

For the Parker and Beaulieu equations, the volume flow rate of the air into the system (i.e. entering the duct) needs to be known. This includes both the inlet air flow and the entrained air and is related to the volumetric flow rate in the duct:[9]

$$V_A = \frac{V}{1 + (\alpha - 1) \cdot \phi} \quad [m^3/s]$$

where V is the volumetric flow rate in the duct as defined above [m^3/s] , α is the molar expansion factor for the fraction of air that was depleted of its oxygen (use 1.105 as a generic value) [-] and φ is the Parker O_2 depletion factor as defined above [-].

ParkerfFactor

The f factor is needed in Parker's heat release rate equation and is defined below:[9]

$$f = \frac{1-\phi}{2\phi} \cdot \frac{X_{CO}}{X_{O_2}} \text{ [-]}$$

Where φ is the Parker oxygen depletion factor as defined above [-] and X_{CO} and X_{O2} are the mole fractions of carbon monoxide and oxygen, respectively.

ConstantsforParkerGeneric

The macro creates and defines the generic values for the net heat of complete combustion per unit mass of oxygen consumed and the net heat of complete combustion per unit volume of oxygen consumed. Both of these variables are needed to calculate the generic Parker heat release rate (i.e. not fuel specific). The generic net heat of complete combustion per unit mass of oxygen consumed, E, is an average of 13100kJ/kg(O_2) for a range of materials.[3] The net heat of complete combustion per unit volume of oxygen consumed, E', is defined in Parker as:[9]

$$E' = E \cdot \rho_o \cdot \frac{W_{O_2}}{W_{AIR}} \text{ [kJ/m}^3\text{(O}_2\text{)]}$$

Where E is the net heat of combustion per unit mass of oxygen consumed as defined above [kJ/kg(O_2)] , ρ_0 is the density of normal dry air at standard temperature and pressure (equal to 1.19kg/m^3), W_{O2} is the

molecular weight of oxygen (equal to 0.032kg/mole) and W_{AIR} is the molecular weight of air (equal to 0.029kg/mole). The equation results in a value of about 17202kJ/m^3(O_2).

ParkerGenericHRR

Since the constants are defined for the generic Parker heat release, it can now be calculated from:[9]

$$Q = \frac{(E' - f(E'' - E')) \cdot X_{O_2}^0 \cdot \phi \cdot V_A}{A} \text{ [kW/m}^2\text{]}$$

Where E' is the generic net heat of complete combustion per unit volume of oxygen consumed defined above as 17202kJ/m^3(O_2), f is the Parker f factor defined above [-], E" is the heat release per unit volume of O_2 consumed in the burning of CO (equal to 23.1MJ/m^3 at 25°C),[9] $X_{O_2}^0$ is the initial mole fraction of the oxygen (from the inlet oxygen analyzer trace) [-], φ is the Parker oxygen depletion factor defined above [-], V_A is the volumetric flow rate into the duct as defined above [m^3/s] and A is the total area burning (i.e. the sample surface area) [m^2].

The value of the Parker heat release rate is also reduced by 1% to account for the error induced by not taking the water in the gas sample into effect in the equation.[10]

ConstantsforParkerHRR

This macro is very similar to ConstantsforParkerGeneric except that the numbers will no longer be constant and instead will depend upon the material properties. The net heat of complete combustion per unit mass of oxygen consumed is defined as the net heat of complete combustion per unit mass of fuel divided by the oxygen fuel mass ratio [kg(O_2)/kg(fuel)]. Both of these variables are material properties that were determined from heat of combustion and elemental analysis testing of the resins used in the composites; more information about the testing that was performed at Schwarzkopf MicroLabs is detailed in Appendix G: Material Properties. The net heat of complete combustion per unit volume of oxygen consumed is

calculated in the same way as in the ConstantsforParkerGeneric macro, except using the fuel specific net heat of complete combustion per unit mass of oxygen consumed.

ParkerHRR

Since the constants are now defined for the fuel specific Parker heat release, it can be calculated using the same equation as in the ParkerGenericHRR macro. However, the fuel specific values for the net heat of complete combustion per unit mass and per unit volume of oxygen will be used instead of the generic values. Everything else is kept the same.

ConstantsforPABEqs

The macro defines two constants that are necessary for the Beaulieu equations: the net heat of complete combustion of the fuel per unit volume CO_2 generated, F', and the heat released per unit volume CO_2 generated in the burning of CO to CO_2, F".[10]

The heat of combustion of the fuel per unit volume CO_2 generated is defined as:[10]

$$F' = \Delta h_{CO_2} \cdot \frac{MW_{CO_2}}{MW_a^0} \cdot \rho_a^0 \qquad [\text{kJ/m}^3]$$

Where Δh_{CO2} is the heat of combustion of the fuel per unit mass CO_2 generated, MW_{CO2} is the molecular weight of carbon dioxide (44g/mole), MW_a^0 is the molecular weight of the incoming gas (initially just air) (28.97 g/mole) and ρ_a^0 represents the density of the incoming gas. To find the heat of combustion of the fuel per unit mass CO_2 generated, the net heat of combustion of the fuel per unit mass fuel is divided by the stoichiometric yield of CO_2, as defined above. The baseline density is an average of the first 20 values listed in the air density column.

The heat released per unit volume CO_2 generated in the burning of CO to CO_2 is defined as:[10]

$$F'' = \Delta h_{CO_2}^{CO \to CO_2} \cdot \frac{MW_{CO_2}}{MW_a^0} \cdot \rho_a^0 \quad [\text{kJ/m}^3]$$

Where $\Delta h_{CO_2}^{CO \to CO_2}$ is the heat of combustion per unit mass CO_2 generated in the burning of CO to CO_2 [kJ/kg(CO_2)] and all other variables are as defined for F'. The heat of combustion for carbon monoxide per unit mass CO is 10.1MJ/kg(CO). This needs to be converted to units of kJ/kg(CO_2). The chemical reaction for the burning of carbon monoxide to carbon dioxide is:

$$CO + 0.5O_2 + 1.88N_2 \Rightarrow CO_2 + 1.88N_2$$

The ratio of interest is the number of moles of CO consumed to the number of moles of CO_2 generated, which is equal to one. The $\Delta h_{CO_2}^{CO \to CO_2}$ variable can then be found using the following equation:

$$\Delta h_{CO_2}^{CO \to CO_2} = \Delta H_{CO} \cdot \frac{MW_{CO}}{MW_{CO_2}} \cdot 1$$

This equation and its result will stay the same no matter what fuel is being burnt. This equation is simply substituted into the equation for F" in the macro.

This macro also rounds all of the constants for the heat release rate equations to three decimal places and pastes them as values back into the worksheet.

PABCO2Generation

Similar to the Parker oxygen depletion factor, the Beaulieu carbon dioxide generation based heat release rate equations require a carbon dioxide generation factor, defined as:[10]

$$\theta = \frac{\frac{X_{CO_2} \cdot (1 - X_{O_2}^0)}{(1 - X_{O_2} - X_{CO})} - X_{CO_2}^0}{X_{CO_2}^0 \cdot (1 - \frac{X_{CO_2}}{(1 - X_{O_2} - X_{CO})})} \text{ [-]}$$

Where X represents the mole fraction of the gas in the subscript. The superscript 0 represents a baseline value, calculating using the first 20s of the trace. The variables with no superscript represent the exhaust gases (in mole fraction).

PABHRR

Since the constants are defined for the Beaulieu heat release equation, it can now be calculated from:[9]

$$Q_{actual} = \frac{F' \cdot \theta \cdot V_A \cdot X_{CO_2}^0 \cdot (1 - \frac{1+\theta}{\theta} \cdot \frac{X_{CO}}{X_{CO_2}} \cdot (\frac{F''}{F'} - 1))}{A} \text{ [kW/m}^2\text{]}$$

Where F' is the heat of combustion of the fuel per unit volume CO_2 generated [kJ/m^3(CO_2)], F" is the heat released per unit volume CO_2 generated in the burning of CO to CO_2, θ is the carbon dioxide generation factor [-], V_A is the volumetric flow rate into the duct as defined above [m^3/s], X_{CO2}^0 is the baseline mole fraction of the carbon dioxide (taken as the first 20s of the trace), X_{CO} and X_{CO2} are the mole fractions of the carbon monoxide and carbon dioxide, respectively, and A is the total area burning (i.e. the sample surface area) [m^2].

The value of the Beaulieu heat release rate is also reduced by 1% to account for the error induced by not taking the water in the gas sample into effect in the equation.[10]

HRRReference

The heat release rate calculated using the mass loss rate can be used as a reference heat release rate because it depends only upon the mass loss rate and the heat of combustion of the material, which was measured for the resins in the composites. The smoothed mass loss rate is multiplied by the heat of combustion and then the product is divided by the sample surface area to get units of kW/m^2.

EHC

The effective heat of combustion is determined for all of the methods of calculating heat release rate in order to compare them against one another and to get a better idea of the accuracy of each method. The effective heat of combustion is defined as:[1]

$$EHC = \frac{Q \cdot \Delta t \cdot A}{M_{loss}} \text{ [kJ/kg]}$$

Where Q is the cumulative heat release rate from one of the methods [kW/m^2], Δt is the time step (typically 0.5s in the FPA) [s], A is the total area burning (i.e. the sample surface area) [m^2] and M_{loss} is the total mass lost [g].

After the macro is run, the range over which the cumulative heat release rate is calculated needs to be adjusted to incorporate only the time during which there is a flame cone on the sample surface. If there is no flame cone, the time should be adjusted from time of ignition to flame out. The mass loss needs to be adjusted to incorporate only the mass lost during the time period over which the effective heat of combustion is determined (see Instructions section in this appendix).

EHCPercentOffCalcs

This macro determines how much the calculated effective heat of combustion differs from the material's known (or assumed) heat of combustion from the following equation:

$$\%Off = 100\% - (\frac{\Delta H_T}{EHC}) * 100 \text{ [\%]}$$

Where ΔH_T is the known (or assumed) heat of combustion and EHC is the effective heat of combustion calculated as defined above.

NaNMFMHFG

This macro simply puts the term "NaN" (stands for Not a Number) into the methane flow meter and calibration heat flux gage columns since these two instruments are typically not used during the test. They should stand out as being nonsensical data so that it is not confusing to anyone looking at the data. If the data needs to be viewed in the analysis of a future test, this macro could simply be commented out in the driver macro by putting an apostrophe before the call to the function.

Fast Fourier Transform

The macros that make up the Fast Fourier transform are run separately than the main driver macro because the user needs to input data based on the 2nd derivative power spectrum. See Appendix A: Operator Independent Ignition for further discussion on the Fast Fourier transform macros. A macro called SecondDerCalc was also created to determine the 2nd derivative of the mass history from the first derivative of the mass history, using the same equation that was used to calculate the 1st derivative of the mass history in the MLR macro.

Instructions

There are step-by-step instructions for successfully running the macro at the beginning of the file FPA Data Reduction.xls and they will be discussed here in detail with additional instruction if necessary.

1.) Fill out calibration information from the day of the test in the "Calibration Information" worksheet

In the Excel worksheet that is output from the Test VI, there is information from the calibration that should be input into the data reduction worksheet so that the data is available if it is needed. The data is used to calculate the daily calibration equation for the compensating photodiode.

2.) Fill out information in the "Test Information" worksheet

Information in the Test Information worksheet includes the time of the start of the test, dimensions of the sample, some material properties and relevant test times (e.g. time to ignition, time to start of flame cone, time to flame out, etc.). This needs to be filled out as completely as possible since many of the parameters are used in various calculations.

3.) Fill out "Observations" worksheet with observations during and after burning, any instrumentation and any special notes about the data

Observations should be made during the test as well as after the test, including observations about the sample itself. Any instrumentation, including surface thermocouples, infrared thermometer, in-depth and back face thermocouples and heat flux gages should be explained in detail in the Observations worksheet. The description of the surface and back face thermocouples should include a measurement of how far the bead is from the edge of the sample. The description of the in-depth thermocouple should include how far the thermocouple hole is from the surface, whether the hole is at an angle and if the hole is tight or loose. The heat flux gage should include a measurement of how far the gage is from the edge of the sample. Special notes about the data may include instrumentation failure during the test, explanation of jumps in the data or any other comments as deemed appropriate.

4.) Cut and paste the raw voltages from the test into the "Test Data" worksheet.

All of the raw data, excluding any instrumentation, should be copied from the VI output file into the Test Data worksheet of the file FPA Data Reduction.xls.

5.) Run the macro entitled "FPADataReduction"

6.) Adjust the definition of the DPT constant, the smoke yields and the oxygen conditioning constants to reflect the length of the test

Unfortunately, a way to automatically update the constants to reflect the length of the test was not determined in this project. This might be able to be accomplished with higher level macros that are not known to the author. The DPT constant and smoke yields are averages over the entire test. The oxygen conditioning constant is for the linear drift so an average of the last 20s of the test is needed to determine the drift correction.

7.) Fix "Final O2" column in the "Oxygen Conditioning" worksheet by filling the 1st 5 spots with the 6th data point and the last five with the 6th to last data point. Copy and paste the values to the "Calculations" WS.

Since the oxygen conditioning requires a 10 point smooth of the data, as discussed in the OxygenConditioning macro subsection above, the first and last five data points of the smooth and drift corrected oxygen trace will be nonsensical. Therefore, the 6^{th} and 6^{th} to last data points are used to fill in the first and last five data points in order to decrease confusion in the heat release rate calculations. The value should then be pasted (as values, not as a formula) to the Calculations worksheet so that the smooth and corrected trace can be used in the calculations.

8.) Delete last two data points from the MLR column.

Since the mass loss rate is calculated using an equation that includes the two data points above and below the current data point,[5] the first and last two data points will be nonsensical. The first two data points are automatically zero, however since it is not known how to determine the length of the test using the macro, the last two data points could not be removed automatically.

9.) Check for explained outliers in the mass history and fix them if necessary. Explain corrections in Observations sheet.

The most common "explained outlier" is the noise caused by the shutter down action in the load cell history. However, there may be other explained causes for spikes in the mass history including accidental touching or bumping of the load cell during the test. If the outliers can be explained, they can be smoothed out manually and explained in the Observations section so that the derivatives can be successfully studied. If they cannot be explained however, the change in the load cell history should not be smoothed out.

10.) **To perform the 2nd derivative FFT: Copy the MLR column to the 2nd Derivative sheet under the appropriately marked column by doing paste special, values. Run SecondDerCalc macro. Trim the end of the data taking the equations into account. Make sure the number of data points is an even power of two by adding zeroes or deleting data (only delete baseline data). Copy the time and second derivative columns over to the next appropriately marked columns. Highlight the data (not the titles) and the blank column next to it. Run ForwardFT macro. Autofill the magnitude column. Go to power spectrum and change x axis range to 0.02-0.03Hz. Look for the first data point in this range that goes above a magnitude of 0.00025 or, if they are all below this value, the highest frequency in this range. Copy the values from the ForwardFT results and paste them into the next appropriately named columns. Put zeroes for data starting at cutoff frequency and ending at negative cutoff frequency. Highlight this data and run InverseFT macro. Change the time on the 2nd derivative graph to reflect the length of the test.**

The process for the 2nd derivative Fast Fourier transform method may be able to be much more automated, however it would require higher level programming with the macros in Excel. For now, pieces of the process need to be completed manually including how to determine the cutoff frequency using the 2nd derivative power spectrum and making the data an even power of two. First, the mass loss rate column needs to be moved into the Fast Fourier transform sheet so that the SecondDerCalc macro can be run; the second derivative calculation should be two data points shorter than the mass loss rate, due to the equation. Since the data must be an even power of two for the Fast Fourier transform macros (see discussion in Appendix A: Operator Independent Ignition), the data must be padded with zeroes or data must be deleted.

Data should only be deleted if it is part of the baseline (i.e. test data should not be deleted). In order to run the Fast Fourier transform macros, three columns must be highlighted since the last column (even it is blank or full of zeroes) represents the imaginary component of the data, which is negligible. After the forward transform is run, the data between the positive and negative cutoff points are changed to zeroes to eliminate that frequency band (assumed to be noise) in the results. The inverse transform is then run on the partially zeroed data to produce the smoothed curve. The time axis on the 2nd derivative graph needs to be updated since the data was padded with zeroes to facilitate the Fast Fourier transform.

11.) To perform the 1st derivative FFT: Copy the time and MLR columns from the 2nd Der worksheet. Highlight this data plus one column to the right and run ForwardFT macro. Autofill the magnitude column. Copy the results over to the next appropriately named column. Use same cutoff frequency from the 2nd derivative to zero data range. Highlight the three data columns and run InverseFT macro. Change the time on the 1st derivative graph to reflect the length of the test.

As for the 2nd derivative, the Fast Fourier transform of the 1st derivative of the mass history may also be able to be more automated but higher level macro programming would be needed. The time and 1st derivative should be copied from the 2nd derivative worksheet since the columns will already be the correct length (i.e. an even power of two). Again, the two data columns plus one (the imaginary column) should be highlighted in order to run the macro. The data between the positive and negative cutoff point from the 2nd derivative power spectrum is used to zero the data. The inverse macro is then run on the partially zeroed data and will produce a smoothed mass loss rate plus an imaginary column that can be ignored since it is typically on the order of 10^{-18}. The time axis on the 1st derivative graph needs to be updated since the graph was padded with zeroes to facilitate the Fast Fourier transform.

12.) Determine how much mass was lost during the test using the mass history and insert this value into the "Test Information" worksheet.

The difference between the average of the first and last twenty seconds of the mass history can be used to determine how much mass was lost during the test.

13.) **Adjust the definition of the EHC and the b parameter (if proper burning) for the time that there was a flame cone over the surface. Use the correct mass based on the time period. If no flame cone, delete b parameter data and calculate EHC from ignition to flameout.**

The idea of the flame cone was extended to the definitions of the effective heat of combustion and the b flame spread parameter in order to get more accurate values for these parameters and to maintain consistency. For the effective heat of combustion, the mass needs to be adjusted to include only the mass lost during that time period. This is done by adjusting the effective heat of combustion for the heat release rate equation that is based on the mass loss rate until the difference between the actual (estimated) heat of combustion and the reference effective heat of combustion is essentially zero. The mass lost found by this method is then applied to the other effective heat of combustion calculations. The variables in the equation for the b parameter, including time to start and end of flame cone, need to be adjusted based on the test data.

14.) **Fill in time to ignition data in the "Observations" worksheet. The time to ignition using the 2nd derivative is the most negative peak (not including shutter down noise). There should be a sharp change in the combustion oxygen, CO, CO2 and THC traces at ignition; record time to ignition from these traces as well. Record visual time to ignition. Subtract shutter down time.**

The time to ignition is determined in a variety of ways in order to determine any systematic differences between the different methods. All times to ignition should be reported from shutter down time.

15.) **Add instrumentation data and any graphs that are needed. If there is no instrumentation for the test, delete the Instrumentation worksheets.**

Any instrumentation that was used for the test such as thermocouples, an infrared thermometer or a heat flux gage needs to be added to the data reduction worksheet and relevant graphs should be made.

Conclusions

The data reduction macro used in Excel was created by the author and was specifically designed to easily incorporate additional macros or changes to the existing macros in the future. The current macro is fully operational for data reduction in the FPA, however more pieces of the macro may be able to be more fully automated using more advanced macro techniques, which would decrease the time needed for data reduction of FPA tests.

Files for Reference

See files FPA Data Reduction.xls in FPA Tests folder for macro workbook and Data Reduction Worksheet Equations.doc in Notes and Lists folder for more information on the equations used, including the page number for each equation in the references.

References

[1] Standard Methods of Test for Measurement of Synthetic Polymer Material Flammability Using a Fire Propagation Apparatus (FPA), ASTM E 2058-03, ASTM, 100 Barr Harbor Drive, West Conshohocken, PA, U.S.

[2]Standard Test Methods for Measurement of Flammability of Materials in Cleanrooms using a Fire Propagation Apparatus (FPA), NFPA 287, National Fire Protection Association, Quincy, MA.

[3] "Chapter 3-4: Generation of Heat and Chemical Compounds in Fires." The SFPE Handbook of Fire Protection Engineering. Ed. Philip J. DiNenno. National Fire Protection Association, Quincy, MA, 2000.

[4] User's Guide for the Fire Propagation Apparatus (FPA) ASTM E-2058, Factory Mutual Research Corporation (FMRC), Norwood, MA.

[5] Standard Test Method for Heat and Visible Smoke Release Rates for Materials and Products Using an Oxygen Consumption Calorimeter, ASTM E 1354-02, ASTM, 100 Barr Harbor Drive, West Conshohocken, PA, U.S.

[6] Department of Chemistry, "Atmospheric Chemistry: Common Units of Measurement and Their Conversions", 2000, University of South Carolina <http://michele.usc.edu/cttc/mak/unit_conv_atmosphere.html>.

[7] Litton, C.D., Lazarra, C.P. and Perzak, F.J., "Fire Detection for Conveyor Belt Entries Document," United States Department of the Interior, Bureau of Mines, Report AA76-COMM-106B-Exhibit#2, 1991 <http://www.msha.gov/regs/comments/03-1307/posthearing/aa76-comm-106exhi2.pdf>.

[8] Babrauskas, V., "Appendix A: Tables and Charts," Fire Protection Handbook, 19th Edition, Ed. Arthur E. Cote, National Fire Protection Association, Quincy, MA, 2003

[9] Parker, W.J., "Calculations of the Heat Release Rate by Oxygen Consumption for Various Applications," NBSIR 81-2427, National Institute of Standards and Technology, Gaithersburg, Maryland, 1982.

[10] Beaulieu, P.A. and Dembsey, N.A., "Enhanced Equations for Carbon Dioxide and Oxygen Calorimetry," *Proceedings of the 9th International Fire and Materials Conference,* p.49 (2005).

Appendix D: Secondary FPA Checks

Introduction

In addition to finding the calibration equations and instrument delays as well as learning additional information about the various instruments in the FPA, secondary checks were also performed. These additional checks included determining the heat flux map at the sample height and the ratio between the convective and radiative portions of the heat flux at various points across the sample surface. Also included is a description of the air velocity profile in the air chamber, a description of the smoke path in the FPA and a study of how the air flow rate affects PMMA results in the FPA. The load cell and the oxygen analyzer both produce results that should be better and attempts were made to better the readings from these instruments.

Heat Flux Gage

Many different aspects of the incident heat flux in the FPA were studied using both the calibration heat flux gage (i.e. the heat flux gage used for the irradiance calibration; located in a metal frame) and the dual heat flux gage which was embedded into the sample in an attempt to determine the flame heat flux. The different secondary checks that were performed on the WPI FPA with these two gages are detailed in the subsections below.

Heat Flux Map

The calibration gage, which is a total heat flux gage, was used to determine the heat flux map in the FPA, shown in Figure 51.

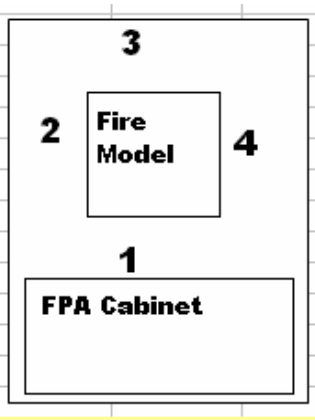

	Heat Flux (kW/m^2)			
Position	**10/26/2006**	**10/30/2006**	**11/2/2006**	**Average**
Center 1	50	50.25	50.14	50.13
Circle 1, Position 1	49.9	50.28	49.68	49.95
Circle 1, Position 2	50.45	51.34	50.42	50.74
Circle 1, Position 3	50.55	51.6	51.24	51.13
Circle 1, Position 4	49.12	49.55	49	49.22
Circle 2, Position 1	52.18	52.72	52.07	52.32
Circle 2, Position 2	54.81	54.92	53.5	54.41
Circle 2, Position 3	54.51	54.74	54.72	54.66
Circle 2, Position 4	52.48	53	52.59	52.69
Center 2		49.82	50.09	49.96

Figure 51: Heat Flux Map in the FPA. The map was repeated on three different days to get a better idea of the variability.

A center point reading (represents the center of the sample) was taken at the beginning and end of the heat flux map (except on day one) in order to determine if there was any hysteresis or drift in the gage or the lamps themselves. "Circle 1" represents a one inch diameter circle from the center of the sample. Positions 1-4 were located right in front of the lamps and the numbering of the lamps is shown in the diagram. "Circle 2" represents a 2 inch diameter circle from the center of the sample so it is essentially the very edge of the sample. For the heat flux map, the quartz was in place and the air was flowing through the air chamber at a rate of 200lpm in order to simulate test conditions as close as possible.

As can be seen from the heat flux map, there is little to no hysteresis or drift in the reading of the gage or the FPA lamps over the course of one day since the center reading at the beginning and end of the heat flux map were approximately the same for both days in which they were measured. It is apparent from Figure 51 that the heat flux increases by approximately 5kW/m^2 as the heat flux gage is moved closer to the lamps (i.e. "Circle 2" readings are higher than "Circle 1" and "Center" readings). From the FPA standard,[1]

the heat flux map readings should be "at most a 5% mean deviation of the readings from the average value," which is the case in the WPI FPA according to the heat flux map.

Issues with the Lamp Voltage Controller

The DigiTech lamp voltage controller is known to be inconsistent with regards to the relationship between the lamp voltage and the applied heat flux at the sample surface. Therefore, it is strongly encouraged that the heat flux be checked via the calibration heat flux gage at the beginning of each day or any time that the applied heat flux is changed during the day. The newest version of the FPA has a different lamp voltage controller. It may be beneficial to research the new lamp voltage controller currently being used and determine (through discussions with personnel at Fire Testing Technology (FTT) and FM Global) whether it will produce more consistent and repeatable values for the relationship between the lamp voltage and the applied heat flux.

Effect of Quartz Cylinder on Heat Flux

Although it is small, there is a systematic difference with heat flux with and without the quartz. The difference is shown in Figure 52 below.

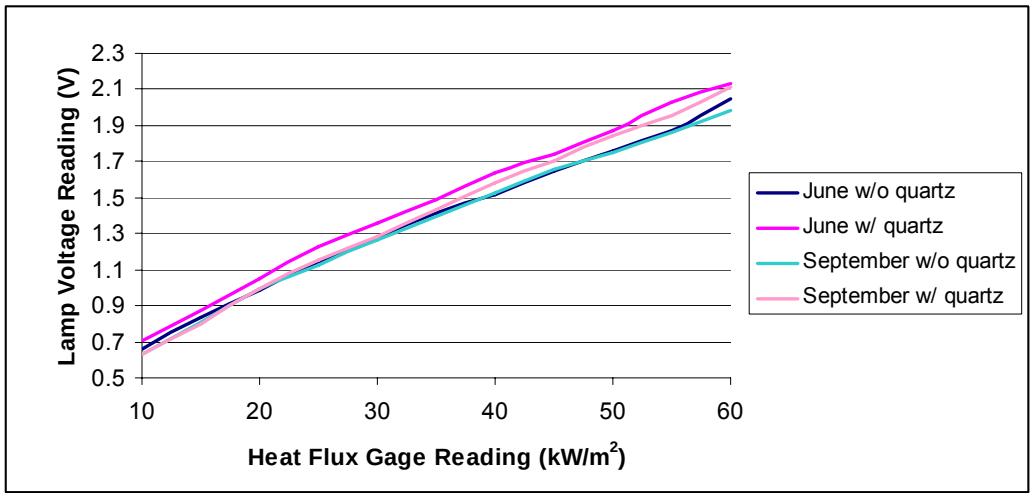

Figure 52: Comparison of Heat Flux Gage Readings With and Without the Quartz Cylinder in Place.

As can be seen from the graph, the vertical axis is the lamp voltage which was determined to be unreliable in the previous section. The study with regards to the effect of the quartz cylinder was done before it was realized that the lamp voltage was unreliable. Although the effect has been seen at different times, it was only systematically studied once. Since there is a consistent trend (i.e. the heat flux reading is lower without the quartz, especially as the heat flux is increased) in the two months the study was performed, it is thought that the lamp voltage reading is somewhat reliable in this case since the two readings (with and without quartz) were taken one right after the other and the comparison was relative instead of absolute.

The quartz cylinder should be used for the irradiance test since the quartz cylinder does make a difference in the heat flux reading and the quartz cylinder will be used for all tests since it helps to control the atmosphere to which the sample is exposed as well as eliminate effects due to drafts in the laboratory.

Convective and Radiative Portions of the Heat Flux Across the Sample Surface

A piece of ceramic fiberboard was cut into the shape of a typical FPA circular sample and holes were drilled at different radii for insertion of the dual heat flux gage to lie flush with the "sample" surface. It was found through testing on two different days that the convective and radiative portions of the heat flux stay constant over the sample surface. The convective and radiative fractions are the same, within the stated heat flux gage uncertainty of 6kW/m^2, although the total tends to read consistently higher than the radiometer, indicating there is a very small amount of convective heating in the FPA. The idea of convective heating appears to be counter-intuitive since there is a relatively cool air flow in the air chamber but a discussion of the air flow patterns in the air chamber later in this appendix help to provide further explanation.

It is suggested that a larger piece of ceramic fiberboard be used to represent the exact dimensions of the combination of the sample and the insulated sample dish in order to determine if there are any differences. The piece of ceramic fiberboard discussed above was the size of a circular sample alone and did not include effects due to the larger sample holder.

Air Flow in the FPA Air Chamber

The air flow in the FPA's air chamber is somewhat complex due to the obstruction in the form of the sample holder and the air flow's effect on the smoke patterns, including the turbulence in the smoke. The following subsections will describe these secondary checks that were performed on the FPA.

Map of the Air Velocity in the FPA Air Chamber

A map of the air velocity in the air chamber with and without the sample holder in place was performed with a wind vane velocity meter. All measurements below are in miles per hour and the wind vane was turning clockwise unless otherwise noted. The asterisk after the reading means that the meter was slowing moving clockwise and then counter-clockwise but was not moving fast enough to get a reading. A superscript "+" means that the vane registered up to 0.3mph counter-clockwise but showed an average reading of zero. The results from the map of the air velocity are shown below.

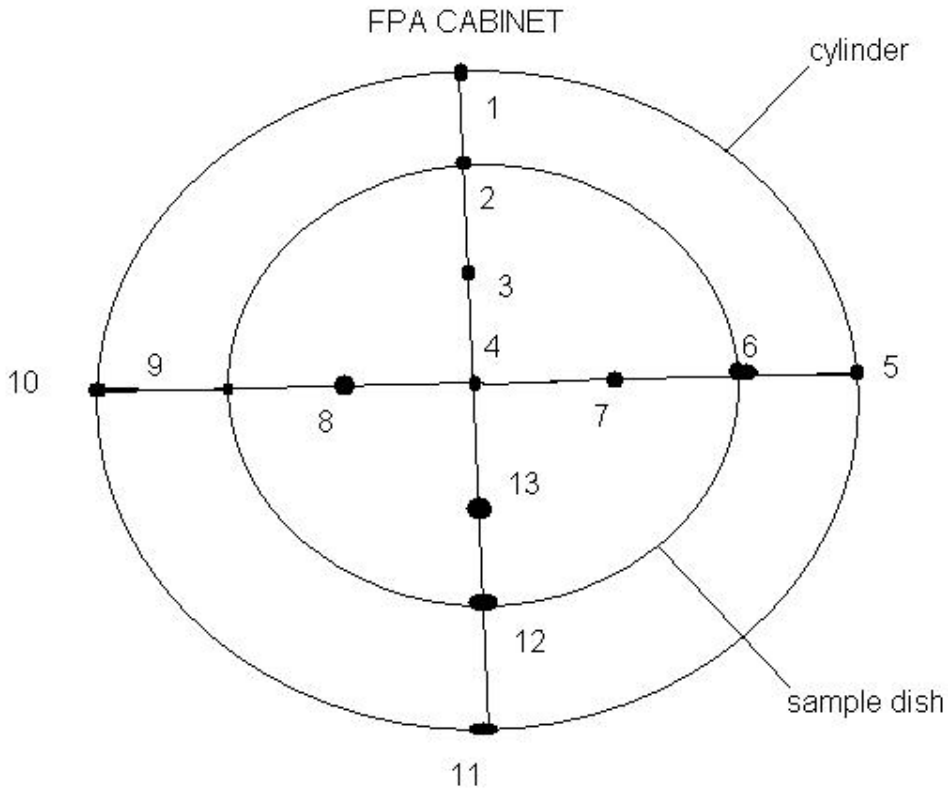

Figure 53: Diagram for Placement of Wind Vane Meter with Sample Dish in Place and No Quartz. The air was on at the normal flow rate of 200lpm.

Measurements Taken at Sample Height
1 2.4
2 2.0
3 0*
4 0*
5 2.3
6 2.0
7 0*
8 0*
9 2.2
10 2.4
11 2.4
12 2.2
13 0*

Measurements Taken 1" Above Sample
1 2.3
2 2.2
3 0^{*+}
4 0
5 2.4

6 2.2
7 0.4CCW
8 0*
9 2.1
10 2.2
11 2.6
12 2.4
13 0.4CCW

Measurements Taken 2" Above Sample
1 2.4
2 2.4
3 0.4-0.8
4 0
5 2.3
6 2.2
7 0
8 0.4-0.8
9 2.1
10 2.2
11 2.3
12 2.3
13 0.4-0.8

Measurements Taken 3" Above Sample
1 2.0
2 2.3
3 1.5
4 0.4-0.8
5 2.0
6 2.3
7 1.4
8 1.7
9 2.2
10 2.2
11 2.2
12 2.2
13 1.7

Measurements Taken 6.5" Above Sample
1 1.7
2 2.1
3 2.0
4 2.0
5 1.7
6 2.0
7 2.0
8 1.7
9 1.5
10 1.3
11 1.5
12 1.6
13 1.6

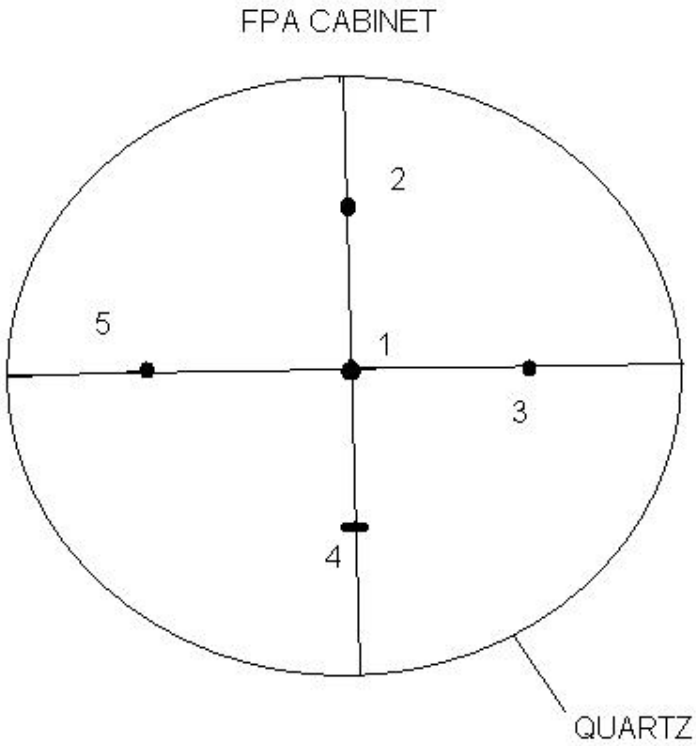

Figure 54: Diagram for Placement of Wind Vane Meter at the Top of the Quartz Cylinder with Sample Dish in Place. The air was on at the normal flow rate of 200lpm.

1 1.5
2 1.4
3 1.4
4 1.2
5 1.4

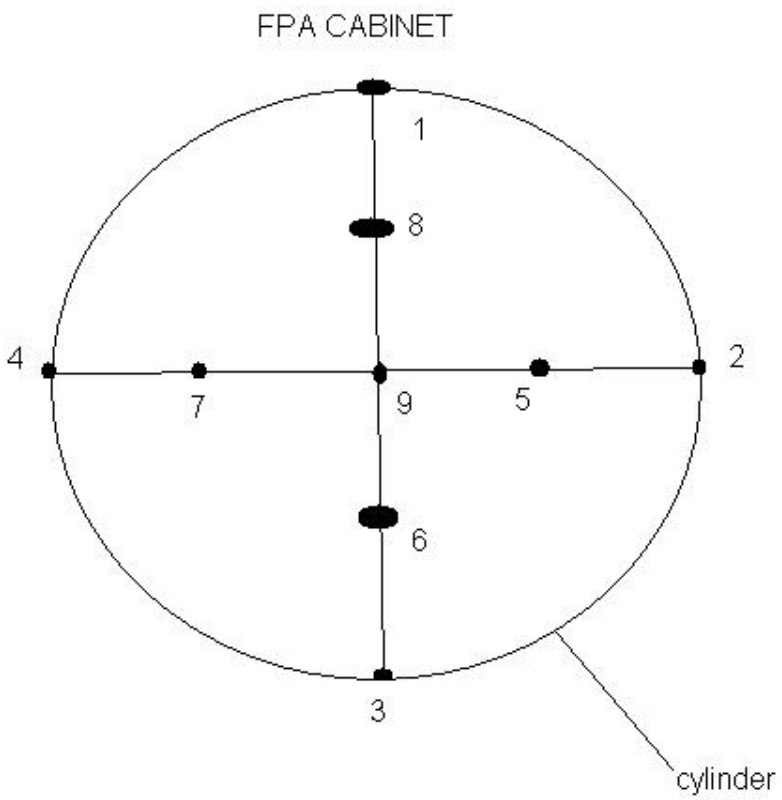

Figure 55: Diagram for Placement of Wind Vane Meter at Approximate Sample Height with Load Cell Pedestal in Place but no Sample Holder and No Quartz. The air was on at the normal flow rate of 200lpm.

1 1.3
2 1.3
3 1.4
4 1.2
5 1.4
6 1.5
7 1.2
8 1.3
9 1.5

From the results of the air velocity profile, it can be seen that the velocity in the air chamber is virtually uniform without the presence of the sample holder. However, when the sample holder in introduced, a wake around the sample holder is created. The disturbance of the air flow around the sample holder leads to turbulence in the smoke layer above the samples, as will be discussed in the next section. The velocity of the air is uniform at the top of the quartz tube assembly even with the sample holder in place, indicating that the air flow recovers from the wake around the sample holder and becomes uniform after a distance shorter than the length of the quartz cylinder.

Smoke Patterns

Due to the 200lpm air flow rate in the air chamber and the disturbance caused by the FPA insulated sample holder (see discussion in previous section), there is an effect on the patterns of smoke in the FPA. When there is smoke coming from the sample, it can be seen that there is turbulence around the perimeter of the sample but the air and smoke directly above the center of the sample is stagnant. The stagnant air may explain the convective heating that the dual heat flux gage records. At a short distance above the sample surface, the smoke begins to curl around back in toward the center and the smoke realigns itself. Therefore, visual observations confirm the findings of the air velocity profile using the wind vane meter.

Effect of Air Flow Rate on Time to Ignition and Flame Height

PMMA tests were done in the FPA with flow rates of 75, 150, 200 (the flow rate specified in the FPA standard[1]), 250 and 325lpm. The time to ignition was the same for all tests, within the uncertainty of 9s; the same result was found by Beaulieu.[2] Although the flame height increased as the flow rate was decreased since the flame became oxygen-starved, there does not seem to be a large effect due to the magnitude of the flow rate on results in the FPA.

Attempts to Improve Readings from the Load Cell and the Oxygen Analyzer

The raw data from both the load cell and the oxygen analyzers are much too noisy to be successfully used in calculations. Currently, the derivatives of the load cell data are being smoothed using the Fast Fourier transform (see Appendix A: Operator Independent Ignition) and the oxygen analyzer is both drift corrected and smoothed using a simple 10 point smooth (see OxygenConditioning section in Appendix C: FPA Data Reduction Macro). Before these smoothing algorithms were applied to the data, experiments were done in an attempt to reduce the noise in the instruments.

Load Cell

Testing to determine if the load cell readings could be made better focused on settings available in the load cell controller as well as vibration issues. Unfortunately, the total error for the load cell is 0.025% of the full scale capacity of the load cell, which was determined from a specification sheet sent from the manufacturer. The full scale capacity of the load cell is 2000g so that is a total error of 500mg. The experimental uncertainty in the mass loss history before any smoothing is performed is approximately 250mg so the WPI FPA load cell is within the manufacturer specifications. However, the manufacturer generally overstates the uncertainty; for example, the rated error on the Cone's load cell is 125mg and its resolution is showing up as 10mg (however, there is smoothing performed in the load cell controller in the Cone).

Even though the load cell was operating within the stated uncertainty, tests were done with isodamp at different locations in the FPA in an attempt to isolate where the noise was coming from after the load cell was properly leveled in the FPA. It was determined that the interaction between the load cell pedestal and the stem coming from the actual load cell was causing a majority of the noise. However, there was still a significant amount of noise when weights were put directly on the load cell stem, indicating that it would be beneficial if the load cell itself had a better resolution.

It was also found that vibrations from pumps and other equipment in the FPA as well as in the lab did not affect the reading of the load cell. Electrical noise was also tested with an oscilloscope but little noise in the electrical signal was found since the load cell controller is connected to the clean power supply.

All smoothing was turned off in the WPI FPA load cell controller because the smoothing algorithms dramatically increased the response time of the load cell. For scientific purposes, obtaining raw volts with no smoothing and using a smoothing technique in Excel was preferred over using an unknown smoothing algorithm in the load cell controller.

In the future, it is highly suggested that springs be used to soften the effect that the shutter down action has on the load cell history. It is also suggested that the load cell itself be replaced with one that has a higher resolution.

Oxygen Analyzer

For the FPA oxygen analyzer, the company claims a peak to peak fluctuation of either ±0.025% O_2 (for control paramagnetic) or ±0.05% (for basic paramagnetic).[3] The actual peak to peak fluctuation is about ±0.025% O_2. Therefore, it seems as though the FPA Servomex analyzer is working within its limits, however a higher resolution is necessary to use the oxygen trace to calculate heat release rate so a number of different possibilities for decreasing the uncertainty were considered.

When the Agilent was being used, the data was being smoothed inadvertently (the smoothing was a default setting in the Agilent software). Therefore, the noise was apparent only when the FPA was switched over to the new LabView software (which does not smooth). The Agilent was reconnected and the smoothing was removed; the oxygen analyzer acted the same as it did with the LabView data acquisition system so it is not the data acquisition hardware.

Air and nitrogen tests were run with VI Data Logger instead of the FPA VI to see if the VI was somehow corrupting the data. The same uncertainty band was found on both so it is not the FPA VI that is the problem.

The noise band is basically the same whether the pump is on or not so it is not the pump oscillations. Both air and nitrogen were run through the data acquisition system with the same uncertainty band showing for both gases so it is not some effect due to the type of gas.

Analog-to-digital calculations were used to determine if the data acquisition equipment was creating a ceiling for the quality of the data; it is definitely not the limiting factor.

A technician from Servomex, Jason Sanders, thinks that some moisture got into the oxygen analyzer. He said that even a drop could cause trouble with the paramagnetic oxygen transducer but would not affect the CO and CO_2 (unless there was a lot of water). It is unknown when the problem started since smoothing was inadvertently being used in the Agilent data acquisition system. However, the idea of a "wet" sample going to the analyzer was studied.

The inlet air goes through one drierite column (as well as the dryer downstairs). The CO/CO_2 and combustion O_2 cells in the analyzer all see the same exhaust sample gas that goes through a 10 micron gamma filter, 2 HEPA filters, a cold trap and 2 drierite columns. It was decided that it would be beneficial to install inline relative humidity meters after the drierite columns for both oxygen cells.

A Vaisala relative humidity meter was used to determine the relative humidity in the gas analyzer sample lines. The temperature and relative humidity in the lab are 25C and 19%, respectively. The meter is a Vaisala HMP 237. All three gases that enter the gas analyzer (air, nitrogen, CO/CO_2) were tested and they are all very dry before they go into the analyzer. The relative humidity meter was inserted inline at a number of different places as listed below (RH = relative humidity; Td = dew point temperature):

Before drierite, inlet oxygen lines, air: RH = 2.3%, Td = -23.4C
Before drierite, inlet oxygen lines, nitrogen: RH = -0.1%, Td = -85.4C
After drierite, inlet oxygen lines, air: RH = 0.9%, Td = -34.4C
Before cold trap, pump and drierite, combustion oxygen lines, air: RH = 15.2%, Td = -2.9C
Before drierite and after cold trap and pump, combustion oxygen lines, air: RH = 9.3%, Td = -7.8C
After drierite, cold trap and pump, combustion oxygen lines, air: RH = 0.3%, Td = -46.6C
At CO/CO_2 inlet to FPA: RH = 0.0%, Td = -86.6C

The accuracy of the meter is +/-1% for relative humidity and +/-2C for the dew point temperature.

Jason Sanders, the Servomex technician, said that absolutely no water should be allowed in the analyzer. However, the manual for Servomex[3] states that the dew point of the sample gas should be 9°F lower than the minimum expected ambient temperature. This relates to a relative humidity of 70% and the testing with the relative humidity meter showed that the conditions are well within this range for the WPI FPA.

Since there are no improvements that can be made on the output of the oxygen analyzer besides drift correction and simple smoothing algorithms, it is suggested that the oxygen analyzer be replaced with one that has a much better resolution.

Conclusions

This appendix showed that while the WPI FPA is fully operational and produces good results for a wide range of materials, there are areas for improvements. The largest two areas of improvement with regards to instrumentation would be the load cell and the oxygen analyzer.

Files for Reference

For additional information on the heat flux map, see Tests with Instrumentation Summary v8.xls in FPA Tests/Data Summaries. For additional information on the effect of the quartz cylinder, see FPA Tests/Older FPA Tests/Heat Flux Gage Reading VS ch14 lamp voltage.xls. For more information on the air velocity in the air chamber, see FPA Documents/FPA SOP Documents/Velocity Profile in the Air Chamber.doc and for its effects on time to ignition and flame height, see FPA Tests/Older FPA Tests/PMMA Airflow Tests folder. For tests and discussions on the study of the uncertainty in the load cell, see Vibration Testing folder and Notes and Lists/Notes on Noise Reduction in Load Cell.doc. For additional information on the oxygen analyzer discussion, see Notes and Lists/Issues with Oxygen Analyzer.doc.

References

[1] Standard Methods of Test for Measurement of Synthetic Polymer Material Flammability Using a Fire Propagation Apparatus (FPA), ASTM E 2058-03, ASTM, 100 Barr Harbor Drive, West Conshohocken, PA, U.S.

[2] Beaulieu, P.A. "Flammability Characteristics at Heat Flux Levels Up to 200kW/m^2 and The Effect of Oxygen on Flame Heat Flux" PhD Dissertation, Worcester Polytechnic Institute, 2005.

[3] Configuration, Operation and Installation Manual for the Servomex Xentra Analyzer, Sugar Land, Texas.

Appendix E: Modifications to the WPI FPA

Introduction

This section details modifications that have been made to the WPI FPA as well as suggested future modifications. Each paragraph will be a discussion about a different modification or area of improvement. A special acknowledgment for this section goes to Tricia Beaulieu, Stephen Ogden, Lawney Crudup and Dana Capron at FM Global for their invaluable help in getting the FPA set up at WPI.

Modifications to the WPI FPA

The regulator marked "Set Pilot Flame" on the fire model and a significant amount of tubing for the pilot flame line were removed since they caused restrictions in the ethylene/air flow. The restriction made it impossible to create the 10mm horizontal blue pilot flame required from the FPA standard.[1]

The air regulator that was positioned before the manifold that splits the air in the FPA cabinet was removed since it caused a major pressure drop and did not allow enough air to flow to the lamps. If the lamps do not have enough air, they will break at a fairly constant rate.

An inline water pump was added to overcome the back pressure in the building's water system. The chilled water system at WPI has the capacity to flow 10GPM, however the difference between the supply and return pressures was only approximately 5-10psi. Therefore, there was no pressure to drive the water flow through the system. The pump was added to boost the supply pressure to 90psi to fully overcome the back pressure.

Permanent pressure gages were added into the water supply, the water return, the air supply and the water pump outlet. Also, fittings were purchased such that a temporary pressure gage could be installed anywhere in the air line (as long as a tube can be cut). There are currently tube unions upstream of the lamps in the water line to ease quick installation of a pressure gage or a water flow meter to determine potential problems. The instrumentation was installed since there were many problems with proper air and

water flow rates and pressures at the beginning of this project, which caused the bulbs in the lamps to break at a very regular interval.

Permanent water flow meters were installed inline before the manifold which splits the water into the four different lamps (located on the fire model) and another one just downstream of the shield water regulator (inside the FPA cabinet). Temporary air flowmeters can be installed anywhere in the air line as long as a tube can be cut.

The plastic water tubing inside the FPA cabinet was replaced with copper piping after the installation of the pump that increased the water pressure to 90psi. There is a lot of sensitive electrical equipment inside the FPA, resulting in a disaster if one of the plastic tubes were to leak or rupture inside. Therefore, copper tubing was used to reduce this possibility.

Modifications were made to allow for the addition of thermocouples and a heat flux gage embedded in the sample. This entailed changing the load cell pedestal to a 3 prong design (instead of a flat plate) and drilling a hole through the bottom of the air chamber for the thermocouple wires and the heat flux gage lines.

A bracket was installed in the FPA exhaust hood in order to mount the infrared thermometer to view the sample surface.

The Agilent data acquisition system was replaced with National Instrument's LabView hardware and software. The LabView software was written by WPI student Todd Hetrick and modified slightly by WPI Student Esther Kim.

The way that the oxygen and nitrogen mix with the air in order to create an oxygen deprived or enhanced environment was changed. In the original design, the oxygen/nitrogen (which is at a very low pressure) and the air (which is at a much higher pressure) were set up to mix by meeting head to head. However, the tubing set up was changed so that the nitrogen or oxygen aspirates into the air flow. The problem with the enhanced/deprived oxygen environment was not solved just by changing the tubing setup, although it is a necessary step. More steps that need to be followed are detailed in the next section.

Suggested Modifications to the WPI FPA

The fiberboard panels on the sides of the fire model are cracked and pieces of it are now falling off completely. Unfortunately, the current design for the installation of the fiberboard panels does not allow for any thermal expansion, resulting in the cracking and breaking of the panels. Lab manager Randy Harris is currently investigating materials to replace the fiberboard panels. The current fix for the missing pieces is layers of Cotronics® insulation held on by aluminum tape.

The pressure tap on the back of the lamps does not work. This is more of a comment than a suggested modification.

When a large pressure is applied to the lamps, the "Air Switches On" LED on the fire model will stay lit for a long time after the air has been shut off. It is assumed that the pressure switch is somehow sticking at the higher pressures. The "air on" light will also just randomly turn on for periods of time, even when the air hasn't been turned on for a while. Also, the cover for the electrical wires on the inside of fire model is bubbled and needs to be repaired. The pressure switches for the lamp cooling air and water turn on when there is only a very slight pressure. It is suggested that the switches for both the air and the water be replaced with pressure switches that only turn on when the appropriate pressure for the air and water is achieved. The switches are part of an interlock that prevents the lamps from being turned on without some water and air flow but they should be upgraded to require the proper air and water pressures in order to operate the lamps.

As discussed before, the oxygen analyzer is nowhere near as accurate as necessary to perform the heat release rate calculations using oxygen consumption calorimetry. The Cone oxygen analyzer is two times better than the FPA oxygen analyzer (see Appendix D: Secondary FPA Checks for additional information).

As discussed before, the load cell should be improved by changing the design of the load cell, finding better bearings for the load cell pedestal or simply getting a load cell with a better resolution (see Appendix D: Secondary FPA Checks for additional information). The bearings must be replaced at the beginning of each day or before every other test. While it does not take a lot of time to change the bearing, they cost $13 each so it would be beneficial to determine another method of getting the pedestal to sit on the load cell.

Currently, the ability to create oxygen deprived or enhanced environments in the WPI FPA is unavailable. The tubing set up for how the oxygen/nitrogen and air mix in the FPA has already been corrected (see discussion in previous section). However, an oxygen-safe check valve also needs to be installed in the vertical position right before the point at which the oxygen/nitrogen aspirates into the air. Currently, the air backs all the way up to the nitrogen or oxygen bottle and does not even allow the gas to flow. The check valve will allow slow aspiration of the oxygen/nitrogen (which should be at a pressure of only a few psi) into the air (which should be at a pressure of around 30psi). A flow regulator is also needed before the air mixes with the oxygen/nitrogen to turn the pressure of the air down to 30psi; it is currently at approximately 90psi. Stephen Ogden at FM Global also found that the addition of a vacuum pump was necessary for the inlet oxygen analyzer to properly read a mixture of oxygen/nitrogen and air. The system currently works by a pressure differential.

Files for Reference

Additional information about modifications and suggestions for improvements to the FPA can be found in the FPA Documents folder under Modifications to the WPI FPA.doc and Questions and Comments About the FPA.doc.

References

[1] Standard Methods of Test for Measurement of Synthetic Polymer Material Flammability Using a Fire Propagation Apparatus (FPA), ASTM E 2058-03, ASTM, 100 Barr Harbor Drive, West Conshohocken, PA, U.S.

Appendix F: Instrumentation

Introduction

In order to obtain as much data as possible while the composite is burning, instrumentation such as an infrared thermometer, surface, in-depth and back face thermocouples as well as an embedded heat flux gage were attempted. Some of the instruments proved to be reliable and consistent, both from test to test and with analytical solutions for the temperature profile, while some did not. The installation, uncertainty and discussion of each instrument used are listed in the following sections.

Infrared Thermometer

Originally, an infrared thermometer was used to measure sample surface temperature. The IR thermometer was mounted on a bracket in the FPA exhaust hood. Due to the distance between the infrared thermometer and the sample surface, the measurement is taken over a spot size that is 0.9" in diameter in the FPA. The center of the spot is located approximately one inch from the edge of the sample, measured by way of a laser attachment to the thermometer, to avoid the pilot flame. In the Cone, the infrared thermometer is closer to the sample surface, resulting in a spot size of 0.5", and is situated to view the center of the sample. The thermometer was water cooled and air was blown across the lens to prevent smoke deposits.

Unfortunately, the infrared thermometer did not provide repeatable results for the polyester composites and did not provide results consistent with the surface thermocouple for any of the composites. The reason for this is not known but there are a number of theories in the literature including absorption of the emitted radiation by gases coming from the sample such as CO, CO_2 and H_2O [1] [2] or the transmissive properties of the resin material [3].

A comparison between the results obtained from the surface thermocouple, which is known to be a good measure of the surface temperature (see next section), versus those obtained using the infrared thermometer will demonstrate the issues with the thermometer.

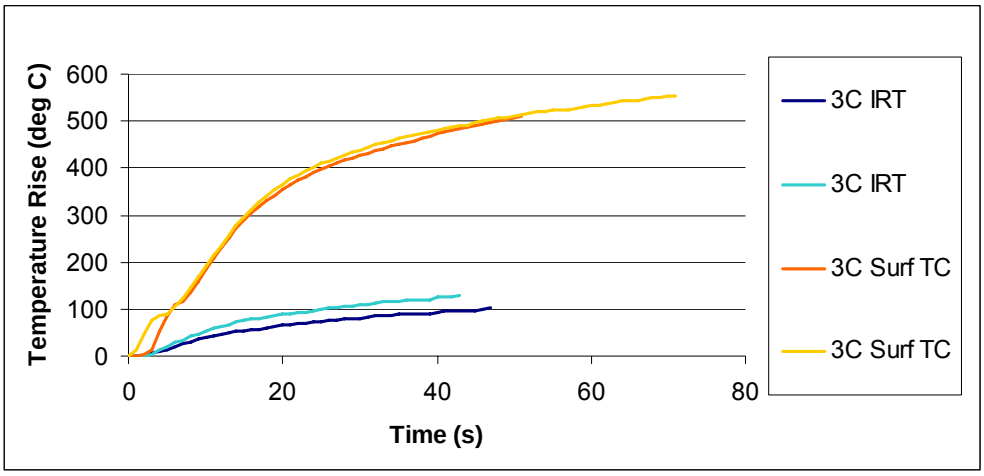

Figure 56: Comparison of Surface Temperature Obtained using the Infrared Thermometer and the Surface Thermocouple for the Phenolic Composite. All tests were performed with the 3C sample at 70kW/m^2 in the Cone.

It is obvious from the figure that the surface thermocouple increases at a much faster rate and that the infrared thermometer is repeatable for the phenolic composite but it not accurate.

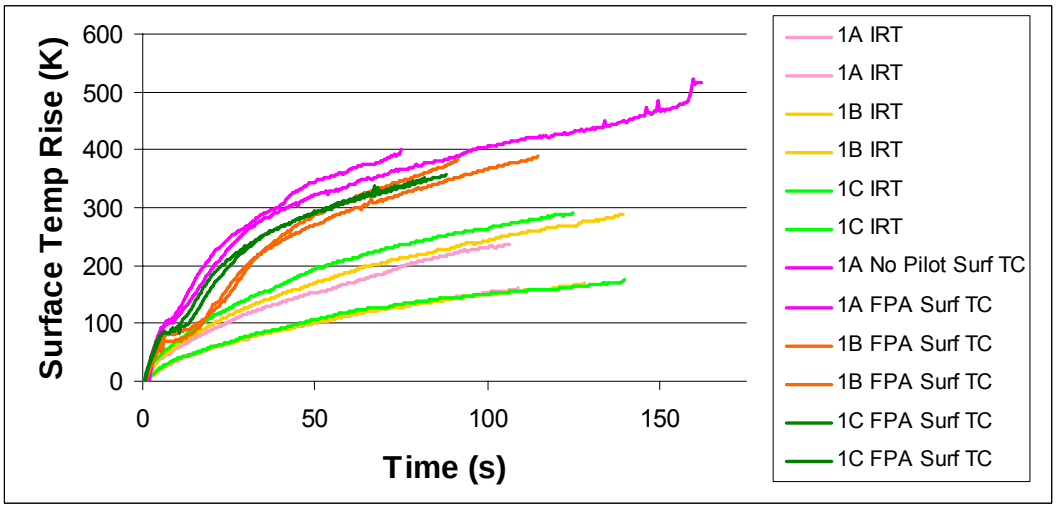

Figure 57: Comparison of Surface Temperature Obtained using the Infrared Thermometer and the Surface Thermocouple for the Polyester Composites. All tests were performed at 50kW/m^2 in the FPA.

From the figure, it can be seen that the surface thermocouple is both repeatable and increases faster than the infrared thermometer. The infrared thermometer was not repeatable for identical tests done with the polyester composite.

Carbon black was applied to the surface of the polyester with the highest glass content to determine if the infrared thermometer would record correctly. As can be seen from the graph below, the infrared thermometer rose steeply, as it should, but it then leveled off before ignition and would not be useful.

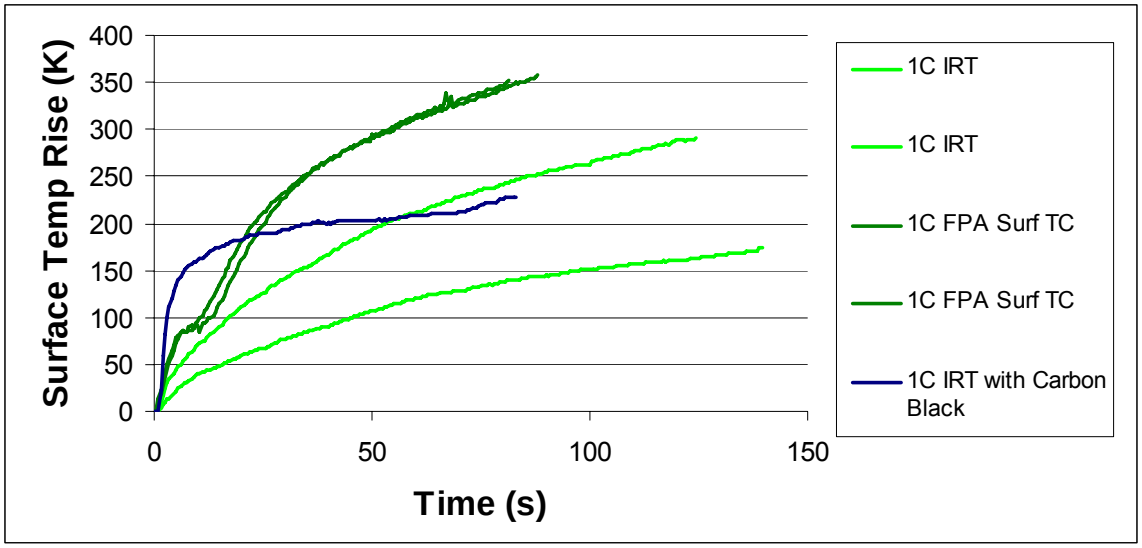

Figure 58: Comparison of Surface Temperature for the 1C Composite using the Infrared Thermometer (IRT), a Surface Thermocouple and the IRT with a layer of carbon black on the surface. All tests were done in the FPA at 50kW/m^2.

It was determined late in the testing matrix that the infrared thermometer was producing results that were not repeatable and that were not consistent with the analytical solution as compared to the in-depth temperatures (see Parameter Estimation section in Chapter 2). Therefore, the surface thermocouple began to be used late in the testing matrix.

Surface Thermocouple

The surface thermocouple (Omega Precision Fine Wire Thermocouples, Model 5TC-GG-K-30-36 from Omega Engineering) was attached with a thin layer of high temperature adhesive (Resbond 907 Industrial Strength Fireproof Adhesive from Cotronics Corp.). The surface thermocouple was located one inch from the edge of the sample so that the bead was in the zone of uniformity but not affected by the pilot flame

(the ignition source used in the FPA). Occasionally, there was a problem with the surface thermocouple paste coming apart from the surface during the test (although it usually held tight to the surface throughout the entire test). If the surface is lightly roughed with a blade or sandpaper, there is typically better adhesion. The surface thermocouple should be touching the surface of the sample before the adhesive is applied. The adhesive has a thermal conductivity that is slightly higher than the composite materials (0.86W/mK) and thus is thought to be a good choice for the particular application.

The surface thermocouple provided results that were very consistent for all of the system 1 (polyester) composites as well as the neat phenolic with the highest glass content (system 3). Since the testing with the surface thermocouple was started after many of the tests had already been completed, there is not currently much data for the surface thermocouple. It would be beneficial to perform additional tests to round out the testing matrix.

When the surface thermocouple is used in the parameter estimation (see Parameter Estimation in Chapter 2), the resultant parameters seem to be more repeatable and all of the curves can be matched with the same set of parameters, especially for 3C, indicating that surface thermocouple trace matches the temperature profile recorded by the in-depth thermocouples. Therefore, there is confidence that the surface thermocouple is a much better record of the surface temperature than the infrared thermometer and it is suggested that it be used in the future.

In-Depth Thermocouples

In order to install the thermocouples at depth, 1.25mm diameter holes were drilled at appropriate depths from the surface. The holes were drilled 38-50mm (1.5-2 inches) into the edge of the sample. From testing with both thermocouples at different radii as well as with the heat flux gage, it was found that there is a zone of uniformity with regards to temperature and heat flux within a 32mm (1.25inch) radius from the center of the specimen. Since the specimens have a diameter of approximately 102mm (4 inches) diameter, the thermocouple bead was located within this zone of uniformity. In order to eliminate air gaps in the holes drilled for the thermocouples, excess thermal grease (OmegaTherm Thermally Conductive Silicone

Paste, Model OT-201 from Omega Engineering) was inserted along with the thermocouples (Omega Precision Fine Wire Thermocouples, Model 5TC-GG-K-30-36 from Omega Engineering).

Heat release rate and mass loss rate curves from identical tests performed with and without embedded thermocouples demonstrated that the thermocouples did not have an effect on the overall burning characteristics of the material. From comparison of the maximum deviation between thermocouple traces from identical tests, an average of the maximum deviations was found to be 27°C, which was used to determine differences with resin type and glass content.

The main difficulty with the thermocouples is ensuring that the holes are properly measured since the largest degree of variability is the depth of the hole from the surface, the angle of the hole and the tightness of the hole. It is helpful if the thermocouple hole is peened before drilling is started because the drill will tend to bow since it has such a small diameter.

Back Face Thermocouples

The back face thermocouple (Omega Precision Fine Wire Thermocouples, Model 5TC-GG-K-30-36 from Omega Engineering) was affixed to the middle of the back surface with Krazy glue, which is inexpensive, dries very fast and has proven to be consistent and repeatable for back face temperature measurements. Before the Krazy glue is applied, the thermocouple bead should be in contact with the back face of the material.

Heat Flux Gage

A heat flux gage was also embedded in the sample to lie flush with the surface. The dual heat flux gage (MedTherm model number 32-15TKS-15R(S)-21846) that was used was able to partition the heat flux into both convective and radiative fractions. However, a resin condensate layer formed on the gage just before ignition or after a prolonged period of non-flaming decomposition. The formation of this layer caused the

radiometer to read essentially zero and caused a change in the reading of the total heat flux gage. Even though the reading from the total heat flux gage after the condensate formation is still being interpreted, the information obtained before this time from both the total and radiative heat flux gage can be used to partition the heat flux from the FPA and Cone into its radiative and convective portions.

Since the heat source in both the FPA and the Cone operate over a wide range of frequencies, a correction needs to be applied for the transmission of the sapphire window on the radiometer. Two graphs for the fractional transmittance of the sapphire window were provided by the manufacturer; the horizontal axis was wavelength on one graph and blackbody source temperature on the other. The wavelength graph is flat over a range of frequencies but both the Cone and the FPA have a range of wavelengths that extend beyond the flat portion of the curve. The correction factor that has already been applied to the sapphire window in the calibration is 0.85 (after speaking with the manufacturer) since the calibration source operates within the flat portion of the wavelength curve and that portion of the curve represents a fractional transmittance of 0.85.

The graph of transmittance versus blackbody source temperature that was used to determine the correction factor for the radiometer is shown below.

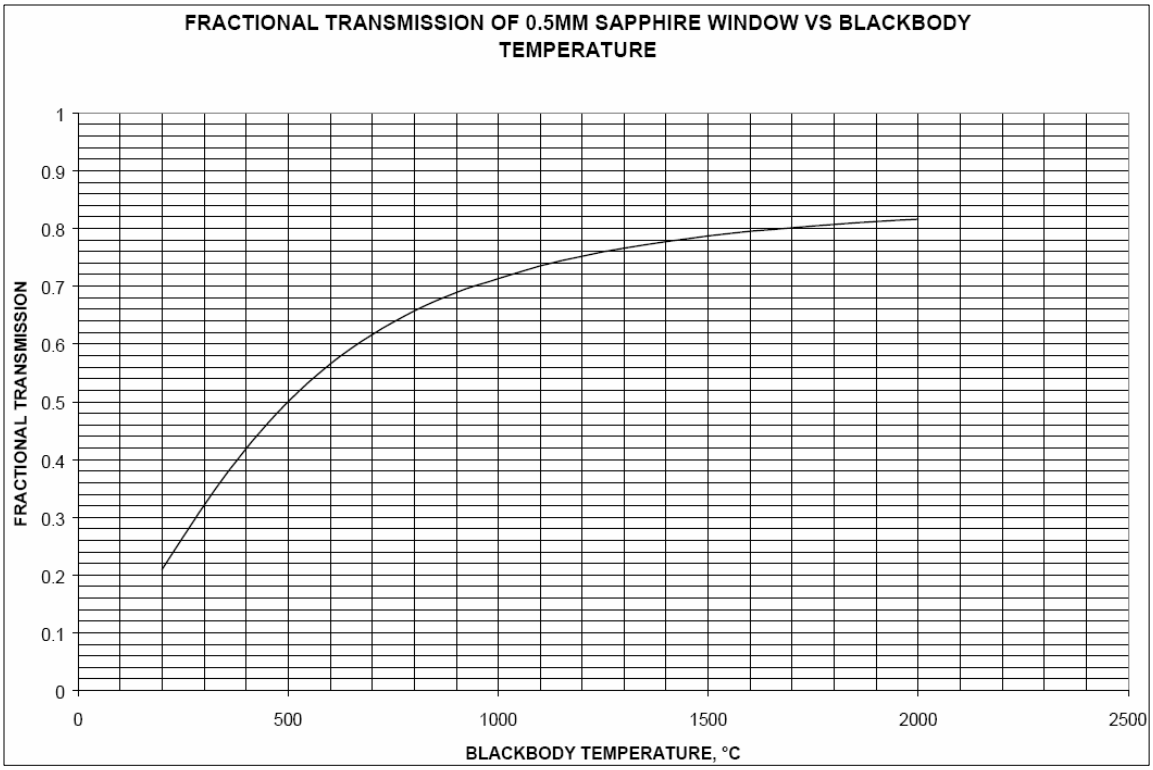

The blackbody source temperature for the FPA is approximately 2000°C, according to the manual for the infrared lamps, which leads to a correction factor of 0.85/0.82=1.04. The blackbody temperature for the Cone varies with the applied heat flux and thus the correction factor will be different for each applied heat flux.

If the ratio between the radiometer (before the correction is applied) and the total heat flux gage is determined before significant decomposition of the sample begins, it is very close to the calculated correction factor for both the FPA and the Cone, indicating that the correct factor was determined from the graph.

Shown below is a graph of the radiometer and total heat flux gage curves for the polyester with the highest glass content at 50kW/m^2 in the FPA with no pilot flame (to prolong the period without resin condensate forming on the gage surface).

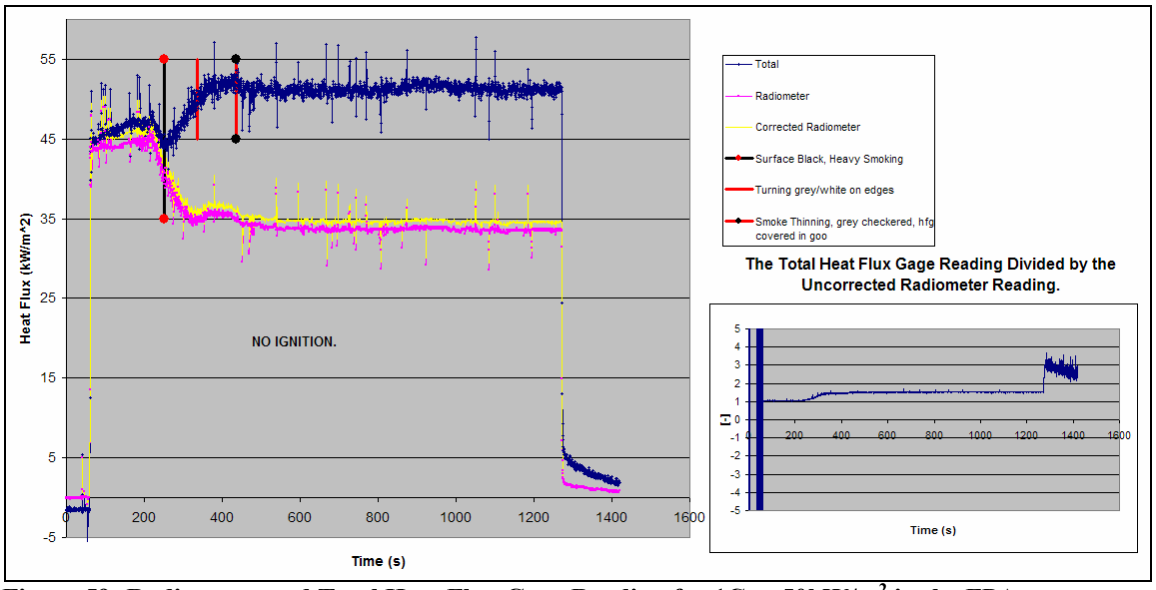

Figure 59: Radiometer and Total Heat Flux Gage Reading for 1C at 50kW/m^2 in the FPA.

Since there is not an abundance of resin due to the lack of pilot flame and the high glass content, the radiometer does not drop all the way to zero but it drops significantly after decomposition of the material begins. The vertical red lines indicate various visual observations regarding decomposition that match up with changes in the radiometer and total heat flux gage curves; this was seen for all other tests as well. The smaller graph is a graph of the total heat flux gage over the uncorrected radiometer reading. The ratio between the two prior to significant decomposition is 1.05 while the calculated correction factor was 1.04.

A similar graph is shown below for a Cone test at 70kW/m^2 with the neat phenolic at the highest glass content.

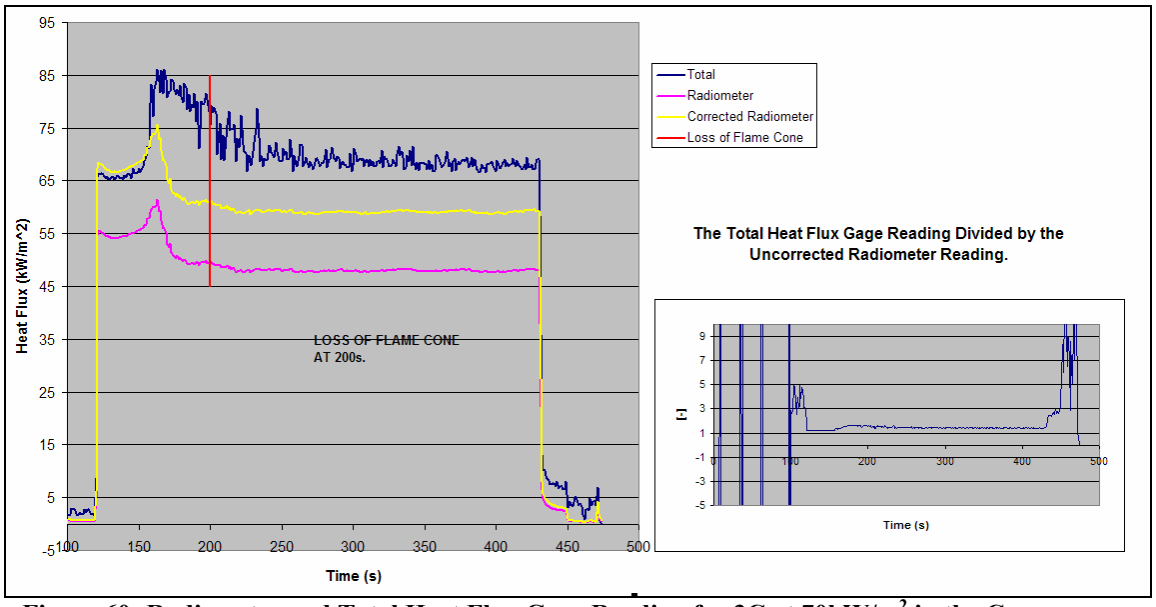

Figure 60: Radiometer and Total Heat Flux Gage Reading for 3C at 70kW/m^2 in the Cone.

Since the heat flux is at 70kW/m^2, the correction factor is 0.85/0.69=1.23 while the ratio between the total and the radiometer before significant decomposition is 1.21. The main difference between the readings from the Cone and the FPA is that there is convective heating in the FPA (i.e. the total heat flux gage reads higher than the radiometer) and convective cooling in the Cone (i.e. the radiometer reads higher than the total heat flux gage). This is thought to be due to the stagnant area of air over the sample surface in the FPA due to the wake caused around the sample holder from the 200lpm flow rate of air. The Cone has a natural convection that sweeps over the entire surface and the flow does not experience a stagnation in the center.

Conclusions

The surface, back face and in-depth thermocouples are producing very good data for analysis, however the infrared thermometer has not proven to provide reliable or consistent data. It is suggested that the surface thermocouple be used over the infrared thermometer to measure sample surface temperature. Additional research is needed on the heat flux gage to determine if the reading of the total heat flux gage can be used after the formation of the resin condensate. The radiometer will not be able to be used after the formation

of the resin condensate because it drops off so significantly (sometimes to zero if there is enough resin and subsequent decomposition of the resin).

Files for Reference

See FPA Tests/Data Summaries/Tests with Instrumentation Summary v8.xls for data showing that the in-depth thermocouples have no effect on the overall burning of the composites. For additional information on the radiometer, see Notes and Lists/Issues with Radiometer.doc and FPA Tests/Data Summaries/Tests with Heat Flux Gage.xls.

References

[1] Omega, Inc. "IR Thermometers and Pyrometers" 02 February 2007 <http://www.omega.com/literature/transactions/volume1/thermometers1.html>.

[2] Blair, Bill. "Atmospheric Transmission." John Hopkins University, Department of Physics and Astronomy. 02 February 2007 <http://fuse.pha.jhu.edu/~wpb/spectroscopy/atm_trans.html>.

[3] Clausing, L.T. "What you really need to know to begin using infrared cameras." The American Society for NonDestructive Testing, May 2006. 02 February 2007 <http://www.asnt.org/publications/materialseval/solution/may06solution/may06sol.htm>.

Appendix G: Material Properties

Introduction

Since very few material properties of the composites were known prior to the start of the project, including the chemical formula, chemical heat of combustion and ash content of the resins, testing needed to be performed in order to determine the properties. These properties are needed for the fuel specific heat release rate equations (see Appendix C: FPA Data Reduction Macro). Fire engineering "properties" of the composites, such as the flame spread b parameter, were determined from test data and can be used to differentiate the composites based on resin type and glass content.

Material Properties

Chemical Formula

The chemical formula of the resins used in the composites in this study was determined from testing at Schwarzkopf Micro Labs.

Table 8: Table of Results from Elemental Analysis Done at Schwarzkopf Micro Labs for the Resins

RESULTS OF ANALYSIS

SAMPLE #	SML#	% Carbon	% Hydrogen	% Nitrogen
Polyester	**E78057**	**57.80**	**4.72**	**<0.10**
Neat Phenolic	**E78058**	**64.71**	**5.88**	**<0.10**
Phenolic with Char Former	**E78059**	**43.45**	**4.92**	**<0.10**
Phenolic with Intumescent	**E78060**	**49.08**	**5.12**	**13.65**
Modar with ATH	**E78061**	**22.56**	**5.18**	**0.15**
Modar	**E78062**	**62.87**	**7.01**	**0.50**

Although the Modar resins were not used in the current study, they will be used in future studies with the composites.

In order to find the subscripts of the chemical formula from these numbers, each percentage should be divided by the appropriate molecular weight. Schwarzkopf Micro Labs do not include oxygen in their elemental analysis so it assumed that the remainder of the resin composition is oxygen.

Using this information, the chemical formulas for the resins are listed below:

Polyester: $C_{2.1}H_2O$
Neat Phenolic: $C_{3.0}H_{3.2}O$
Phenolic with Char Former: $C_{1.1}H_{1.5}O$
Phenolic with Intumescent: $C_{4.2}H_{5.2}NO_{2.1}$
Modar with ATH: $C_{188}H_{514}NO_{451}$
Modar: $C_{130.8}H_{173.8}NO_{46.2}$

From a discussion with Schwarzkopf Micro Labs, the uncertainty in the elemental analysis is ±0.3 in the subscripts of the chemical formula.

The oxygen fuel mass ratio can be calculated using the chemical formula. A chemical reaction assuming complete combustion to carbon dioxide and water in air was created for all of the composites. The oxygen fuel mass ratio is defined as the ratio of the grams of oxygen needed to fully combust one mole of fuel. The values of r that were calculated are shown below.

Table 9: Table of Oxygen Fuel Mass Ratio, r, for the Resins

System	r Value
Polyester	1.54
Neat Phenolic	1.9
Phenolic with Char Former	1.03
Phenolic with Intumescent	1.39
Modar with ATH	0.29
Modar	1.93

The mass fraction of carbon in the fuel, which is another material property needed for the fuel specific heat release rate equations, is easy to calculate from the elemental analysis. It is simply the fractional equivalent of the percentage given in Table 8.

Heat of Combustion

The heat of combustion of the resins, which is needed for the fuel specific heat release rate equations, was also determined from additional testing at Schwarzkopf Micro Labs. The results are shown in the table below.

Table 10: Heat of Combustion of the Resins Determined by Schwarzkopf Micro Labs.

	HoC Determined by Schwarzkopf	
Resin	Total HoC (BTU/lb)	Total HoC (kJ/kg)
System 1	10374	24107.0
System 3	10669	24792.5
System 4	7858	18260.3
System 5	8944	20784.0
System 7	4063	9441.6
System 8	11589	26930.4

From discussions with Schwarzkopf Micro Labs, the uncertainty in the heat of combustion is ±100BTU/lb (±232kJ/kg). The heat of combustion shown in Table 10 is based on the initial mass instead of the mass lost. Therefore, tests were done at WPI to determine the approximate ash percent in the resins.

Resin Ash Percent

The ash percent in the resins was determined using the procedure outlined in ASTM D5630: Standard Test Method for Ash Content in Plastics. The process requires a muffle furnace to cook the resins for a specified amount of time until they do not lose more than 2mg during that time period. The results from the testing are shown below.

Table 11: Ash Percent of the Resins from Testing with the Muffle Furnace. The average and standard deviation are based on three tests.

Resin Type	Average % Mass Lost	Std Dev % Mass Lost
Polyester	98.76	0.13
Neat Phenolic	96.95	0.25
Char Former Phenolic	72.16	0.08
Intumescent Phenolic	90.78	3.58
Modar + ATH	57.62	0.09
Modar	99.90	0.04

Three tests were performed with each resin to determine the average and standard deviation. The phenolic resins took many hours in the furnace in order to lose less than 2mg but the polyester and the modar resins depleted relatively quickly.

The percent mass lost in each of the composites, determined from testing, was compared to the glass content and it was found that the percent mass lost for the polyester matched the glass content to within about 5% but this was not true for any of the phenolics. This finding is consistent with the muffle furnace testing since the polyester was almost completely depleted and was depleted fairly readily. Even though the neat phenolic lost almost all of its mass, it took much longer to do so than the polyester and thus is a much more stable resin with regards to reaction to fire.

Fire Engineering Property: b Flame Spread Parameter

Quintiere's[1] flame spread parameter is given as:

$$b = k_f \cdot Q'' - 1 - \frac{t_{ig}}{t_b} \qquad [1]$$

Where b is the flame spread parameter
Q" is the average or the peak HRRpuA [kW/m^2]
k_f is a constant equal to 0.01m^2/kW
t_{ig} is the time to ignition [s]
t_b is the total burning time [s]

This approach was chosen over the others in the literature because it is the classical approach and has values that are easy to determine in the FPA. Some of the methods in the literature use peak heat release rate and some use an average heat release rate in the equation for the b parameter. In this study, both the average and the peak heat release rate were used because the values were significantly different in some cases due to a strong initial peak (see Figure 2). Since the same burn duration was used for both the peak and the average heat release rate in the b parameter equation, the b parameter calculated using the peak heat release rate assumes that the heat release rate is at its peak value for the entire burn duration and thus represents a worst case scenario.

Since all of the information about the sample is not known (e.g. the chemical formula), the generic heat release rate formulas were used. As stated before, the heat release rate for the FPA is calculated using

carbon dioxide generation calorimetry and that for the Cone is calculated using oxygen consumption calorimetry.

Related to the idea of proper ignition discussed in a previous section, the time to ignition was defined as the time to the start of the flame cone. In most cases, this was the same as the time to ignition but was slightly longer in some cases. Along the same line, the total burning time was defined as the time from the beginning to the end of the fully developed flame cone on the specimen surface, which was determined from visual observations. The observations of the end of the flame cone generally correlated with a change in the heat release rate trace. For System 1, which properly ignited at much lower heat fluxes than any other system, the disappearance of the flame cone usually correlated with the beginning of the decay tail or, in some cases, with the beginning of the second rounded peak in the heat release rate trace. For every other system, the flame cone generally ended after the initial peak.

Referring to the literature,[2,1] the flame spread is considered to be accelerating if the b parameter is greater than zero and decelerating otherwise. Beyler et. al.[3] extend this idea to correlate a b parameter based on a test performed at an applied heat flux of 50kW/m^2 to the probability of flashover. They concluded, based on their data, that a material with a b parameter less than 0.3 is not expected to flashover in a room/corner test. However, materials with a b parameter larger than 0.3 are much more likely to flashover (although there were some outliers in their data set). Beyler et. al. did not publish any uncertainties related to the b parameter in their report.[3]

The b parameter for both the FPA and the Cone tests are given in Table 12 and Table 13 below. From the FPA calibration tests, it was determined that the uncertainty in the heat release rate trace is 45kW/m^2. The uncertainty in the time to ignition and the burn duration were found to be 9s and 101s, respectively. Given these uncertainties, the equation for the propagation of uncertainty[4] was used to determine that the uncertainty in the b parameter is approximately 0.45 full scale (±0.225).

Table 12: System 1 FPA Tests and the Corresponding b Parameter Using both the Average and the Peak Heat Release Rate Determined from the Generic CO_2 Based Formula in ASTM 2058. The maximum b parameter (the actual b parameter plus the uncertainty) is also included.

FRP Sample	Heat Flux (kW/m^2)	Avg -- Generic 2058	Peak -- Generic 2058	Avg -- Generic 2058 +0.45	Peak -- Generic 2058 +0.45
1A	50	0.0	1.1	0.45	1.55
1A	50	0.0	1.3	0.45	1.75
1A	40	-0.1	0.8	0.35	1.25
1A	30	-10.6	-10.2	-10.15	-9.75
1B	50	0.0	0.6	0.45	1.05
1B	50	0.1	0.5	0.55	0.95
1B	30	-0.8	-0.3	-0.35	0.15
1B	25	-3.6	-3.1	-3.15	-2.65
1C	50	-0.4	0.0	0.05	0.45
1C	50	-0.5	-0.2	-0.05	0.25
1C	30	-2.1	-1.7	-1.65	-1.25
1C	25	-3.9	-3.7	-3.45	-3.25

Table 13: Cone Tests and the Corresponding b Parameter Using both the Average and the Peak Heat Release Rate Determined from the Generic O_2 Based Formula in ASTM E 1354. The maximum b parameter (the actual b parameter plus the uncertainty) is also included.

FRP Sample	Heat Flux (kW/m^2)	Average -- Generic 1354	Peak -- Generic 1354	Avg -- Generic 1354 +0.45	Peak -- Generic 1354 +0.45
1A	50	-0.7	-0.4	-0.25	0.05
1A	50	-0.3	-0.1	0.15	0.35
1B	50	0.0	0.4	0.45	0.85
1C	50	-0.4	-0.2	0.05	0.25
3A	50	-6.3	-6.2	-5.85	-5.75
3A	60	-2.3	-2.1	-1.85	-1.65
3A	65	-3.8	-3.6	-3.35	-3.15
3A	70	-0.3	0.1	0.15	0.55
3A	80	-0.3	0.2	0.15	0.65
3C	65	-2.2	-2.1	-1.75	-1.65
3C	70	-1.7	-1.6	-1.25	-1.15
3C	80	-1.5	-1.4	-1.05	-0.95
4A	60	-4.0	-3.9	-3.55	-3.45
4A	65	-2.9	-2.7	-2.45	-2.25
4A	70	-2.9	-2.7	-2.45	-2.25
4A	80	-0.9	-0.7	-0.45	-0.25
4B	80	-1.4	-1.1	-0.95	-0.65
4C	100	-4.4	-4.3	-3.95	-3.85
5A	100	-0.1	0.1	0.35	0.55
5B	100	-0.3	0.1	0.15	0.55

The tests performed at 50kW/m^2 are highlighted because the correlation from Beyler et. al.[3] is based on tests done at this applied heat flux. Considering those tests done at 50kW/m^2 in both Table 12 and Table 13, 1A and 1B based on a peak heat release rate in the FPA and 1B based on a peak heat release rate in the Cone are the only composite samples that would be expected to flashover in a room/corner test based on the actual b parameter (not the maximum). The b parameter based on the peak heat release rate is significantly higher than that based on the average heat release rate due to the strong initial peak in the heat release rate trace for the 1A and 1B sample.

However, the uncertainty in the b parameter is 0.45 so, in order to truly determine if the b parameter has a chance of obtaining the threshold value of 0.3 for flashover, this uncertainty needs to be

added to the value that was obtained from the data. Table 12 and Table 13 display the maximum possible values of the b parameter in the last two columns. The maximum possible value of the b parameter for each FRP sample was determined by taking the actual value of the b parameter and adding the uncertainty of 0.45.

From the data in the tables, it can be seen that all of the polyester (System 1) samples have a maximum b parameter larger than 0.3 and thus have the potential to flashover in the room/corner test based on the Beyler et. al.[3] correlation. The 1C sample displays maximum b parameter values for the calculations based on the average heat release rate that are less than 0.3 but those calculated using the peak heat release rate are either very close or over this threshold value. Therefore, it is assumed that the 1C sample has a potential for flashover, especially when compared to the phenolic composites. 3A displays very negative b parameters, which indicate that the phenolic is not expected to flashover in the room/corner test. Comparing the tests done at 50kW/m^2, it is apparent that the phenolic has better fire performance than the polyester resin.

For the tests that are not completed at 50kW/m^2, the Beyler et. al.[3] correlation cannot be reliably used. Therefore, the discussion will be based on other references[2,1] that correlate a negative b parameter with decelerating flame spread and a positive b parameter with accelerating flame spread. If the maximum possible value of the b parameter is again considered (i.e. the b parameter plus the uncertainty of 0.45), the only samples that are expected to exhibit accelerating flame spread are 1A at 40kW/m^2 in the FPA, 3A at both 70kW/m^2 and 80kW/m^2 in the Cone, and 5A and 5B at 100kW/m^2 in the Cone. This again demonstrates that the phenolics are superior to the polyester resin and that the additives (System 4 with the charring additive and System 5 with the intumescent additive) make the phenolic perform better.

An important observation regarding the b parameter is the significant increase in the b parameter with applied heat flux for the System 1 composites. Since the uncertainty in the b parameter is 0.45, it can be seen that there is a very significant difference between low and medium heat fluxes but it seems to level off as the applied heat flux increases up to 50kW/m^2. From Table 12 and Table 13, it can also be seen that the b parameter makes a significant drop (see, for example, the b parameter for 1A in the FPA with applied heat flux) to become more negative just before the minimum heat flux for ignition (30kW/m^2 for 1A).

Files for Reference

See Sample Info folder for more information on the composites.

References

[1] Cleary, T. and J. Quintiere, "A Framework for Utilizing Fire Property Tests," *Fire Safety Science, Proceedings of the Third International Symposium,* International Association of Fire Safety Science (IAFSS), Scotland, U.K., Cox and Langford Editors, Elsevier Applied Science London and New York, July 8-12 (1991) 647-656.

[2] Dembsey, N.A., J.J. Alston and S.D. Ayers, "Using Cone Calorimeter Data and Half-Scale Corner Test Data to Assess the Fire Performance of Composite Materials," submitted to Cinnabar-Florida, Orlando, FL, USA as part of the project *Phenolics vs. Other Thermosets for Theme Parks* (2001).

[3] Beyler, C., S. Hunt, B. Lattimer, N. Iqbal, C. Lautenberger, N. Dembsey, J. Barnett, M. Janssens, S. Dillon and A. Grenier, "Prediction of ISO 9705 Room/Corner Test Results," US Department of Transportation, Report No. R&DC-215-99, 1999.

[4] Coleman, H. W. and W. G. Steele, Experimentation and Uncertainty Analysis for Engineerings, 2nd Edition, New York: John Wiley & Songs., Inc., 1999.

Appendix H: Paper from Composites 2006

COMPOSITES 2006 Convention and Trade Show American Composites Manufacturers Association October 18-20, 2006
St. Louis, MO USA

Effect of Resin Type and Glass Content on the Fire Engineering Properties of Typical FRP Composites

by

Melissa Avila, Graduate Student, WPI
Nicholas Dembsey, Associate Professor, WPI
Charles Dore, Partner, Abate Fire Technologies

Abstract

This study is designed to provide the composites industry as well as the fire engineering industry baseline data and engineering "properties" of common fiber reinforced polymer (FRP) systems. Four resin systems and three glass contents will be considered. This matrix of FRP systems has been carefully fabricated and documented so as to provide "transparency" as to the system compositions. An important and interesting aspect of these FRP systems is that all the resins used are listed by the manufacturers as Class 1 or Class A per ASTM E 84. The FRP systems are being evaluated in bench scale modern fire test apparatuses (FPA, ASTM E 2058, and the Cone Calorimeter, ASTM E 1354). These apparatuses provide a range of measurements such as heat release rate that can be used to calculate engineering "properties" of these FRP systems. The "properties", such as minimum heat flux for proper ignition and the b flame spread parameter, can then be used to compare the fire performance of these FRP systems according to resin type and glass content. The fire performance criterion to be used is flashover (full room involvement). Modern building codes in general require the fire engineer to design to prevent flashover from occurring.

Introduction

Traditionally, the UL Steiner Tunnel Test has been used to evaluate the fire hazard of interior wall finishes, such as composite materials. The sample in the Tunnel Test is placed horizontally on a ceiling of a tunnel-like test apparatus. Although it has been used for over 50 years, the Tunnel Test has a number of important shortcomings. First, the results of the test only provide a classification scheme for ranking materials; the results do not include useful engineering data. The result of the test is a flame spread index (FSI), which is an arbitrary scale in which fiber-cement board represents zero and red oak represents 100.[1] The FSI is used in modern building codes to determine where to allow installation of certain materials in a building. A rating of Class 1 or A, such as the resins that were tested in this study, means that the FSI is less than 25 and the material can be installed anywhere in the building. Second, some materials do not behave in the Tunnel Test as they would in a real fire scenario. In a real world scenario, fire will spread most quickly in the upward direction due to the effect of the buoyancy-induced flows aiding flame spread. Since the sample in the Tunnel Test is a horizontal sample, upward flame propagation is not modelled.[2, 3]

A more appropriate test would be one in which both concurrent flow (up a wall and under a ceiling) and opposed flow (lateral and down a wall) flame spread were possible, such as in the room/corner test (ISO 9705, NFPA 265 and NFPA 286). In this test method, a large ($4m^2$) sample is placed on the walls as well as on the ceiling of a corner in a standard test room. The corner is then exposed to an incident heat flux from a large flame. This more closely represents a realistic fire scenario however, the main disadvantage of the room/corner test is that it is expensive and time-consuming. Therefore, many different researchers have worked toward developing a model to use bench-scale data (such as the Fire Propagation Apparatus (FPA), ASTM E 2058[4], or the Cone Calorimeter, ASTM E 1354[5]) to predict room/corner test results.[2, 3]

In this study, properties such as the heat release rate, minimum heat flux for proper ignition and the Quintiere[6] flame spread parameter, b, will be used to differentiate the composite systems based on resin type and glass content. The b parameter will also be used to estimate whether flashover might occur in the room/corner test from bench scale experiments done in the FPA and the Cone Calorimeter on the fiber reinforced polymer (FRP) composite systems.

The FPA and the Cone Calorimeter

The FPA[7] is a bench-scale fire test apparatus in which the sample is heated by four radiant lamps. Each IR lamp consists of 6 bulbs with a tungsten wire in argon gas, which provides a uniform heat flux over the specimen surface of up to 60kW/m^2. The lamps emit with spectral energy peaks of 1.15 and 0.89 microns.[7] A long quartz tube can be used to create an atmosphere for the test that is different than the ambient (i.e. enhanced oxygen up to 40% and pure nitrogen). A flowrate of air at 200lpm is run through the bottom of the air chamber so that the sample is in a flow field during the test. The ignition source is a 10mm long blue pilot flame located 10mm above the center of the sample. The combustion products are collected into a duct where smoke obscuration, oxygen consumption, CO/CO_2 generation, total hydrocarbons and temperature are recorded. The mass loss history of the sample is also recorded. This raw data can be used to calculate useful engineering data such as heat release rate, mass loss rate, smoke yield and smoke extinction coefficient. The standard specifies a carbon dioxide generation based heat release rate, which will be used for the FPA in this study.[7]

The Cone Calorimeter[8] is similar to the FPA but it also has some important differences. The heater in the Cone is an electrically heated rod in the shape of a cone, instead of the IR lamps in the FPA. The Cone is designed to compute heat release rate based on oxygen consumption instead of carbon dioxide generation as in the FPA, so oxygen consumption calorimetry will be used for the Cone in this study. The sample in the Cone is exposed to the ambient environment and is not in a flow field so the apparatus can only perform tests under ambient conditions.[8]

The difference in the radiant source between the Cone and the FPA is noteworthy because the FPA radiation apparently tends to absorb at depth into the composites evaluated in this study while the Cone does not. This difference causes a discrepancy in the time to ignition and burn duration between results obtained from the Cone and the FPA. An attempt was made to resolve this issue by applying carbon black powder to the surface of the specimen in the FPA to prevent in-depth absorption. The carbon black decreased the time to ignition in the FPA to match that of the Cone but did not affect the overall burning duration as compared to tests in the FPA without carbon black. In some cases, this is thought to be due to near surface effects preventing the carbon black from covering the whole surface after initial radiant

exposure and subsequent reactions (e.g. jetting at the specimen surface causing disruptions in the carbon black layer). The carbon black did not affect the heat release rate or the b parameter from results without carbon black in the FPA but it did increase the range of the minimum heat flux for proper ignition compared to tests without carbon black in the FPA for the System 1 composites. The results from the tests with carbon black on the specimen surface in the FPA are not reported in this study due to inconsistencies in the results; future work is needed.

Sample Holder

Instead of the non-insulated aluminium dish that is specified in ASTM E 2058[7], an insulated sample dish described by de Ris and Khan[8] is used. The sample is surrounded by Cotronics® paper insulation on the back and sides as shown in Figure 61 to provide a barrier to heat loss. The assumptions that can be made based on the presence of the insulation (e.g. no heat loss from the back face or sides of the sample) are very useful in modelling the sample's reaction to the applied heat flux. The sample holder is also beneficial for installing thermocouples on the surface, center and back of the sample as well as embedding a heat flux gage to lie flush with the sample surface, which is the next step to be completed in the current work.

Apparatus Calibration

Before any testing of the composite samples was started, tests were done with well-known materials in an attempt to determine the uncertainty in the time to ignition, burn duration and heat release rate in the FPA,[7] since it is a new apparatus at WPI. The analysis for the uncertainty in the time to ignition and the burn duration for the FPA is based on three PMMA tests. A sample set of three is believed to be sufficient in this case because the FPA standard calls for three identical tests to be performed to correctly determine other properties.[7] From these tests, the uncertainty in the time to ignition and the burn duration were found to be 9s and 101s, respectively. These uncertainties are full scale (as opposed to ± half scale).

FPA tests were done with methane, propylene and acetone, as well as PMMA, and the heat release rate was calculated using three different methods. The ASTM E 2058[7] and the Beaulieu[9] methods are based on carbon dioxide generation while the Parker[10] method is based on oxygen consumption. All three

methods can be formulated as either fuel specific or generic (i.e. published average values). The effective heat of combustion was found by dividing the cumulative heat release rate by the total mass lost. This effective heat of combustion was compared to the chemical heat of combustion (equal to the published total heat of combustion corrected for the published smoke yield); this method is specified as a heat release rate calibration procedure in ASTM E 2058, using acetone as a model material. The standard states that the effective heat of combustion, calculated using the fuel specific heat release rate equation, must be within ±5% of the published value for acetone.[7] As can be seen from Table 14, the accuracy (defined as a deviation of the average value from all of the tests as compared to the published value; all of the reported uncertainties are full scale as opposed to ± half scale) in the acetone heat of combustion, calculated from the fuel specific equation, was found to be 7.9%. Therefore, the heat release rate for the FPA was found to be calibrated according to ASTM E 2058. Effective heat of combustion accuracies determined using the other methods of calculating heat release rate are also shown in Table 14 to demonstrate that there is not a significant difference between the results from the different methods.

In Table 14, the number listed as the accuracy in kW is the maximum value that the heat release rate trace derived from the ASTM E 2058,[7] Parker[8] and Beaulieu[7] equations deviates from the reference heat release rate trace (the mass loss rate multiplied by the published chemical heat of combustion). There is an asterisk in the last column for both propylene and methane because both of these gases were coming from the FPA's gas burner. The mass flowrate of the gas was stepped up and down during the experiment, which increased the heat release rate of the fire. In the case of both propylene and methane, it was found that the absolute difference between the calculated and the reference heat release rate curves got larger as the mass flowrate was increased. The value listed in Table 14 is the maximum value of the deviation.

The absolute accuracy in Table 14 is listed in kW even though units of kW/m^2 are generally used. Since the propylene and the methane are in the gaseous state and are coming through the FPA's gas burner, there is no specimen surface to divide by to achieve units of kW/m^2. Since the average specimen surface of the composites is $0.007m^2$, the uncertainty in kW/m^2 is then approximately $70kW/m^2$, full scale, based on data from Table 14.

The uncertainty in the time to ignition and the burn duration for the Cone are expected to be within the same range as the FPA. Therefore, the uncertainty values for these variables from the FPA will be used

for the Cone as well. The heat release rate uncertainty in the Cone is governed by the C factor, which is determined by calculating the heat release rate of a methane fire at different mass flow rate steps and inserting the subsequent values into an equation for the C factor that is provided in ASTM E 1354.[8] The required uncertainty from the standard is 5% and it is known that the Cone meets this requirement. Therefore, no additional calibration testing was required on the Cone for the purposes of this study.[8]

Description of Composite Systems

In the following discussions, the term "system" will be used to differentiate between resin types (e.g. System 1 is a polyester). The term "sample" will be used to differentiate between glass contents (e.g. sample 1A has a lower glass content than 1B). Lastly, the term "specimen" will be used to represent one individual composite from the sample that will be tested.

Eleven different fiber reinforced polymer (FRP) samples are being tested for the current work. There is a total of 4 different resin systems, each with three different glass contents (except for System 3, which has only two glass contents). Table 15 shows the base resin and the glass content for all of the FRP composites that were tested in the current study. Antimony trioxide was added to the polyester (System 1) as a smoke inhibitor. The neat resole phenolic (System 3) is comprised of formaldehyde and phenol and was modified with the addition of a char forming, fire retardant plasticizer that lowers the viscosity of the resin and further enhances its physical and resistance properties. An inorganic fire retardant for System 4 is used to create a high charring effect while an organic fire retardant for System 5 creates an intumescent effect. All of the resins used in this study are listed as Class 1 or A with regards to ASTM E 84.[1]

The fiberglass in each of the composites is Vectorply's 0/90 biaxial glass with a chopped strand mat stitched to it. In an attempt to keep all of the FRP composites approximately the same thickness (see Table 15 for a range of thickness for each sample), one pair of glass layers (chopped strand mat plus the 0/90 biaxial) was removed as the glass content was decreased. For example, sample 1A has one less pair of glass layers than 1B and two less than 1C.

Proper and Improper Ignition

The concept of proper ignition that was used in this study is an extension of the concept of "sustained flaming" that was developed in ASTM E 2058.[7] The standard defines sustained flaming as the "existence of flame on or over most of the specimen surface for at least a 4s duration".[7] Since one of the goals of this study is to produce useful data for the development of a pyrolysis model, a fully developed flame cone is necessary to make the simplifying assumption of one-dimensional burning. Another benefit to this definition is that it does not count edge burning as significant burning because the end use of this product (i.e. a wall, ceiling, floor) would be so large that edge effects would be very minor. A flame is considered to be effectively one-dimensional if it is even over the entire sample surface and is unified into a single flame cone (not necessarily axisymmetric). A distinction was made between cellular burning (flamelets over most or all of the surface) and edge burning. If a sample started to burn with cellular flaming and then progressed into a flame cone, it was still called proper ignition for the purposes of this study. Visual observations were made as to the time of the beginning and end of the flame cone so that data could be properly truncated for modelling purposes. This definition of proper ignition was also used in the calculation of the b parameter[9] (where the time to ignition is defined as the start of the flame cone and the burn out is defined as the loss of the flame cone) and in determining the minimum heat flux for proper ignition.

FPA and Cone Testing

After tests were done to calibrate the FPA,[7] testing on the composites was started. In order to get a good initial set of data, each sample was tested twice in the FPA at an incident heat flux of 50kW/m^2 with the quartz tube in place. This is a practical choice for a heat flux because it represents an average between the heat fluxes typically observed in room/corner tests. In these tests, the lateral flames have a heat flux of approximately 25kW/m^2 while upward flame spread generates about 100kW/m^2.[11]

After this initial set of tests was performed at 50kW/m^2, additional tests were done to determine the minimum heat flux for proper ignition. System 3, 4 and 5 (the phenolic samples) did not properly ignite at 50kW/m^2 so some tests were also performed at 60kW/m^2. None of the Systems 3, 4 and 5 composites

would ignite in the FPA at 60kW/m^2, which is the highest heat flux that the FPA can achieve. Therefore, the minimum heat flux for proper ignition for these systems had to be determined in the Cone,[8] which can achieve up to 100kW/m^2. The minimum heat flux for proper ignition for the System 1 (polyester) composites was determined with the FPA.

FPA Results

The only system that properly ignited at 50kW/m^2 in the FPA[7] was the polyester (System 1), which had significant amounts of black smoke with large stringy particulates of styrene in the smoke. The neat phenolic with the low glass content (3A) delaminated violently and the test had to be stopped in one case. The rest of the samples had only edge burning (i.e. flames emerging from between the sample and the layers of Cotronics®) after hundreds of seconds of exposure.

Figure 62 is a graph of the heat release rate traces from FPA tests done at 50kW/m^2 for the System 1 composites. The end of the trace is truncated based on visual observations of the loss of the fully developed flame cone. Recalling that the heat release rate uncertainty for the FPA is a maximum of 70kW/m^2, it can be seen that the top layer has a significantly higher heat release rate than the rest of the layers for 1A and 1B but 1C does not have a significant initial peak. Considering the difference in the initial peak with changing glass content, it can be seen that the magnitude of the initial peak is significantly different between 1A and 1B as well as between 1A and 1C but there is not a significant difference between the initial peaks of 1B and 1C. However, the graph shows a trend that as the glass content is increased, the magnitude of the initial peak decreases. These differences are believed to be related to the surface texture. The surface texture of 1A and 1B is smooth and 1A is highly glossy, which seems to indicate that there is a resin film on the surface. However, 1C has a very bumpy surface due to the weave from the glass layers, which may indicate that there is much less resin near the surface than for 1A or 1B and thus a less significant initial peak in the heat release rate trace.

Given the accuracy with which the heat release rate can be determined in the FPA, the difference in the plateau region of the curve is insignificant (see Figure 62) across all of the System 1 samples. Once the top layer of resin is burnt off, the glass layers block the heat transfer into and the mass transfer out of

the specimen, slowing the decomposition of the resin. This effect appears to be present irregardless of the glass content for the range of glass contents studied.

From the test data, the time to ignition for samples 1A, 1B and 1C are 124s, 145s and 159s, respectively. Given that the uncertainty in the time to ignition is 9s, there is a significant increase in the time to ignition with glass content for all of the polyester composites. Recalling from previous discussion that the burn duration uncertainty is 101s, it can be seen from Figure 62 that the burn duration significantly shortens as the glass content increases. The burn duration would be expected to be shorter for the higher glass content specimen since there is less resin to burn off in the sample than for those with a lower glass content (higher resin content).

Another interesting view on the results was observed by looking at the sample's response to a range of applied heat flux. Figure 63 and Figure 64 show that neither the average nor the peak heat release rate for System 1 significantly changed over an applied heat flux range of 20-50kW/m^2. This demonstrates that the System 1 composites have a similar burning rate over the range of applied heat fluxes considered, given the heat release rate uncertainty. Figure 65 and Figure 66 show how the time to the start of the flame cone, which is essentially the time to ignition for the System 1 composites, and the burnout time vary with applied heat flux. Considering the uncertainty in the time to ignition and burnout previously stated, the time to the start of the flame cone significantly decreases and the burn duration significantly increases as the applied heat flux is increased. The higher heat flux will heat the sample up to ignition faster and will provide sufficient energy to decompose more of the resin and expel it through the glass layers.

Minimum Heat Flux for Proper Ignition

The only composite system that properly ignited in the FPA[7] was System 1 so the rest of the samples had to be tested in the Cone[8] at higher heat fluxes. The last column in Table 15 gives the minimum heat flux for proper ignition as a range. A change in the range of the minimum heat flux for proper ignition is considered to be significant if it is greater than or equal to the step that is being taken (i.e. 5kW/m^2 or 10kW/m^2).

There is a significant change over all of the systems with resin type. The polyester resin (System 1) has a lower minimum heat flux for proper ignition range than any of the phenolic resins. Among the

phenolics, the neat phenolic (System 3) has the lowest minimum heat flux for proper ignition, which shows that the additives (Systems 4 and 5) are having a significant effect on the fire performance. The intumescent additive, System 5, tends to have a significantly higher minimum heat flux for proper ignition than the charring additive, System 4.

There also appeared to be a trend for most of the systems with changing glass content, except for System 1. The data in Table 15 seem to indicate that the minimum heat flux for proper ignition increases as the glass content increases. That is, as the glass content of the sample increased, more energy was needed to overcome the blocking effect of the glass and release enough vapors at the sample surface to create a steady flame cone over the entire surface.

System 1 seems to have an effect that is unexpected (i.e. the lowest glass content has the lowest minimum heat flux for proper ignition) however, more tests should be done to fully confirm this effect. Only one test was done with each sample at each heat flux.

System 3 appears to show a significant change with glass content. It should be noted that 3A was tested in the FPA at 50kW/m^2 and did not properly ignite due to significant delamination and violent popping early in the test. While 3A did pop and delaminate in the Cone, it properly ignited before severe popping and delamination occurred. The difference in reaction of the 3A sample between the two different apparatuses is thought to be due to in-depth absorption of the FPA lamp's wavelength into the specimen, as discussed before. Therefore, the 3A sample was tested in the Cone even though the minimum heat flux for proper ignition range would indicate that it could be tested in the FPA.

System 4 showed an increase in minimum heat flux for proper ignition at each change in glass content (i.e. 4A, 4B and 4C all have different minimum heat flux for proper ignition ranges) while System 5 only demonstrated a change for the highest glass content. Sample 5C has a minimum heat flux for proper ignition that is higher than the maximum applied heat flux that the Cone can achieve.

Analysis

A bench scale test, such as those outlined in this study are useful for preliminary observations regarding the fire characteristics of a particular material. They are also relatively inexpensive and not as time consuming

as large scale tests. However, the end use of the composites that were studied in these experiments is not to use them as small circles. Rather, the end use would be to use them as building materials to make walls, ceilings and floors, which is a completely different situation that involves different types of physics (e.g. concurrent versus opposed flow flame spread as is described in the next section). Experiments that would test these composites in a situation that would be more similar to their end use would be a room/corner test, such as ISO 9705 in Europe and NFPA 265 and 286 in the United States. In these tests, a corner of a standard size fire room is lined with the material and a propane burner is used as the ignition source. The ISO 9705 is the most severe due to the higher applied heat fluxes that it requires as compared to the NFPA standards.[11]

Although room/corner tests are more close to the end use of the product, the test has its own drawbacks, including the significant time and money that each test consumes. Therefore, it would be beneficial if the bench scale tests could predict results from the room/corner test. In the next few sections, the idea of a flame spread b parameter[9] will be introduced. The b parameter can be used to estimate flashover potential in the room/corner test from results obtained in a bench scale test, such as the FPA.

Flame Spread Theory

Although flame spread is not important in a bench scale apparatus, such as the FPA[7] and the Cone,[8] due to the small size of the specimen, it is extremely important in a real world environment. The flame spread velocity determines how the heat release rate increases with time and thus will be a large factor in the outcome of the fire (e.g. how many items will ignite, if the room will flashover, etc.) The general theory of flame spread is that there is a pyrolysis front in which the material is currently burning and the flame that it is produced is causing the material right next to it to preheat. This preheating may eventually cause enough vapors to be released from the surface to create a mixture that is in the flammable range. The flame will then be the ignition source that will ignite the flammable mixture and the flame will spread slightly and the process will continue. Therefore, flame spread can be thought of as a series of ignitions along the sample surface. If the flame spread is very slow (i.e. the burn time is fast compared to the time to preheat the sample to release vapors in the flammable region), then the fire will decelerate with time. However, if the flame spread is very fast, then the fire will accelerate.[12]

There are other factors that will affect flame spread including ambient conditions (e.g. presence of wind) and the orientation of the burning surface. Concurrent flow spread, either by natural convection or ambient flows, will be faster than identical conditions with no wind because the flame will be leaning in the direction of the flame spread and will create a higher incident heat flux for the target elements. Flame spread up a wall is aided by natural buoyancy induced flows and thus is much faster than opposed flow flame spread.[12]

This theory demonstrates how the Steiner Tunnel Test cannot accurately predict real world scenarios because it only models flame spread along a ceiling in a forced flow field. It is unclear how forced concurrent flow spread, such as in the Steiner Tunnel Test, relates to buoyancy-induced concurrent flow spread, such as that found when a vertical wall is burning. There are also many other issues with the Tunnel Test that are detailed in the literature[3], including in the standard itself.[1] Quintiere[9] developed a flame spread b parameter to help correlate bench scale data to room/corner tests to determine flashover, which will be discussed in the next section.

Quintiere b Parameter

Quintiere's[9] flame spread parameter is given as:

$$b = k_f \cdot Q'' - 1 - \frac{t_{ig}}{t_b}$$

Where b is the flame spread parameter
Q" is the average or the peak HRRpuA [kW/m^2]
k_f is a constant equal to 0.01m^2/kW
t_{ig} is the time to ignition [s]
t_b is the total burning time [s]

This approach was chosen over the others in the literature because it is the classical approach and has values that are easy to determine in the FPA. Some of the methods in the literature use peak heat release rate and some use an average heat release rate in the equation for the b parameter. In this study, both the average and the peak heat release rate were used because the values were significantly different in some cases due to a strong initial peak (see Figure 62). Since the same burn duration was used for both the peak

and the average heat release rate in the b parameter equation, the b parameter calculated using the peak heat release rate assumes that the heat release rate is at its peak value for the entire burn duration. Therefore, the b parameter calculated using the peak heat release rate and the overall burn duration represents a worst case scenario.

Since all of the information about the sample is not known (e.g. the chemical formula), the generic heat release rate formulas were used. As stated before, the heat release rate for the FPA[7] is calculated using carbon dioxide generation calorimetry and that for the Cone[5] is calculated using oxygen consumption calorimetry.

Related to the idea of proper ignition discussed in a previous section, the time to ignition was defined as the time to the start of the flame cone. In most cases, this was the same as the time to ignition. However, it was slightly longer in some cases. Along the same line, the total burning time was defined as the time from the beginning to the end of the fully developed flame cone on the specimen surface, which was determined from visual observations. The observations of the end of the flame cone generally correlated with a change in the heat release rate trace. For System 1, which properly ignited at much lower heat fluxes than any other system, the disappearance of the flame cone usually correlated with the beginning of the decay tail or, in some cases, with the beginning of the second rounded peak in the heat release rate trace. For every other system, the flame cone generally ended after the initial peak.

From the FPA calibration tests, it was determined that the uncertainty in the heat release rate trace is a maximum of 70kW/m^2. The uncertainty in the time to ignition and the burn duration were found to be 9s and 101s, respectively. Given these uncertainties, the equation for the propagation of uncertainty[13] was used to determine that the uncertainty in the b parameter is approximately 0.7 full scale (±0.35).

Referring to the literature,[2, 9] the flame spread is considered to be accelerating if the b parameter is greater than zero and decelerating otherwise. Beyler et. al.[11] extend this idea to correlate a b parameter based on a test performed at an applied heat flux of 50kW/m^2 to the probability of flashover. They concluded, based on their data, that a material with a b parameter less than 0.3 is not expected to flashover in a room/corner test. However, materials with a b parameter larger than 0.3 are much more likely to flashover (although there were some outliers in their data set). Beyler et. al. did not publish any uncertainties related to the b parameter in their report.[11]

The b parameter for both the FPA and the Cone Calorimeter tests are given in Table 17. The tests performed at 50kW/m^2 are highlighted because the correlation from Beyler et. al.[11] is based on tests done at this applied heat flux. Considering those tests done at 50kW/m^2 in both Table 16 and Table 17, 1A and 1B based on a peak heat release rate in the FPA and 1B based on a peak heat release rate in the Cone are the only composite samples that would be expected to flashover in a room/corner test. The b parameter based on the peak heat release rate is significantly higher than that based on the average heat release rate due to the strong initial peak in the heat release rate for the 1A and 1B samples (see Figure 62).

However, the uncertainty in the b parameter is 0.7 so, in order to truly determine if the b parameter has a chance of obtaining the threshold value of 0.3 for flashover, this uncertainty needs to be added to the value that was obtained from the data. Table 18 represents the maximum possible values of the b parameter based on the data in Table 17. The maximum possible value of the b parameter for each FRP sample was determined by taking the value of the b parameter from Table 17 (the largest value was taken if there were duplicate tests) and adding 0.7.

From the data in Table 18, it can be seen that all of the polyester (System 1) samples have a b parameter larger than 0.3 and thus have the potential to flashover in the room/corner test based on the Beyler et. al.[11] correlation. 3A displays very negative b parameters, which indicate that the phenolic is not expected to flashover in the room/corner test. Comparing the tests done at 50kW/m^2, it is apparent that the phenolic has better fire performance than the polyester resin.

For the tests that are not completed at 50kW/m^2, the Beyler et. al.[11] correlation cannot be reliably used. Therefore, the discussion will be based on other references[2,9] that correlate a negative b parameter with decelerating flame spread and a positive b parameter with accelerating flame spread. If the maximum possible value of the b parameter is again considered (i.e. the b parameter plus the uncertainty of 0.7), the only samples that are expected to exhibit accelerating flame spread are 1A at 40kW/m^2 in the FPA, 1B at 30kW/m^2 in the FPA, 3A at both 70kW/m^2 and 80kW/m^2 in the Cone, and 5A and 5B at 100kW/m^2 in the Cone. This again demonstrates that the phenolics are superior to the polyester resin and that the additives (System 4 with the charring additive and System 5 with the intumescent additive) make the phenolic perform better.

An important observation regarding the b parameter is the significant increase in the b parameter with applied heat flux for the System 1 composites (see Figure 67). Since the uncertainty in the b parameter is 0.7, it can be seen that there is a very significant difference between low and medium heat fluxes but it seems to level off as the applied heat flux increases up to 50kW/m^2. From Table 16 and Table 17, it can also be seen that the b parameter makes a significant jump (see, for example, the b parameter for 1A in the FPA with applied heat flux) to become more negative just before the minimum heat flux for ignition (30kW/m^2 for 1A).

Conclusions and Future Work

The work being done in this study is important to the composites industry because it is a beginning to research into how the resin type and the glass content affect the overall fire performance of the composites. The resin type was found to greatly affect the resultant fire performance, however the effect of glass content is a little more subtle. For example, there is a difference in the peak heat release rate with glass content for the System 1 composites (see Figure 62) but there is no significant difference in the average heat release rate in the plateau region of the trace. There is an increase in the time to ignition and a decrease in the burning time with glass content for the System 1 composites (see Figure 62). The minimum heat flux for proper ignition greatly changed with resin type with the polyester resin (System 1) having a significantly lower minimum heat flux for proper ignition range than the phenolic resins and the phenolics with additives (Systems 4 and 5) improving over the performance of the neat phenolic (System 3). Except for System 1, the minimum heat flux for proper ignition range increased with glass content (see Table 15).

This work is also very important to the fire industry because the industry is leaning toward performance based design in modern building codes. This requires fire engineers to determine whether a room will flashover or not. From the results of the b parameter, it is expected that the FRPs with the polyester resin (System 1) would be expected to flashover in a room/corner test while the phenolics (Systems 3, 4 and 5) are not expected to flashover based on tests done at 50kW/m^2. Based on the large uncertainty in the b parameter and to verify the results of this study, it would be very interesting to perform large scale room/corner tests with the specimens. It will also be very important to relate the results obtained from the FPA with the results obtained with the Cone since much work has been done with the

Cone. A correlation between the two apparatuses will be needed to compare the FPA to past work done with other materials.

In the near future, there are plans to instrument the sample with embedded and surface thermocouples as well as an embedded heat flux gage and an IR thermometer in order to determine additional information such as temperatures at depth and the flame heat flux. This is especially useful information for modelling purposes.

Acknowledgments

The continued significant support for this project from FM Global Research (FM Global Fellow Avila and FM Global Scholar Dembsey) is greatly appreciated. The authors greatly appreciate the materials donated by: Trevor Humphries of VectorPly, Phoenix City, AL (glass); and Chad Fester of Airtech International Inc. of Huntington Beach, CA (vacuum bagging and peal ply) as well as Cinnabar, FL (lamination of the FRP composite panels). Many thanks also to Randall Harris, Mihyun (Esther) Kim and Jacqueline Shea at WPI for performing the Cone tests.

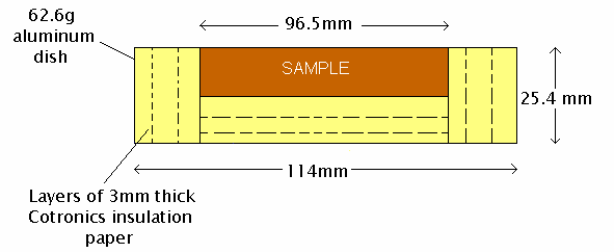

Figure 61: Insulated Sample Holder Designed by de Ris and Khan[15]

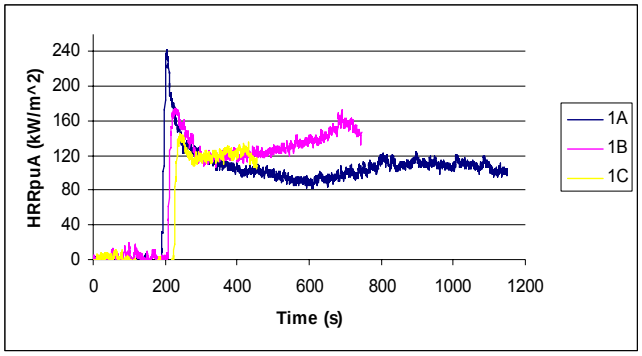

Figure 62: Comparison of the Generic CO_2 Based Heat Release Rate per Unit Area (HRRpuA) for System 1 at an Applied Heat Flux of 50kW/m^2 in the FPA[7], Truncated at Loss of Flame Cone

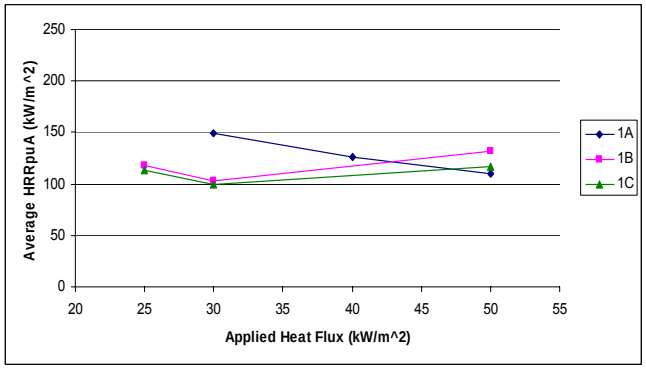

Figure 63: Comparison of Average CO_2 Based Heat Release Rate per Unit Area (HRRpuA) for System 1 over a Range of Applied Heat Flux in the FPA[7]

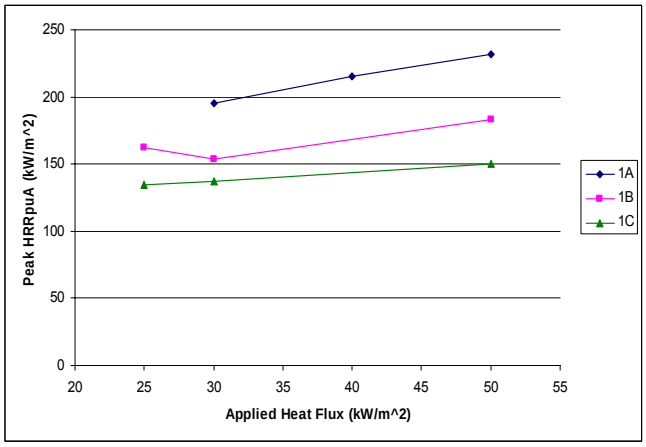

Figure 64: Comparison of Peak CO_2 Based Heat Release Rate per Unit Area (HRRpuA) for System 1 over a Range of Applied Heat Flux in the FPA[7]

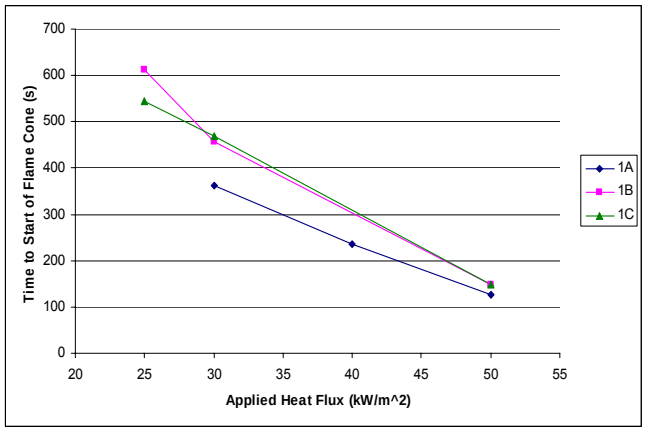

Figure 65: Comparison of Time to Start of Flame Cone for System 1 Composites at a Range of Applied Heat Flux in the FPA[7]

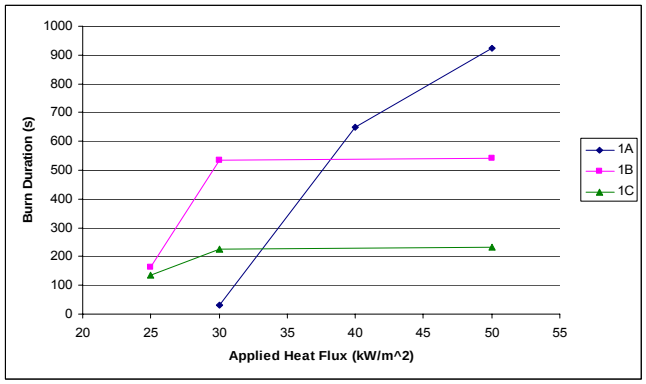

Figure 66: Comparison of Burnout Time for System 1 Composites at a Range of Applied Heat Flux in the FPA[7]

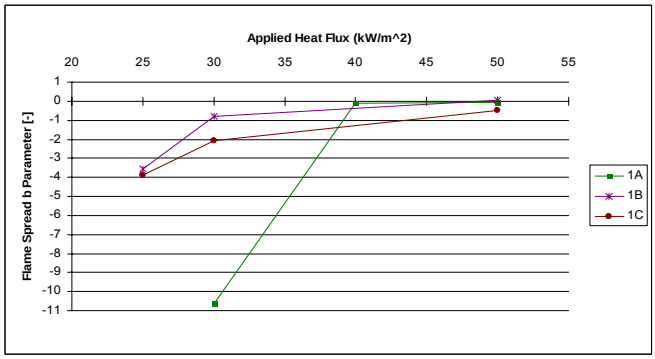

Figure 67: b Parameters Based on Average Values of CO_2 Based Heat Release Rate for System 1 Tests in the FPA[7]

Table 14: Results from FPA[7] Calibration Tests. The accuracy in percent is defined as a deviation of the average value from all of the tests as compared to the published value. The accuracy in kW is the maximum value that the heat release rate trace derived from the ASTM E 2058,[7] Parker[8] and Beaulieu[7] equations deviates from the reference heat release rate trace (the mass loss rate multiplied by the published chemical heat of combustion). All of the reported uncertainties are full scale as opposed to ± half scale. EHC stands for Effective Heat of Combustion (the cumulative heat release rate divided by the total mass lost). The Phase column represents the phase the material was when it was burnt (G=Gas, L=Liquid, S=Solid).

EHC -- 2058[4] Fuel Specific (CO2 Generation)				
Material	**Phase**	**# Tests**	**Accuracy (%)**	**Accuracy (kW)**
Propylene	G	6	-1.2	<0.5 *
Methane	G	6	8.6	<0.5 *
Acetone	L	4	7.9	<0.5
PMMA	S	3	-2.9	<0.5
EHC -- Parker[10] Fuel Specific (O2 Consumption)				
Material	**Phase**	**# Tests**	**Accuracy (%)**	**Accuracy (kW)**
Propylene	G	6	5	<0.5*
Methane	G	6	11	<1 *
Acetone	L	4	9	<0.5
PMMA	S	3	-1.4	<0.5
EHC -- Beaulieu[9] Fuel Specific (CO2 Generation)				
Material	**Phase**	**# Tests**	**Accuracy (%)**	**Accuracy (kW)**
Propylene	G	6	4.3	<0.5*
Methane	G	6	14.2	<1 *
Acetone	L	4	12.2	<0.5
PMMA	S	3	3.9	<0.5

Table 15: Description of the FRP Composites and the Minimum Heat Flux for Proper Ignition Range for each Composite Sample. The Thickness of the Sample and the Minimum Heat Flux for Proper Ignition are listed as ranges. The Minimum Heat Flux for Proper Ignition was determined in the Cone[8] except for System 1, which was determined in the FPA.[7] %RFG = % Refined Glass Content.

FRP Sample	Resin System	Glass (%RFG)	Thickness (mm)	Min HF (kW/m^2)
1A	Brominated Polyester	33	8.5-10	25-30
1B	Brominated Polyester	46.5	8.0-9.0	20-25
1C	Brominated Polyester	73.3	6	20-25
3A	Neat Resole Phenolic	38	6-9.5	40-50
3C	Neat Resole Phenolic	79.1	7-8	60-65
4A	Resole Phenolic w/ Charring Additive	30	7-8	50-60
4B	Resole Phenolic w/ Charring Additive	38	7.5-8	70-80
4C	Resole Phenolic w/ Charring Additive	48	8.5-10.5	90-100
5A	Resole Phenolic w/ Intumescent Additive	30	6	90-100
5B	Resole Phenolic w/ Intumescent Additive	45	8-9	90-100
5C	Resole Phenolic w/ Intumescent Additive	59	8-9	>100

Table 16: Table of FPA Tests for System 1 and the Corresponding b Parameters Using both the Average and the Peak Heat Release Rate Determined from the Generic CO_2 Based Formula Presented in ASTM E 2058[7]

FRP Sample	Heat Flux (kW/m^2)	Average -- Generic 2058	Peak -- Generic 2058
1A	50	0.0	1.1
1A	50	0.0	1.3
1A	40	-0.1	0.8
1A	30	-10.6	-10.2
1B	50	0.0	0.6
1B	50	0.1	0.5
1B	30	-0.8	-0.3
1B	25	-3.6	-3.1
1C	50	-0.4	0.0
1C	50	-0.5	-0.2
1C	30	-2.1	-1.7
1C	25	-3.9	-3.7

Table 17: Table of Cone Calorimeter Tests and the Corresponding b Parameter Using both the Average and the Peak Heat Release Rate Determined from the Generic O_2 Based Formula Presented in ASTM E 1354[8]

FRP Sample	Heat Flux (kW/m^2)	Average -- Generic 1354	Peak -- Generic 1354
1A	50	-0.7	-0.4
1A	50	-0.3	-0.1
1B	50	0.0	0.4
1C	50	-0.4	-0.2
3A	50	-6.3	-6.2
3A	60	-2.3	-2.1
3A	65	-3.8	-3.6
3A	70	-0.3	0.1
3A	80	-0.3	0.2
3C	65	-2.2	-2.1
3C	70	-1.7	-1.6
3C	80	-1.5	-1.4
4A	60	-4.0	-3.9
4A	65	-2.9	-2.7
4A	70	-2.9	-2.7
4A	80	-0.9	-0.7
4B	80	-1.4	-1.1
4C	100	-4.4	-4.3
5A	100	-0.1	0.1
5B	100	-0.3	0.1

Table 18: Table of Maximum Possible Values of the b Parameter for Tests Performed at 50kW/m^2 in both the FPA[7] and the Cone[8]. The Maximum Possible Value is Obtained by Taking the Value from Table 16 and Table 17 (the Maximum Value was taken if there were Two Identical Tests) and adding the Maximum Uncertainty in the b Parameter,[9] equal to 0.7. There is no Data for 3A at 50kW/m^2 in the FPA because this FRP Sample Popped and Delaminated Violently in this apparatus (see discussion in text).

FRP Sample	Avg. -- Generic 2058	Peak -- Generic 2058	Avg. -- Generic 1354	Peak -- Generic 1354
1A	0.7	2.0	0.4	0.6
1B	0.8	1.3	0.7	1.1
1C	0.3	0.7	0.3	0.5
3A	[-]	[-]	-5.6	-5.5

[Authors:]

Melissa Avila is a graduate student at WPI in the field of Fire Protection Engineering. She has a BS degree in Mechanical Engineering from WPI and is the FM Global Research Fellow. This study is part of her Master's thesis.

Nicholas A. Dembsey is an Associate Professor with the Fire Protection Engineering Department at WPI as well as FM Global Research Scholar. He is the Chair of ACMA's Fire Committee.

Charles H. Dore is a BS (Chemistry) and BA (Business) graduate of Widener University. Since 1950 he has been involved in formulation and lamination of resins, gel coats and composites. He holds 3 patents including development of sprayable syntactic foam, Spray Core™.

References

[1] Standard Test Method for Surface Burning Characteristics of Building Materials, ASTM E 84-05, ASTM, 100 Barr Harbor Drive, West Conshohocken, PA, U.S.

[2] Dembsey, N.A., J.J. Alston and S.D. Ayers, "Using Cone Calorimeter Data and Half-Scale Corner Test Data to Assess the Fire Performance of Composite Materials," submitted to Cinnabar-Florida, Orlando, FL, USA as part of the project *Phenolics vs. Other Thermosets for Theme Parks* (2001).

[3] Williamson, R.B. and F.W. Mowrer, "The Role of Interior Finish in Fire Development," *Fire Protection Engineering*, 2004, No. 24, pp. 26-40.

[4] Standard Methods of Test for Measurement of Synthetic Polymer Material Flammability Using a Fire Propagation Apparatus (FPA), ASTM E 2058-03, ASTM, 100 Barr Harbor Drive, West Conshohocken, PA, U.S.

[5] Standard Test Method for Heat and Visible Smoke Release Rates for Materials and Products Using an Oxygen Consumption Calorimeter, ASTM E 1354-02, ASTM, 100 Barr Harbor Drive, West Conshohocken, PA, U.S.

[6] Cleary, T. and J. Quintiere, "A Framework for Utilizing Fire Property Tests," *Fire Safety Science, Proceedings of the Third International Symposium,* International Association of Fire Safety Science (IAFSS), Scotland, U.K., Cox and Langford Editors, Elsevier Applied Science London and New York, July 8-12 (1991) 647-656.

[7] User's Guide for the Fire Propagation Apparatus (FPA) ASTM E-2058, Fire Testing Technology Limited, PO Box 116, East Grinstead, West Sussex, England.

[8] de Ris, J.L. and Khan, M.M., "A sample holder for determining material properties," *Fire and Materials*, 24, 219-226 (2000).

[9] Beaulieu, P.A. and Dembsey, N.A., "Enhanced Equations for Carbon Dioxide and Oxygen Calorimetry," *Proceedings of the 9th International Fire and Materials Conference,* p.49 (2005).

[10] Parker, W.J., "Calculations of the Heat Release Rate by Oxygen Consumption for Various Applications," National Bureau of Standards Report # NBSIR 81-2427 (1982).

[11] Beyler, C., S. Hunt, B. Lattimer, N. Iqbal, C. Lautenberger, N. Dembsey, J. Barnett, M. Janssens, S. Dillon and A. Grenier, "Prediction of ISO 9705 Room/Corner Test Results," US Department of Transportation, Report No. R&DC-215-99, 1999.

[12] Quintiere, J.G. "Surface Flame Spread." SFPE Handbook of Fire Protection Engineering, 3rd Edition. Ed. Philip J. DiNenno. Quincy, MA: National Fire Protection Association, 2002.

[13] Coleman, H. W. and W. G. Steele, Experimentation and Uncertainty Analysis for Engineerings, 2nd Edition, New York: John Wiley & Songs., Inc., 1999.

Appendix I: Paper for Fire and Materials 2007

Effect of Resin Type and Glass Content on the Fire Engineering Properties of Typical FRP Composites

Melissa Avila & Nicholas Dembsey
Worcester Polytechnic Institute, Worcester, MA

Charles Dore
Abate Fire Technologies

Abstract

This study is designed to provide the composites industry as well as the fire engineering industry engineering "properties" and baseline data for pyrolysis modelling of common fiber reinforced polymer (FRP) systems. Four resin systems and three glass contents will be considered. This matrix of FRP systems has been carefully fabricated and documented so as to provide "transparency" as to the system compositions. An important and interesting aspect of these FRP systems is that all the resins used are listed by the manufacturers as Class 1 or Class A per ASTM E 84. The FRP systems are being evaluated in bench scale modern fire test apparatuses (FPA, ASTM E 2058, and Cone, ASTM E 1354). These apparatuses provide a range of measurements such as heat release rate that can be used to calculate engineering "properties" of these FRP systems. The "properties", such as minimum heat flux for proper ignition (found to range from 20 to over 100 kW/m^2) and the b flame spread parameter, can then be used to compare the fire performance (flashover potential) of these FRP systems according to resin type and glass content. Additional instrumentation has also been added to the specimens to allow surface and in-depth temperatures to be measured. The additional measurements complete a set of data useful for pyrolysis

modelling. The effect of environment oxygen concentration and flaming and non-flaming decomposition are investigated in terms of fundamental pyrolysis behavior of the FRP systems.

Introduction

Traditionally, the UL Steiner Tunnel Test, ASTM E84[1], has been used to evaluate the fire hazard of interior wall finishes, such as composite materials. The sample in the Tunnel Test is placed horizontally on a ceiling of a tunnel-like test apparatus. Although it has been used for over 50 years, the Tunnel Test has a number of important shortcomings. First, the results of the test only provide a classification scheme for ranking materials; the results do not include useful engineering data. Second, some materials do not behave in the Tunnel Test as they would in a real fire scenario. Since the sample in the Tunnel Test is a horizontal sample, upward flame propagation is not modelled.[2,3] A more appropriate test would be one in which both concurrent and opposed flow flame spread were possible, such as in the room/corner test (ISO 9705[4], NFPA 265[5] and NFPA 286[6]). In this test method, a large ($4m^2$) sample is placed on the walls as well as on the ceiling of a corner in a standard test room. The corner is then exposed to an incident heat flux from a large flame. This more closely represents a realistic fire scenario but has the disadvantages of being expensive and time-consuming. Therefore, many different researchers have worked toward developing a model to use bench-scale data (such as the Fire Propagation Apparatus (FPA), ASTM E 2058[7], or the Cone Calorimeter, ASTM E 1354[8]) to predict room/corner test results.[2, 3] Other researchers have developed pyrolysis models to predict behavior directly from these bench-scale tests.[9]

In this study, properties such as the heat release rate, minimum heat flux for proper ignition and the Quintiere[10] flame spread parameter, b, will be used to differentiate the composite systems based on resin type and glass content. The b parameter will also be used to estimate whether flashover might occur in the room/corner test from bench-scale experiments done in the FPA and the Cone Calorimeter. Embedded thermocouples and an infrared thermometer to measure sample surface temperature as well as changing the environment to which the sample is exposed give additional insight into the behavior of the composites and provide the beginning of a data set useful for modelling purposes.

The FPA and the Cone Calorimeter

The FPA[7] is a bench-scale fire test apparatus in which the sample is heated by four radiant lamps. Each IR lamp consists of 6 bulbs with a tungsten wire in argon gas, which provides a uniform heat flux (to within 5kW/m^2, determined from testing) over the specimen surface of up to 60kW/m^2. The lamps emit with spectral energy peaks of 1.15 and 0.89 microns.[11] A long quartz tube can be used to create an atmosphere for the test that is different than the ambient (i.e. enhanced oxygen up to 40% or pure nitrogen). A flow rate of air at 200lpm is run through the bottom of the air chamber so that the sample is in a flow field during the test. The ignition source is a 10mm long blue pilot flame located 10mm above the center of the sample. The FPA can be used to calculate useful engineering data such as heat release rate, mass loss rate, smoke yield and smoke extinction coefficient. The standard specifies a carbon dioxide generation based heat release rate, which will be used for the FPA in this study.[7]

The Cone Calorimeter[8] is similar to the FPA but it also has some important differences. The heater in the Cone is an electrically heated rod in the shape of a cone, instead of the IR lamps in the FPA. The sample in the Cone is exposed to the ambient environment and is not in a flow field so the apparatus can only perform tests under ambient conditions. The ignition source is an intermittent sparker instead of the pilot flame used by the FPA. The Cone standard specifies an oxygen consumption based heat release rate, which will be used for the Cone in this study.[8]

Sample Holder

Instead of the non-insulated aluminium dish that is specified in ASTM E 2058[7], an insulated sample dish described by de Ris and Khan[12] is used. The sample is surrounded by Cotronics® paper insulation on the back and sides as shown in Figure 61 below to provide a barrier to heat loss.

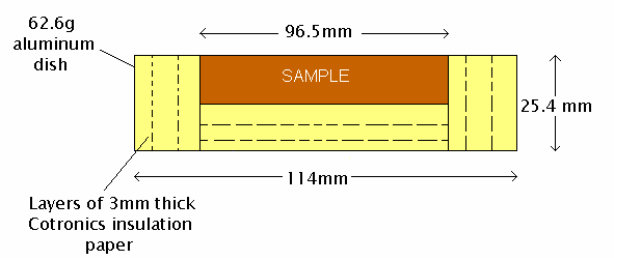

Figure 68: Insulated Sample Holder Designed by de Ris and Khan[15]

The assumptions that can be made based on the presence of the insulation (e.g. no heat loss from the back face or sides of the sample) are very useful in modelling the sample's reaction to the applied heat flux. The sample holder is also beneficial for installing embedded and back face thermocouples as well as embedding a heat flux gage to lie flush with the sample surface, which is the next step to be completed in the current work.

Radiant Source Comparison - Cone and FPA

The difference in the radiant source between the Cone and the FPA is noteworthy because the FPA radiation apparently tends to absorb at depth into the composites evaluated in this study while the Cone does not. This difference causes a discrepancy in the time to ignition and burn duration between results obtained from the Cone and the FPA, as can be seen in Figure 69 below for the polyester with the lowest glass content.

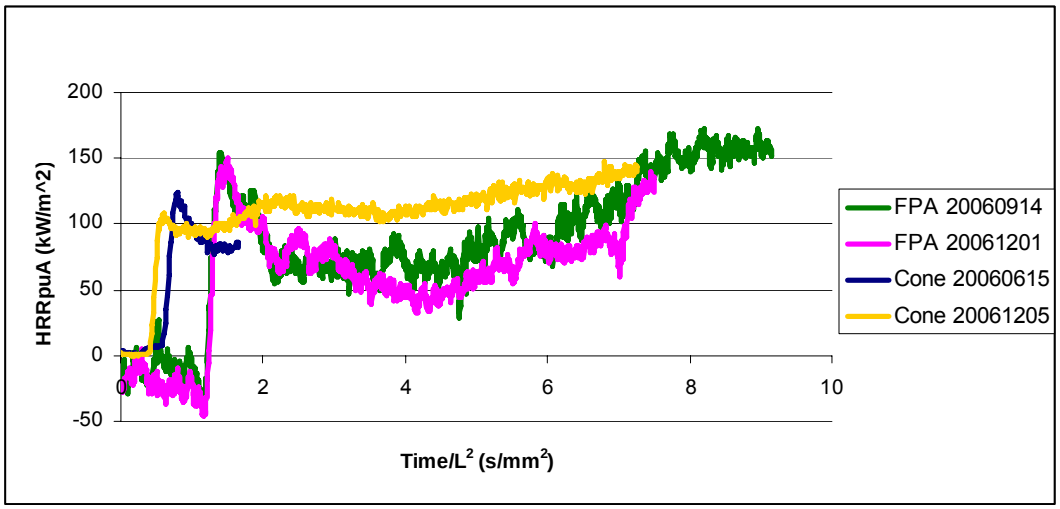

Figure 69: HRR Traces for two Cone Tests and two FPA Tests. All tests were done with sample 1A at 50kW/m^2. Time zero is shutter down time. The data is truncated at loss of flame cone. The date of the test is shown in the legend.

The time axis in the graph is normalized with respect to thickness, as all graphs will be reported in this paper. This normalization assumes that the thermal diffusivity is the same for all samples in this study and is used to eliminate the effect of thickness on the results. There was a variability of 6-10.5mm in thickness over all of the composite systems used.

Figure 69 demonstrates that there is a definitive difference in the time to ignition between the Cone and the FPA tests, however the difference in the burn duration is unclear. The variability in the Cone burn duration seen in the graph is unexplained at this time although it could be due to inherent variability in the composite samples, difference in ambient conditions on test days or many other factors. For example, if there was less resin close to the surface for one of the Cone 1A samples and there was little to no in-depth absorption of the radiation (as is thought to be the case for the Cone), the result may be a quicker burn out time because the resin near the surface burns out before it can sufficiently preheat the in-depth resin to continue burning. More work is needed to solve these issues.

Testing performed with thermocouples to demonstrate differences between FPA and Cone test results were inconclusive. Figure 70 shows a comparison between thermocouple traces for identical tests done in the Cone and the FPA on the polyester sample with the lowest glass content (1A) at 50kW/m^2.

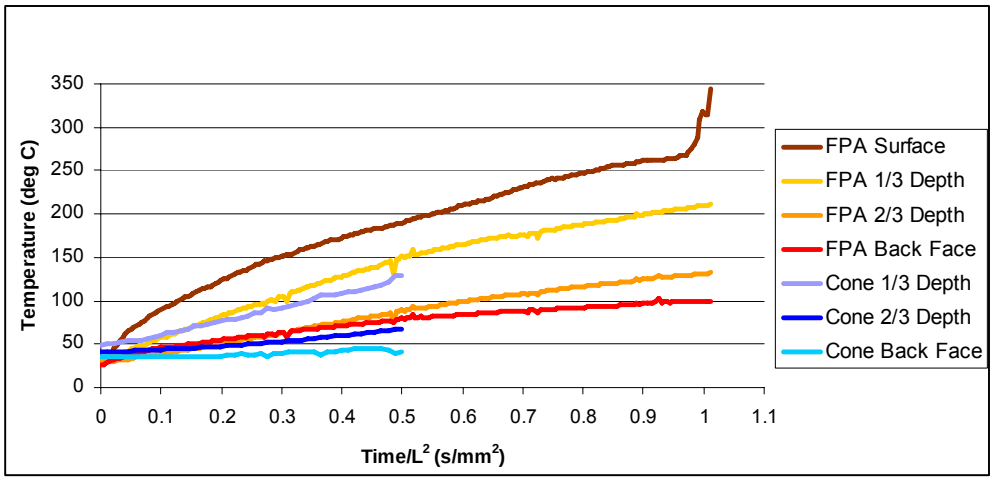

Figure 70: Comparison of Surface and In-Depth Temperature on the Cone and the FPA at 50kW/m^2 for the 1A sample. Data is truncated at ignition. Time zero is shutter down time. The surface temperature data for the Cone test did not record properly and is not included.

The Cone test for the 1A sample ignites before the FPA test of the same material and the temperature begins to rise a bit slower than the FPA test. After the initial period however, the thermocouple traces between the two tests match each other fairly well. The results from this testing are inconclusive at this time and future work is needed.

An attempt was also made to resolve the absorption issue by applying carbon black powder to the surface of the specimen in the FPA to prevent in-depth absorption. The carbon black decreased the time to ignition in the FPA to match that of the Cone but did not affect the overall burning duration as compared to tests in the FPA without carbon black. In some cases, this is thought to be due to near surface effects (e.g. jetting at the specimen surface causing disruptions in the carbon black layer) preventing the carbon black from covering the whole surface after initial radiant exposure. The carbon black did not affect the heat release rate or the b parameter as compared to results without carbon black in the FPA but it did increase the range of the minimum heat flux for proper ignition compared to tests without carbon black in the FPA for the System 1 composites. The results from the tests with carbon black are not reported in this study due to inconsistencies in the results; future work is needed.

Apparatus Calibration

Before any testing of the composite samples was started, tests were done with well-known materials in an attempt to determine the uncertainty in the time to ignition, burn duration, mass loss rate and heat release rate in the FPA,[7] since it is a new apparatus at WPI. The analysis for the uncertainty in the time to ignition, burn duration and mass loss rate for the FPA is based on three PMMA tests. A sample set of three is believed to be sufficient in this case because the FPA standard calls for three identical tests to be performed to correctly determine other properties.[7] From these tests, the maximum uncertainty in the time to ignition and the burn duration were found to be 9s and 101s, respectively. The uncertainty in the mass loss rate was found to be 17mg/s. These uncertainties are full scale (as opposed to ± half scale).

FPA tests were done with methane, propylene and acetone, as well as PMMA, and the heat release rate was calculated using three different methods. The ASTM E 2058[7] and the Beaulieu[13] methods are based on carbon dioxide generation while the Parker[14] method is based on oxygen consumption. All three methods can be formulated as either fuel specific or generic (i.e. published average values). The effective heat of combustion was found by dividing the cumulative heat release rate by the total mass lost. This effective heat of combustion was compared to the chemical heat of combustion (equal to the published total heat of combustion corrected for the published smoke yield); this method is specified as a heat release rate calibration procedure in ASTM E 2058, using acetone as a model material. The standard states that the effective heat of combustion, calculated using the fuel specific heat release rate equation, must be within ±5% of the published value for acetone.[7] As can be seen from Table 19, the accuracy (defined as the deviation of the average value from all of the tests as compared to the published value; all of the reported uncertainties are full scale as opposed to ± half scale) in the acetone heat of combustion, calculated from the fuel specific equation, was found to be 7.9%. Therefore, the heat release rate for the FPA was found to be calibrated according to ASTM E 2058. Effective heat of combustion accuracies determined using the other methods of calculating heat release rate are also shown in Table 19 to demonstrate that there is not a significant difference between the results from the different methods.

Table 19: Results from FPA[7] Calibration Tests. All of the reported uncertainties are full scale as opposed to ± half scale. EHC=Effective Heat of Combustion; G=Gas; L=Liquid; S=Solid.

EHC--Fuel Specific 2058						
Material	**Phase**	**# Tests**	**Accuracy (%)**	**Precision (%)**	**Avg Deviation (kW)**	**Max Deviation (kW)**
Propylene	G	6	-1.2%	+/-2.5%	0.3	<0.5 *
Methane	G	6	8.6%	+/-1.5%	0.4	<0.5 *
Acetone	L	4	7.9%	+/-5%	0.3	<0.5
PMMA	S	3	-2.9%	+/-2.5%	0.2	<0.5
EHC--Parker						
Material	**Phase**	**# Tests**	**Accuracy (%)**	**Precision (%)**	**Avg Deviation (kW)**	**Max Deviation (kW)**
Propylene	G	6	5.0%	+/-1.5%	0.8	<1*
Methane	G	6	11.0%	+/-2%	0.7	<1 *
Acetone	L	4	9.0%	+/-5%	0.5	<0.5
PMMA	S	3	-1.4%	+/-2%	0.2	<0.5
EHC--Beaulieu						
Material	**Phase**	**# Tests**	**Accuracy (%)**	**Precision (%)**	**Avg Deviation (kW)**	**Max Deviation (kW)**
Propylene	G	6	4.3%	+/-2.5%	0.4	<0.5*
Methane	G	6	14.2%	+/-0.5%	0.6	<1 *
Acetone	L	4	12.2%	+/-5%	0.4	<0.5
PMMA	S	3	3.9%	+/-3%	0.2	<0.5

In Table 19, the number listed as the accuracy in kW is the average or maximum value that the heat release rate trace calculated from the ASTM E 2058,[7] Parker[8] and Beaulieu[7] equations deviates from the reference heat release rate trace (the mass loss rate multiplied by the published chemical heat of combustion). There is an asterisk in the last column for both propylene and methane because both of these gases were coming from the FPA's gas burner. The mass flow rate of the gas was stepped up and down during the experiment, which increased the heat release rate of the fire. In the case of both propylene and methane, it was found that the absolute difference between the calculated and the reference heat release rate traces got larger as the mass flow rate was increased.

The absolute accuracy in Table 19 is listed in kW even though units of kW/m^2 are generally used. Since the propylene and the methane are in the gaseous state and are coming through the FPA's gas burner, there is no specimen surface to divide by to achieve units of kW/m^2. Since the average specimen surface of the composites is $0.007m^2$, the uncertainty in kW/m^2 is an average of $45kW/m^2$ and a maximum of $70kW/m^2$. These uncertainties are determined by averaging all of the uncertainties in the table, except for the cases in which the maximum deviation was <1 instead of <0.5. These uncertainties are believed to be erroneously high since the gas burner was turned to a high heat release rate during the test, which increased the uncertainty. The average heat release rate uncertainty of $45kW/m^2$ will be used to evaluate differences in this study.

The uncertainty in the infrared thermometer and thermocouple measurements was determined from comparing the traces from identical tests, including PMMA and composite testing. Population statistics were calculated based on this comparison and it was found that the uncertainty in the infrared thermometer, which measures sample surface temperature, clustered around 0°C or 70°C so an uncertainty of 70°C will be used. The high degree of uncertainty in this measurement is thought to be due to installation issues; more work is needed. The thermocouple measurements were found to have an average uncertainty of 17°C with a standard deviation of 17°C; the average uncertainty will be used to evaluate significant differences in the thermocouple traces.

The uncertainties calculated above for the FPA will also be used for evaluating significant differences in Cone tests. The heat release rate uncertainty in the Cone is governed by the C factor, which is determined by calculating the heat release rate of a methane fire at different mass flow rate steps and inserting the subsequent values into an equation for the C factor that is provided in ASTM E 1354.[8] The required uncertainty from the standard is 5% and it is known that the Cone meets this requirement. Therefore, no additional calibration testing was required on the Cone for the purposes of this study.

Description of Composite Systems

In the following discussion, the term "system" will be used to differentiate between resin types (e.g. System 1 is a polyester). The term "sample" will be used to differentiate between glass contents (e.g. sample 1A has a lower glass content than sample 1B). Lastly, the term "specimen" will be used to represent one individual composite from the sample that will be tested.

Eleven different fiber reinforced polymer (FRP) samples are being tested for the current work. There is a total of 4 different resin systems, each with three different glass contents (except for System 3, which has only two glass contents). Table 2 shows the base resin and the glass content for all of the FRP composites that were tested in the current study.

Table 20: Description of the FRP Composites and the Minimum Heat Flux for Proper Ignition Range for each Composite System. The Sample Thickness and the Minimum Heat Flux for Proper Ignition (determined in the FPA[7] for System 1 and in the Cone[8] for all others) are listed as ranges. %RFG = % Refined Glass Content.

FRP Sample	Resin System	Glass (%RFG)	Thickness (mm)	Min HF (kW/m^2)
1A	Brominated Polyester	33	8.5-10	25-30
1B	Brominated Polyester	46.5	8.0-9.0	20-25
1C	Brominated Polyester	73.3	6	20-25
3A	Neat Resole Phenolic	38	6-9.5	40-50
3C	Neat Resole Phenolic	79.1	7-8	60-65
4A	Resole Phenolic w/ Charring Additive	30	7-8	50-60
4B	Resole Phenolic w/ Charring Additive	38	7.5-8	70-80
4C	Resole Phenolic w/ Charring Additive	48	8.5-10.5	90-100
5A	Resole Phenolic w/ Intumescent Additive	30	6	90-100
5B	Resole Phenolic w/ Intumescent Additive	45	8-9	90-100
5C	Resole Phenolic w/ Intumescent Additive	59	8-9	>100

Antimony trioxide was added to the polyester (System 1) as a smoke inhibitor. The neat resole phenolic (System 3) is comprised of formaldehyde and phenol and was modified with the addition of a char forming, fire retardant plasticizer that lowers the viscosity of the resin and further enhances its physical and resistance properties. An inorganic fire retardant for System 4 is used to create a high charring effect while an organic fire retardant for System 5 creates an intumescent effect. The fiberglass in each of the composites is Vectorply's 0/90 biaxial glass with a chopped strand mat stitched to it. All of the resins used in this study are listed as Class 1 or A with regards to ASTM E 84.[1]

Proper and Improper Ignition

The concept of proper ignition that was used in this study is an extension of the concept of "sustained flaming" that was developed in ASTM E 2058.[7] The standard defines sustained flaming as the "existence of flame on or over most of the specimen surface for at least a 4s duration".[7] Since one of the goals of this study is to produce useful data for the development of a pyrolysis model, a fully developed flame cone is necessary to make the simplifying assumption of one-dimensional burning. Another benefit to this definition is that it does not count edge burning as significant burning because the end use of this product (i.e. a wall, ceiling, floor) would be so large that edge effects would be very minor. A flame is considered to be effectively one-dimensional if it is even over the entire sample surface and is unified into a single

flame cone (not necessarily axisymmetric). A distinction was made between cellular burning (flamelets over most or all of the surface) and edge burning. If a sample started to burn with cellular flaming and then progressed into a flame cone, it was still called proper ignition for the purposes of this study. Visual observations were made as to the time of the beginning and end of the flame cone so that data could be properly truncated for modelling purposes. This definition of proper ignition was also used in the calculation of the b parameter[9] (where the time to ignition is defined as the start of the flame cone and the burn out is defined as the loss of the flame cone) and in determining the minimum heat flux for proper ignition.

The concept of a critical mass flux is used by modellers as a cut-off point for when the sample ignites and when there is flame out. When the mass flux reaches a critical value, the sample is assumed to have ignited and when it decreases past this value near the end of the test, the flame is assumed to have gone out.[15] The critical mass flux at proper ignition was determined for the samples studied and the results are displayed in Table 21 below.

Table 21: Table of Critical Mass Flux at Proper Ignition. 5A and 5B are based on only one test.

Sample	Average (g/sm^2)	Standard Deviation (g/sm^2)
PMMA	9	6.5
1A	13	2.9
1B	10	4.1
1C	8	1.5
3A	8	2.6
3C	7	5.3
4A	11	4.5
4C	10	5.2
5A	7	NA
5B	5	NA

As can be seen from the table, there is a high degree of uncertainty in the critical mass flux. The critical mass flux is based on the time to ignition (uncertainty of 9s) and on the mass loss rate (uncertainty of 17mg/s) and therefore has a large degree of variability. Also, all tests that experienced proper ignition, including FPA and Cone tests at a variety of heat fluxes, were included to obtain the statistics displayed in the table. Despite the high degree of uncertainty, it is interesting to note that there is a significant downward trend in the critical mass flux at proper ignition with increasing glass content for the system 1 composites (polyester). The PMMA is included as a reference from the literature to ensure consistency.

From Nelson, PMMA has a critical mass flux at ignition of 4-5g/sm^2, which matches with the value obtained with the FPA (within the uncertainty). Another interesting note with regards to the table is that the critical mass flux at proper ignition is approximately 10g/sm^2 for all of the materials studied, including the PMMA and all of the composite systems.

FPA and Cone Testing

After tests were done to calibrate the FPA,[7] testing on the composites was started. In order to get an initial set of data, each sample was tested twice in the FPA at an incident heat flux of 50kW/m^2 with the quartz tube in place. This is a practical choice for a heat flux because it represents an average between the heat fluxes typically observed in room/corner tests. In these tests, the lateral flames have a heat flux of approximately 25kW/m^2 while upward flame spread generates about 100kW/m^2.[16]

After this initial set of tests was performed at 50kW/m^2, additional tests were done to determine the minimum heat flux for proper ignition. System 3, 4 and 5 (the phenolic samples) did not properly ignite at 50kW/m^2 so some tests were also performed at 60kW/m^2. None of the Systems 3, 4 and 5 composites would ignite in the FPA at 60kW/m^2, which is the highest heat flux that the FPA can achieve. Therefore, the minimum heat flux for proper ignition for these systems had to be determined in the Cone,[8] which can achieve up to 100kW/m^2. The minimum heat flux for proper ignition for the System 1 (polyester) composites was determined with the FPA.

A testing matrix was created after the initial round of testing in an effort to compile a good set of data for modeling purposes. The matrix consisted of tests to fully develop potential differences with glass content and resin type for certain composites, perform non-flaming tests, study environmental effects and compare results between the Cone and the FPA. All tests had instrumentation including embedded thermocouples, a back face thermocouple and an infrared thermometer to measure sample surface temperature. In order to better determine differences with glass content and resin type, tests were done with the polyester composites at all three glass contents in the FPA at 50kW/m^2 and with the neat phenolic with the highest glass content at 70kW/m^2 in the Cone; all of these tests experienced proper ignition. Tests

were also done with the 1A and 3C samples at 50kW/m^2 in the FPA under nitrogen and air atmospheres as well as on 1A samples at 50kW/m^2 in the FPA and the Cone.

FPA Results

The only system that properly ignited at 50kW/m^2 in the FPA[7] was the polyester (System 1), which had significant amounts of black smoke with large stringy particulates of styrene in the smoke. The neat phenolic with the low glass content (3A) delaminated violently and the test had to be stopped in one case. The rest of the samples had only edge burning (i.e. flames emerging from between the sample and the layers of Cotronics®) after hundreds of seconds of exposure.

Figure 71 below is a graph of the heat release rate traces from FPA tests done at 50kW/m^2 for the System 1 composites. The end of the trace is truncated based on visual observations of the loss of the fully developed flame cone.

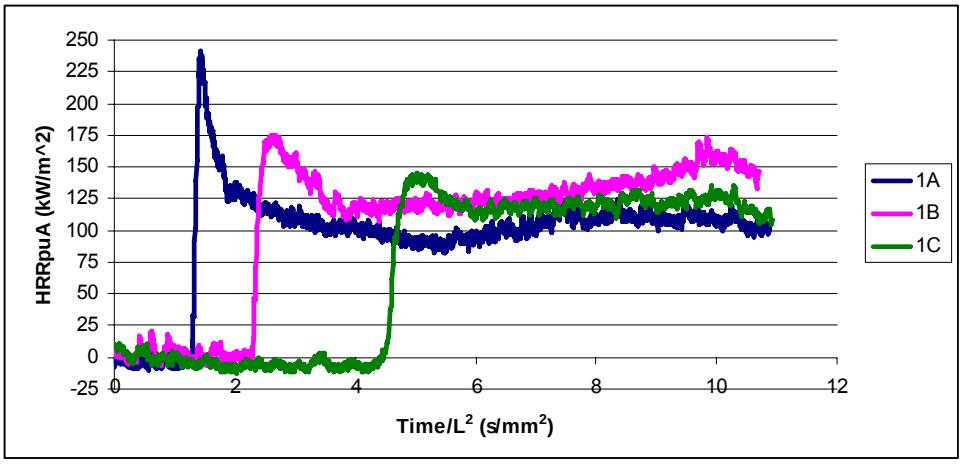

Figure 71: Comparison of the Generic CO_2 Based Heat Release Rate per Unit Area (HRRpuA) for System 1 at an Applied Heat Flux of 50kW/m^2 in the FPA[7], Truncated at Loss of Flame Cone. The thicknesses of the samples are: 1A 10mm; 1B 8mm; and 1C 6mm.

Recalling that the heat release rate uncertainty for the FPA is 45kW/m^2, it can be seen that the top layer has a significantly higher heat release rate than the rest of the layers for 1A and 1B but 1C does not have a significant initial peak. Considering the difference in the initial peak with changing glass content, it can be seen that the magnitude of the initial peak is significantly different between 1A and 1B as well as between

1A and 1C but there is not a significant difference between the initial peaks of 1B and 1C. However, the graph shows a trend that as the glass content is increased, the magnitude of the initial peak decreases. These differences are believed to be related to the surface texture. The surface texture of 1A and 1B is smooth and 1A is highly glossy, which seems to indicate that there is a resin film on the surface. However, 1C has a very bumpy surface due to the weave from the glass layers, which may indicate that there is much less resin near the surface than for 1A or 1B and thus a less significant initial peak in the heat release rate trace.

Given the accuracy with which the heat release rate can be determined in the FPA, the difference in the plateau region of the curve is insignificant (see Figure 71) across all of the System 1 samples. Once the top layer of resin is burnt off, the glass layers block the heat transfer into and the mass transfer out of the specimen, slowing the decomposition of the resin. This effect appears to be present irregardless of the glass content for the range of glass contents studied.

From the test data, the time to ignition for samples 1A, 1B and 1C are 124s, 145s and 159s, respectively. Given that the uncertainty in the time to ignition is 9s, there is a significant increase in the time to ignition with glass content for all of the polyester composites. In Figure 71, the test is truncated at the loss of flame cone, which is approximately the same for all three glass contents if the time axis is normalized with the thickness of the specimen, as it appears in the graph. This result apparently indicates that the three different glass contents reach the same sort of condition at the loss of the flame cone but more work is needed to understand the results. An interesting note is that if the time is not normalized (graph is not shown in this paper), there is a significant decrease in the burn duration with increasing glass content across all three system 1 composites.

Another view on the results was observed by looking at the sample's response to a range of applied heat flux. It was found that neither the average nor the peak heat release rate for System 1 significantly changed over an applied heat flux range of 20-50kW/m^2. This demonstrates that the System 1 composites have a similar burning rate over the range of applied heat fluxes considered, given the heat release rate uncertainty. It was also found that the time to the start of the flame cone significantly decreases and the burn duration significantly increases as the applied heat flux is increased. The higher heat flux will

heat the sample up to ignition faster and will provide sufficient energy to decompose more of the resin and expel it through the glass layers.

Minimum Heat Flux for Proper Ignition

The only composite system that properly ignited in the FPA[7] was System 1 so the rest of the samples had to be tested in the Cone[8] at higher heat fluxes. The last column in Table 20 gives the minimum heat flux for proper ignition as a range. A change in the minimum heat flux for proper ignition range is considered to be significant if it is greater than or equal to the step that is being taken (i.e. 5kW/m^2 or 10kW/m^2).

There is a significant change in the minimum heat flux for proper ignition over all of the systems with resin type. The polyester resin (System 1) has a lower minimum heat flux for proper ignition range than any of the phenolic resins. Among the phenolics, the neat phenolic (System 3) has the lowest minimum heat flux for proper ignition, which shows that the additives (Systems 4 and 5) are having a significant effect on the fire performance. The intumescent additive, System 5, tends to have a significantly higher minimum heat flux for proper ignition than the charring additive, System 4.

There also appeared to be a trend for most of the systems with changing glass content, except for System 1. The data in Table 20 seem to indicate that the minimum heat flux for proper ignition increases as the glass content increases. That is, as the glass content of the sample increased, more energy was needed to overcome the blocking effect of the glass and release enough vapors at the sample surface to create a steady flame cone over the entire surface.

System 1 seems to have an effect that is unexpected (i.e. the lowest glass content has the lowest minimum heat flux for proper ignition) however, more tests should be done to fully confirm this effect. Only one test was done with each sample at each heat flux.

System 3 appears to show a significant change with glass content. It should be noted that 3A was tested in the FPA at 50kW/m^2 and did not properly ignite due to significant delamination and violent popping early in the test. In the Cone, the 3A sample properly ignited before severe popping and delamination occurred. The difference in reaction of the 3A sample between the two different apparatuses is thought to be due to in-depth absorption of the FPA lamp's wavelength into the specimen, as discussed

before. Therefore, the 3A sample was tested in the Cone even though the minimum heat flux for proper ignition range would indicate that it could be successfully tested in the FPA.

System 4 showed an increase in minimum heat flux for proper ignition at each change in glass content (i.e. 4A, 4B and 4C all have different minimum heat flux for proper ignition ranges) while System 5 only demonstrated a change for the highest glass content. Sample 5C has a minimum heat flux for proper ignition that is higher than the maximum applied heat flux that the Cone can achieve.

Thermocouple and Infrared Thermometer

The introduction of embedded thermocouples and the infrared thermometer provides additional data to compare the composites based on resin type and glass content and is the beginning of a data set useful for modelling purposes. This data is preliminary and testing and analysis on the data is ongoing. A comparison of temperatures in-depth and on the back face of the specimen can demonstrate further differences with glass content for the polyester composites, as shown in Figure 72 below.

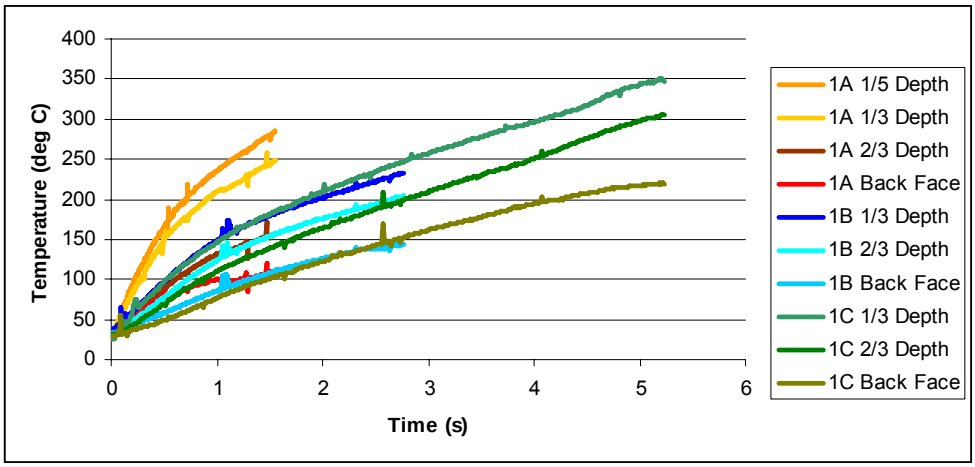

Figure 72: Comparison of In-Depth Temperatures for the System 1 Composites. All tests were done in the FPA at 50kW/m^2. Time zero is shutter down time. Data is truncated at ignition.

Since the samples are different thicknesses, the time axis was normalized by the thickness of the sample. This assumes that all of the samples have the same thermal diffusivity. The heating rate is apparently slowing down slightly with glass content. The graph also clearly demonstrates the difference in time to ignition with glass content, as discussed before.

A comparison was also made between the polyester with the highest glass content and the char former phenolic with the highest glass content to determine differences with resin type, as seen in Figure 73. Both tests were done at 50kW/m^2 in the FPA.

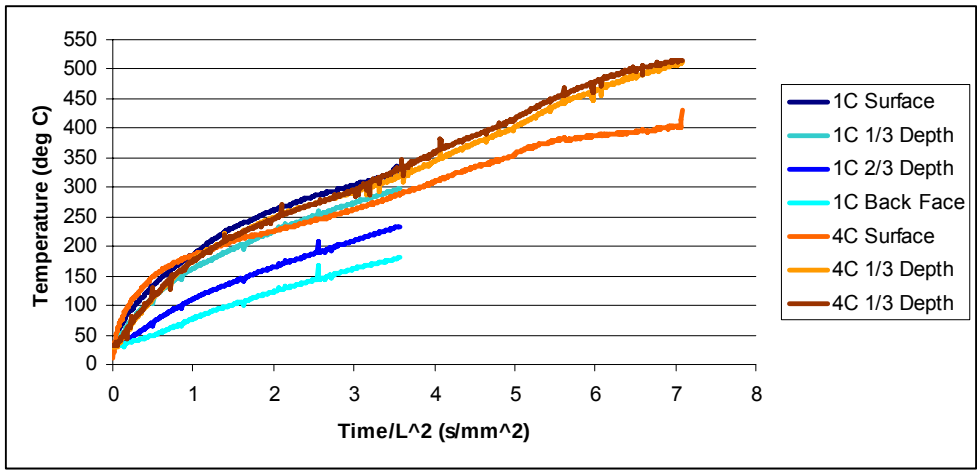

Figure 73: Comparison of 1C and 4C in the FPA at 50kW/m^2. Time zero is shutter down time. The data is truncated at time of ignition.

From Figure 73, it can be seen that the polyester (1C) and the char former phenolic (4C) have approximately the same heating rate, within the thermocouple uncertainty of 17°C and the surface temperature uncertainty of 70°C (as discussed before). The 2/3 and back face thermocouples for the 1C sample lag behind, as would be expected.

Tests were also done under nitrogen and under air with no pilot flame to determine any effects due to a change in atmosphere as well as to prolong the non-flaming condition to achieve more useful temperature data for modelling purposes. A comparison of the 1A sample at 50kW/m^2 in the FPA under these two environments is shown in Figure 74 below.

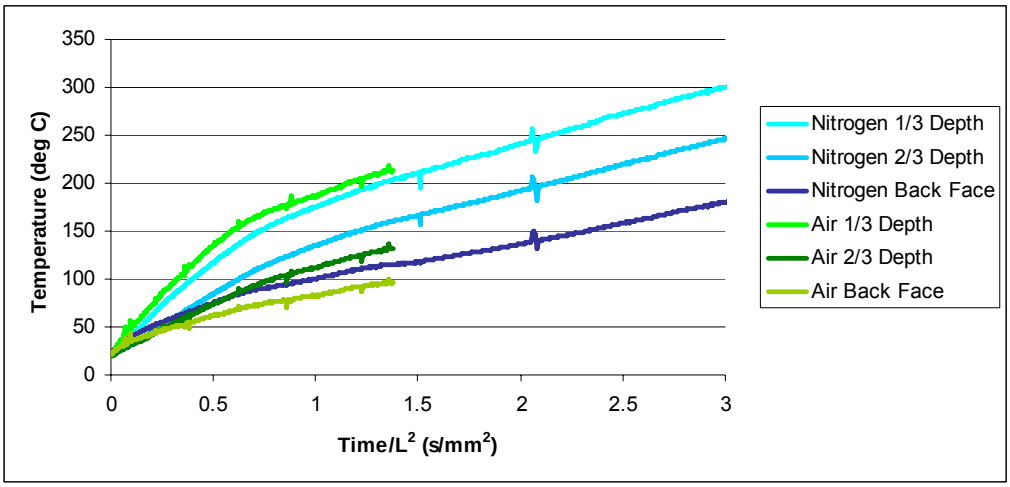

Figure 74: Comparison between 1A Tests Done in the FPA under Air with No Pilot Flame and under Nitrogen. Both tests were done at 50kW/m^2 in the FPA. Time zero is shutter down time. Data is truncated at ignition for the air test. The surface temperature measurements for the air and nitrogen tests did not record properly and are not included.

As can be seen, there does not appear to be a significant difference in the in-depth thermocouple measurements under an air (no pilot flame) or a nitrogen atmosphere for the 1A sample at 50kW/m^2 in the FPA. The polyester auto ignited fairly readily at this heat flux under the air condition. Additional testing is necessary to confirm these findings.

Analysis

A bench scale test, such as those outlined in this study, are useful for preliminary observations regarding the fire characteristics of a particular material. They are also relatively inexpensive and not as time consuming as large scale tests. However, the end use of the composites that were studied in these experiments is not to use them as small circles. Rather, the end use would be to use them as building materials to make walls, ceilings and floors, which is a completely different situation that involves different types of physics (e.g. concurrent and opposed flow flame spread). Experiments that would test these composites in a situation that would be more similar to their end use would be a room/corner test, such as ISO 9705[4] in Europe and NFPA 265[5] and 286[6] in the United States. In these tests, a corner of a standard size fire room is lined with the material and a propane burner is used as the ignition source. ISO 9705 is

the most severe test method due to the higher applied heat fluxes that it requires as compared to the NFPA standards.[11]

Although room/corner tests are more close to the end use of the product, the test has its own drawbacks, including the significant time and money that each test consumes. Therefore, it would be beneficial if the bench scale tests could predict results from the room/corner test. In the next section, the idea of a flame spread b parameter[9] will be introduced. The b parameter can be used to estimate flashover potential in the room/corner test from results obtained in a bench scale test, such as the FPA.

Quintiere b Parameter

Quintiere's[9] flame spread parameter is given as:

$$b = k_f \cdot Q'' - 1 - \frac{t_{ig}}{t_b} \qquad [1]$$

Where b is the flame spread parameter
Q" is the average or the peak HRRpuA [kW/m^2]
k_f is a constant equal to 0.01m^2/kW
t_{ig} is the time to ignition [s]
t_b is the total burning time [s]

This approach was chosen over the others in the literature because it is the classical approach and has values that are easy to determine in the FPA. Some of the methods in the literature use peak heat release rate and some use an average heat release rate in the equation for the b parameter. In this study, both the average and the peak heat release rate were used because the values were significantly different in some cases due to a strong initial peak (see Figure 71). Since the same burn duration was used for both the peak and the average heat release rate in the b parameter equation, the b parameter calculated using the peak heat release rate assumes that the heat release rate is at its peak value for the entire burn duration and thus represents a worst case scenario.

Since all of the information about the sample is not known (e.g. the chemical formula), the generic heat release rate formulas were used. As stated before, the heat release rate for the FPA[7] is calculated using

carbon dioxide generation calorimetry and that for the Cone[8] is calculated using oxygen consumption calorimetry.

Related to the idea of proper ignition discussed in a previous section, the time to ignition was defined as the time to the start of the flame cone. In most cases, this was the same as the time to ignition but was slightly longer in some cases. Along the same line, the total burning time was defined as the time from the beginning to the end of the fully developed flame cone on the specimen surface, which was determined from visual observations. The observations of the end of the flame cone generally correlated with a change in the heat release rate trace. For System 1, which properly ignited at much lower heat fluxes than any other system, the disappearance of the flame cone usually correlated with the beginning of the decay tail or, in some cases, with the beginning of the second rounded peak in the heat release rate trace. For every other system, the flame cone generally ended after the initial peak.

Referring to the literature,[2, 9] the flame spread is considered to be accelerating if the b parameter is greater than zero and decelerating otherwise. Beyler et. al.[11] extend this idea to correlate a b parameter based on a test performed at an applied heat flux of 50kW/m^2 to the probability of flashover. They concluded, based on their data, that a material with a b parameter less than 0.3 is not expected to flashover in a room/corner test. However, materials with a b parameter larger than 0.3 are much more likely to flashover (although there were some outliers in their data set). Beyler et. al. did not publish any uncertainties related to the b parameter in their report.[11]

The b parameter for both the FPA and the Cone tests are given in Table 4 and Table 5 below. From the FPA calibration tests, it was determined that the uncertainty in the heat release rate trace is 45kW/m^2. The uncertainty in the time to ignition and the burn duration were found to be 9s and 101s, respectively. Given these uncertainties, the equation for the propagation of uncertainty[17] was used to determine that the uncertainty in the b parameter is approximately 0.45 full scale (±0.225).

Table 22: System 1 FPA Tests and the Corresponding b Parameter Using both the Average and the Peak Heat Release Rate Determined from the Generic CO_2 Based Formula in ASTM 2058[7]. The maximum b parameter (the actual b parameter plus the uncertainty) is also included.

FRP Sample	Heat Flux (kW/m^2)	Avg -- Generic 2058	Peak -- Generic 2058	Avg -- Generic 2058 +0.45	Peak -- Generic 2058 +0.45
1A	50	0.0	1.1	0.45	1.55
1A	50	0.0	1.3	0.45	1.75
1A	40	-0.1	0.8	0.35	1.25
1A	30	-10.6	-10.2	-10.15	-9.75
1B	50	0.0	0.6	0.45	1.05
1B	50	0.1	0.5	0.55	0.95
1B	30	-0.8	-0.3	-0.35	0.15
1B	25	-3.6	-3.1	-3.15	-2.65
1C	50	-0.4	0.0	0.05	0.45
1C	50	-0.5	-0.2	-0.05	0.25
1C	30	-2.1	-1.7	-1.65	-1.25
1C	25	-3.9	-3.7	-3.45	-3.25

Table 23: Cone Tests and the Corresponding b Parameter Using both the Average and the Peak Heat Release Rate Determined from the Generic O_2 Based Formula in ASTM E 1354.[8] The maximum b parameter (the actual b parameter plus the uncertainty) is also included.

FRP Sample	Heat Flux (kW/m^2)	Average -- Generic 1354	Peak -- Generic 1354	Avg -- Generic 1354 +0.45	Peak -- Generic 1354 +0.45
1A	50	-0.7	-0.4	-0.25	0.05
1A	50	-0.3	-0.1	0.15	0.35
1B	50	0.0	0.4	0.45	0.85
1C	50	-0.4	-0.2	0.05	0.25
3A	50	-6.3	-6.2	-5.85	-5.75
3A	60	-2.3	-2.1	-1.85	-1.65
3A	65	-3.8	-3.6	-3.35	-3.15
3A	70	-0.3	0.1	0.15	0.55
3A	80	-0.3	0.2	0.15	0.65
3C	65	-2.2	-2.1	-1.75	-1.65
3C	70	-1.7	-1.6	-1.25	-1.15
3C	80	-1.5	-1.4	-1.05	-0.95
4A	60	-4.0	-3.9	-3.55	-3.45
4A	65	-2.9	-2.7	-2.45	-2.25
4A	70	-2.9	-2.7	-2.45	-2.25
4A	80	-0.9	-0.7	-0.45	-0.25
4B	80	-1.4	-1.1	-0.95	-0.65
4C	100	-4.4	-4.3	-3.95	-3.85
5A	100	-0.1	0.1	0.35	0.55
5B	100	-0.3	0.1	0.15	0.55

The tests performed at 50kW/m^2 are highlighted because the correlation from Beyler et. al.[11] is based on tests done at this applied heat flux. Considering those tests done at 50kW/m^2 in both Table 22 and Table 23, 1A and 1B based on a peak heat release rate in the FPA and 1B based on a peak heat release rate in the Cone are the only composite samples that would be expected to flashover in a room/corner test based on the actual b parameter (not the maximum). The b parameter based on the peak heat release rate is significantly higher than that based on the average heat release rate due to the strong initial peak in the heat release rate trace for the 1A and 1B samples (see Figure 71).

However, the uncertainty in the b parameter is 0.45 so, in order to truly determine if the b parameter has a chance of obtaining the threshold value of 0.3 for flashover, this uncertainty needs to be

added to the value that was obtained from the data. Table 22 and Table 23 display the maximum possible values of the b parameter in the last two columns. The maximum possible value of the b parameter for each FRP sample was determined by taking the actual value of the b parameter and adding the uncertainty of 0.45.

From the data in the tables, it can be seen that all of the polyester (System 1) samples have a maximum b parameter larger than 0.3 and thus have the potential to flashover in the room/corner test based on the Beyler et. al.[11] correlation. The 1C sample displays maximum b parameter values for the calculations based on the average heat release rate that are less than 0.3 but those calculated using the peak heat release rate are either very close or over this threshold value. Therefore, it is assumed that the 1C sample has a potential for flashover, especially when compared to the phenolic composites. 3A displays very negative b parameters, which indicate that the phenolic is not expected to flashover in the room/corner test. Comparing the tests done at 50kW/m^2, it is apparent that the phenolic has better fire performance than the polyester resin.

For the tests that are not completed at 50kW/m^2, the Beyler et. al.[11] correlation cannot be reliably used. Therefore, the discussion will be based on other references[2,9] that correlate a negative b parameter with decelerating flame spread and a positive b parameter with accelerating flame spread. If the maximum possible value of the b parameter is again considered (i.e. the b parameter plus the uncertainty of 0.45), the only samples that are expected to exhibit accelerating flame spread are 1A at 40kW/m^2 in the FPA, 3A at both 70kW/m^2 and 80kW/m^2 in the Cone, and 5A and 5B at 100kW/m^2 in the Cone. This again demonstrates that the phenolics are superior to the polyester resin and that the additives (System 4 with the charring additive and System 5 with the intumescent additive) make the phenolic perform better.

An important observation regarding the b parameter is the significant increase in the b parameter with applied heat flux for the System 1 composites. Since the uncertainty in the b parameter is 0.45, it can be seen that there is a very significant difference between low and medium heat fluxes but it seems to level off as the applied heat flux increases up to 50kW/m^2. From Table 22 and Table 23, it can also be seen that the b parameter makes a significant drop (see, for example, the b parameter for 1A in the FPA with applied heat flux) to become more negative just before the minimum heat flux for ignition (30kW/m^2 for 1A).

Conclusions and Future Work

The work being done in this study is important to the composites industry because it is a beginning of systematic research into how the resin type and the glass content affect the overall fire performance of the composites. The resin type was found to greatly affect the resultant fire performance, however the effect of glass content is a little more subtle. For example, there is a difference in the peak heat release rate (see Figure 71) and heating rates (see Figure 72) with glass content for the System 1 composites but there is no significant difference in the average heat release rate in the plateau region of the trace. There is an increase in the time to ignition and a decrease in the burning time with glass content for the System 1 composites (see Figure 71). The minimum heat flux for proper ignition greatly changed with resin type with the polyester resin (System 1) having a significantly lower minimum heat flux for proper ignition range than the phenolic resins and the phenolics with additives (Systems 4 and 5) improving over the performance of the neat phenolic (System 3). Except for System 1, the minimum heat flux for proper ignition range increased with glass content (see Table 20).

This work is also very important to the fire industry because the industry is leaning toward performance based design in modern building codes. This requires fire engineers to determine whether a room will flashover or not. From the results of the b parameter, it is expected that the FRPs with the polyester resin (System 1) would be expected to flashover in a room/corner test while the phenolics (Systems 3, 4 and 5) are not expected to flashover based on tests done at 50kW/m^2. Based on the large

uncertainty in the b parameter and to verify the results of this study, it would be very interesting to perform large scale room/corner tests with the specimens. It will also be very important to relate the results obtained from the FPA with the results obtained with the Cone since much work has been done with the Cone.

The thermocouple and infrared thermometer measurements provide the beginning to a complete data set for modelling purposes. In the near future, there are also plans to instrument the sample with an embedded heat flux gage to enhance the data set as well as to perform tests under an enhanced oxygen environment in the FPA.

Acknowledgements

The continued significant support for this project from FM Global Research (FM Global Fellow Avila and FM Global Scholar Dembsey) is greatly appreciated. The authors greatly appreciate the materials donated by: Trevor Humphries of VectorPly, Phoenix City, AL (glass); and Chad Fester of Airtech International Inc. of Huntington Beach, CA (vacuum bagging and peal ply) as well as Cinnabar, FL (lamination of the FRP composite panels). Information regarding the heat of combustion and other properties of the composites used in this study by Mike Stevens from Ashland was very useful. Many thanks also to Randall Harris, Mihyun (Esther) Kim and Jacqueline Shea at WPI for performing the Cone tests.

References

[1] Standard Test Method for Surface Burning Characteristics of Building Materials, ASTM E 84-05, ASTM, 100 Barr Harbor Drive, West Conshohocken, PA, U.S.

[2] Dembsey, N.A., J.J. Alston and S.D. Ayers, "Using Cone Calorimeter Data and Half-Scale Corner Test Data to Assess the Fire Performance of Composite Materials," submitted to Cinnabar-Florida, Orlando, FL, USA as part of the project *Phenolics vs. Other Thermosets for Theme Parks* (2001).

[3] Williamson, R.B. and F.W. Mowrer, "The Role of Interior Finish in Fire Development," *Fire Protection Engineering*, 2004, No. 24, pp. 26-40.

[4] Fire Tests – Full-Scale Room Test for Surface Products, ISO 9705, International Standards Organization, Geneva, Switzerland, 1993.

[5] Standard Methods of Fire Tests for Evaluating Room Fire Growth Contribution on Textile Coverings of Full Height Panels and Walls, NFPA 265, National Fire Protection Association, Quincy, MA.

[6] Standard Methods of Fire Tests for Evaluating Contribution of Wall and Ceiling Interior Finish to Room Fire Growth, NFPA 286, National Fire Protection Association, Quincy, MA.

[7] Standard Methods of Test for Measurement of Synthetic Polymer Material Flammability Using a Fire Propagation Apparatus (FPA), ASTM E 2058-03, ASTM, 100 Barr Harbor Drive, West Conshohocken, PA, U.S.

[8] Standard Test Method for Heat and Visible Smoke Release Rates for Materials and Products Using an Oxygen Consumption Calorimeter, ASTM E 1354-02, ASTM, 100 Barr Harbor Drive, West Conshohocken, PA, U.S.

[9] Lautenberger, C and Fernandez-Pello, C., "A Generalized Pyrolysis Model for Simulating Charring, Intumescent, Smoldering, and Noncharring Gasification," 2006, University of California eScholarship Repository, <http://repositories.cdlib.org/cpl/fs/LautenbergerGenPyro>.

[10] Cleary, T. and J. Quintiere, "A Framework for Utilizing Fire Property Tests," *Fire Safety Science, Proceedings of the Third International Symposium,* International Association of Fire Safety Science (IAFSS), Scotland, U.K., Cox and Langford Editors, Elsevier Applied Science London and New York, July 8-12 (1991) 647-656.

[11] User's Guide for the Fire Propagation Apparatus (FPA) ASTM E-2058, Fire Testing Technology Limited, PO Box 116, East Grinstead, West Sussex, England.

[12] de Ris, J.L. and Khan, M.M., "A sample holder for determining material properties," *Fire and Materials*, 24, 219-226 (2000).

[13] Beaulieu, P.A. and Dembsey, N.A., "Enhanced Equations for Carbon Dioxide and Oxygen Calorimetry," *Proceedings of the 9th International Fire and Materials Conference,* p.49 (2005).

[14] Parker, W.J., "Calculations of the Heat Release Rate by Oxygen Consumption for Various Applications," National Bureau of Standards Report # NBSIR 81-2427 (1982).

[15] Nelson, Mark, "Combustion of Polymers: The critical mass flux concept", 2004, University of Wollongong, Australia <http://www.uow.edu.au/~mnelson/review.dir/cmf.html>.

[16] Beyler, C., S. Hunt, B. Lattimer, N. Iqbal, C. Lautenberger, N. Dembsey, J. Barnett, M. Janssens, S. Dillon and A. Grenier, "Prediction of ISO 9705 Room/Corner Test Results," US Department of Transportation, Report No. R&DC-215-99, 1999.

[17] Coleman, H. W. and W. G. Steele, Experimentation and Uncertainty Analysis for Engineerings, 2nd Edition, New York: John Wiley & Songs., Inc., 1999.